ACTIVATION OF *n*-HEXANE USING VANADIUM-EXCHANGED ZEOLITES

BY

THIRUSHA NAICKER

Submitted in fulfilment of the academic requirements for the degree of Doctor of Philosophy in the School of Chemistry, University of KwaZulu-Natal, Durban

July 2010

As the candidate's supervisor I have/have not approved this thesis/dissertation for submission

Signed: _____ Name: _____ Date: _____

DEDICATION

To my dad and mum, I love you lots.

ABSTRACT

The influence of the form of the ZSM-5 zeolite, vanadium content and the elimination of the exterior surface acidity on the activity and selectivity of *n*-hexane oxidation was studied using a fixed bed reactor. Blank reactor studies (carborundum packed reactor) showed no conversion below 450°C with the highest conversion (8%) at 500°C. The dominant products were found to be carbon oxides (Sel./% = 90) with minor selectivities to the hexene isomers (7%) and the remainder being cracked products, THF and benzene. H-ZSM-5 with different SiO_2/Al_2O_3 ratios (100 and 320) and Na-ZSM-5 (SiO_2/Al_2O_3 ratio of 100) were tested under non-oxidative and oxidative conditions. Under oxidative conditions as the ratio of the SiO_2/Al_2O_3 increased, the aluminium content decreased and so too did the cracking ability of the zeolite (i.e. yield of cracked products dropped from 36% to 8%). However, the use of the Na- form of ZSM-5 completely eliminated acid cracking. Under oxidative conditions H-ZSM-5 (100) was found to be more active and resulted in higher formation of cyclic and aromatic compounds. With increasing time on-stream and higher temperatures the catalyst was found to deactivate. Evidence of this was seen by a decrease in surface area and pore volumes of the spent catalyst. The Na-ZSM-5 (100) showed lower activity, but deactivation was shown to be lower. These findings led to the investigation of vanadium ion-exchanged Na-ZSM-5 catalyst for *n*-hexane activation. Catalysts with different vanadium loadings were prepared using the solid state ion-exchange method. Catalysts were characterised using various methods. These techniques showed that vanadium was successful loaded onto the catalyst and that the highest vanadium loading that could be achieved was 2.5%. The lower loadings were not found to alter the catalyst structure while the highest loading of 2.5% was found to show some pore blockage and to possibly alter the structural environment of the zeolite. Time on stream experiments were conducted and temperature (350, 400 and 450°C), contact time (0.5, 0.8, 1.1 and 1.5 s) and fuel-air ratios (0.7, 1.3 and 2) were varied. The optimum conditions (Conv./% = 39) for terminally activated products were found using the Na-V-ZSM-5 (0.9%) at a temperature of 400°C, a contact time of 1.1 s and fuel-air ratio of 1.3. With the lower fuel-air ratio of 0.7 (oxygen rich conditions), hexanal formation was favoured. The Na-V-ZSM-5 catalyst could be regenerated with initial activity and selectivity being regained. Silanisation was found to be possible, however, the extent and degree of silanisation was difficult to control. Pore blockage was possibly responsible for the lower activity and selectivity obtained using the silanised Na-V-ZSM-5.

PREFACE

The experimental work described in this thesis was carried out in the School of Chemistry, University of KwaZulu-Natal, from July 2006 to December 2009, under the supervision of Professor Holger B. Friedrich.

These studies represent original work by the author and have not otherwise been submitted in any form for any degree or diploma to any tertiary institution. Where use has been made of the work of others it is duly acknowledge in the text.

DECLARATION 1 – PLAGIARISM

I, _____, declare that

1. The research reported in this thesis, except where otherwise indicated, is my original work.
2. This thesis has not been submitted for any degree or examination at any other university.
3. This thesis does not contain other person's data, pictures, graphs or other information, unless specifically acknowledged as being sourced from other persons.
4. This thesis does not contain other person's writing unless specifically acknowledged as being sourced from other researchers. Where other written sources have been quoted, then:
    a. Their words have been re-written but the general information attributed to them has been referenced.
    b. Where the exact words have been used, then their writing has been placed in italics and inside quotation marks, and referenced.
5. This thesis does not contain text, graphics or tables copied and pasted from the internet, unless specifically acknowledged, and the source being detailed in the thesis and in the References sections.

Signed: _____

DECLARATION 2 – PUBLICATIONS

Publication 1:

n-Hexane activation over vanadium modified zeolite ZSM-5 (submitted to Applied Catalysis: General)

Signed: _____

DECLARATION 3 – CONFERENCE CONTRIBUTIONS

Contribution 1:

CATSA conference 2007, Richards Bay, Poster presentation*: n*-Hexane activation using Vanadium doped Zeolites

Contribution 2:

CATSA conference 2008, Parys, Poster presentation*: n*-Hexane activation using Vanadium exchanged Zeolites

Contribution 3:

SACI conference 2008, Cape Town, Poster presentation*: n*-Hexane activation using Vanadium exchanged Zeolites

Signed: _____

TABLE OF CONTENTS

LIST OF ABBREVIATIONS

µmol	micro mole
3D	three dimensional
AAS	atomic absorption spectrometry
BET	Braunauer Emmet Teller
C mol.%	carbon mole percent
cm	centimeter
conv.	conversion
COx	carbon oxides
CVD	chemical vapour deposition
DSC	differential scanning calorimetry
DTA	differential thermal analysis
ESR	electronic spin resonance
FAU	faujasite
FID	flame ionization detector
FT-IR	Fourier transform infrared
g	gram
GC	gas chromatography
GIS	gismondine
h	hour
H_2-TPR	hydrogen - temperature programmed reduction
HDPE	high-density polyethylene
HF	hydrofluoric acid
HPLC	high performance liquid chromatography
ICP-OES	inductively coupled plasma-optical emission spectroscopy
IFP	Institute Francais du Pétrole
K	Kelvin
KHz	kilo Hertz
kPa	kilo Pascal
LLDPE	linear-low density polyethylene
LTA	Linde Type A

m	meter
MAS-NMR	magic angle spinning-nuclear magnetic resonance
MHz	mega Hertz
mL	milli litres
mm	milli metres
mmol	milli moles
MOR	mordenite
M_w	molecular weight
NH_3-TPD	ammonia - temperature programmed desorption
ODH	oxidative dehydrogenation
Pacol	paraffin catalyst olefin
ppm	parts per million
PVC	polyvinylchloride
R_f	response factor
s	second
SHOP	Shell Higher Olefins Process
SS-IE	solid state-ion exchange
TBHP	tert-butyl hydrogen peroxide
TCD	thermal conductivity detector
Temp.	temperature
TEOS	tetraethylorthosilicate
TGA	thermogravimetric analysis
THF	tetrahydrofuran
UV-vis	ultra-violet-visible
V_μ	micropore volume
vol	volume
V_T	total pore volume
wt	weight
XRD	X-ray diffraction
XRF	x-ray fluorescence
ZSM	Zeolite Socony-Mobil

LIST OF FIGURES

LIST OF SCHEMES

LIST OF TABLES

ACKNOWLEDGEMENTS

I would like to thank my parents and brother for their support, constant encouragement, love and patience throughout my studies. I would like to thank my husband, Avinash for his love and encouragement as well as for his advice and knowledge throughout my PhD studies.

I would also like to take this opportunity to thank my supervisor, Dr. F, for his guidance and valuable advice throughout the course of this project. It has been a long journey together but it has been a pleasure working under your supervision.

I thank the technical staff of the University of KwaZulu-Natal, School of Chemistry whom have helped me along the way.

And lastly many thanks to all the friends that I have encountered along the way.

CHAPTER ONE
INTRODUCTION

1

1.1 *n*-Hexane

n-Hexane is produced as a by-product from either natural gas, petroleum or coal and coal derivatives processes. Like most saturated hydrocarbons only a limited amount is used as raw materials in the chemical industry. Other than its use in fuel, the main application of *n*-hexane is in the extraction of vegetable oils from seeds, e.g. soybean and cottonseed. It is ideal for this process because of its high solvency for oil, low boiling point and is also cheaply available. It is also used as a solvent in chemical reactions e.g. for the coordination complex catalysed polymerisation of olefins and in the manufacture of synthetic rubbers and some pharmaceuticals. As a solvent it serves as a catalyst carrier and in some systems works as a molecular regulator by precipitation of the polymer when it reaches a certain molecular size. These processes are fairly old and in time will likely be replaced by more efficient nonsolvent processes **[1, 2]**.

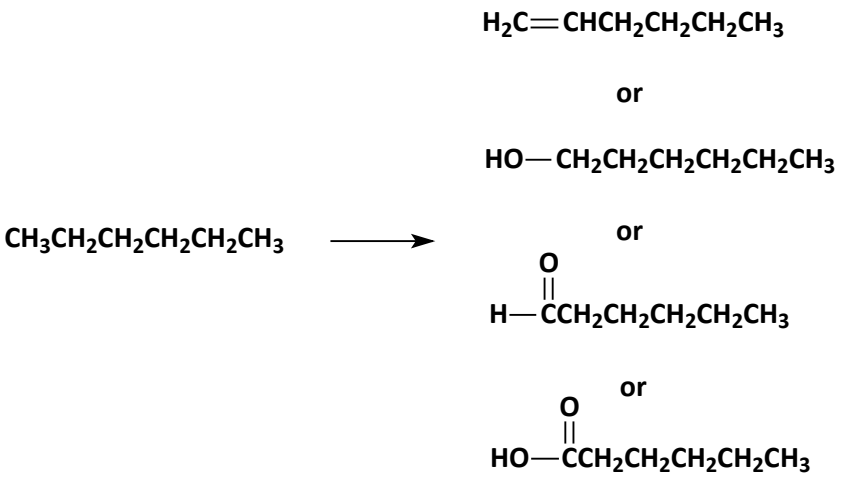

Scheme 1.1 Some important derivatives from *n*-hexane

However partially oxidised hexane (Scheme 1.1) holds an economical interest as most partially oxidised hydrocarbons are used as important building blocks for the manufacture of specialty and everyday chemicals and are also used in the manufacture of plastics and synthetic fibres **[3]**.

1.2 C_6 Olefinic type compounds

1.2.1 Commercial processes used in the manufacture of C_6 olefins

Linear *α*-olefins are more desired than internal olefins and processes that have gained industrial importance are those that start with cheap raw materials. From 1962 to 1985, wax cracking was used to produce linear *α*-olefins. Thermal cracking of long chain linear paraffins yields mainly *α*-olefins. The process occurs *via* a radical mechanism with cleavage of the C–C bond leading to carbon radicals which are converted to olefins by loss of a hydrogen atom (Scheme 1.2). The paraffins are obtained from petroleum, diesel oil, and lubricant fractions of paraffin-based crude oils. These are separated from this mixture and cracked by heating, followed by thermolysis and then rapid quenching of the reaction. To obtain C_6 – C_{20} *α*-olefins, starting materials consisting of C_{18} – C_{36} paraffins are required. Unwanted products such as internal olefins, conjugated and nonconjugated olefins and traces of aromatics are also present **[1]**.

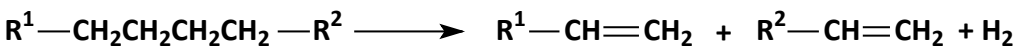

Scheme 1.2 Thermal cracking of waxes **[1]**

Catalytic dehydrogenation of paraffins provides an alternate route to olefins with the same number of carbon atoms but a random location of the double bond. The energy required to cleave the C–H bond (365 kJ/mol) is significantly higher than the cleavage of the C–C bond (245 kJ/mol) thus thermodynamics do not favour economic interest **[1]**.

However, the use of a catalyst facilitates linear olefins with the same number of carbon atoms as the linear paraffin (Scheme 1.3). The Pacol (paraffin catalyst olefin) process is the most important industrial process which makes use of this technology. The reaction is carried out using a hydrogen to carbon ratio of 9:1 with a platinum catalyst supported on alumina under very low conversions to minimise the formation of by-products. The paraffin olefin products are separated using molecular sieves **[1]**.

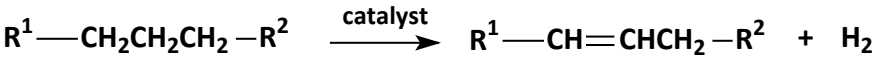

Scheme 1.3 Catalytic dehydrogenation of paraffins **[1]**

A chlorination-dehydrochlorination method exists that can generate linear olefins from linear paraffins. The method consists of chlorinating paraffins to chloroalkanes, followed by a catalysed step using iron or iron alloy catalysts in which hydrogen chloride is eliminated. However, a random mixture of linear olefins results from the dehalogenation **[1, 4]**.

Alternative routes in the production of olefins are based on the oligomerisation of ethylene. In the 1950s, Ziegler developed an ethylene oligomerisation process and in 1965 this became the first commercial process **[5]**. It is a two-step stoichiometric process which consists of the oligomerisation of ethylene on triethylaluminum followed by the second step in which ethylene is used to displace the olefins and regenerate the triethylaluminum for recycle to step one (Scheme 1.4). The disadvantage of this process is the requirement of stoichiometric amounts of reactants, thus industrial plants require large quantities of aluminium alkyls **[1, 6]**.

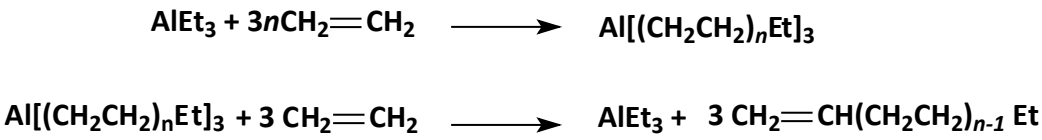

Scheme 1.4 Two step Ziegler process **[1]**

Consequently, the Gulf Oil process and Ethyl process were developed. Both processes require less triethylaluminum with the former requiring only catalytic quantities of triethylaluminum with the growth step and elimination reactions occurring simultaneously in the same reactor. The process produces purer α-olefins than wax cracking. Again, unwanted products are produced and include β-branched α-olefins **[7]**. The Ethyl process has a combination of a stoichiometric and a catalytic stage. In this process, ethylene is first oligomerised using catalytic quantities of triethylaluminum in analogy to the Gulf process. Fractionation then results in fractions containing C_4, C_6 – C_{10} and C_{12} – C_{18}. The shorter α-olefins i.e. C_4 are subjected to transalkylation with long chain aluminium alkyls whilst the longer chain may be used directly. The reactions result in the desired long chain α-olefins being released with the simultaneous formation of short chain trialkylaluminum compounds. These chains are then separated in a second distillation step and transformed by a stoichiometric reaction of ethylene in another reactor to longer chain alkyls. These are then recycled to the transalkylation reactor. The processes results in a higher conversion of ethylene but suffers the disadvantage of lower quality long chain α-olefins **[8]**.

A large scale commercial process that incorporates olefin metathesis is the Shell Higher Olefins Process (SHOP). This three step process produces linear higher olefins from ethene. In the first stage, ethylene is oligomerised in a polar solvent (1,4-butanediol) to give a mixture of linear even numbered α-olefins ranging from C_4 to C_{40}. A nickel-phospine catalyst is used to drive the reaction (Scheme 1.5).

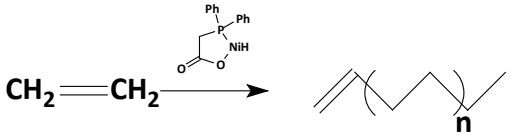

Scheme 1.5 Step one in the SHOP process **[8]**

The C_6 – C_{18} α-olefins fractions are separated from the mixture by distillation and then fractionated into individual components. The second step results in the lighter and heavier olefins undergoing double-bond isomerisation over a solid potassium catalyst which results in

an equilibrium mixture of internal olefins. In the last step the mixture is passed over an alumina-supported molybdate metathesis catalyst. This results in a statistical distribution of linear olefins with both odd and even numbers of carbon atoms *via* cross-metathesis reactions. The product consists of more than 96% linear internal olefins (C_{11} – C_{14}) **[9]**.

Other industrial processes that use ethylene as the starting materials include the Imeditsu process **[10]** and IFP (Institute Francais du Pétrole) process for 1-butene from ethylene **[6]**.

In South Africa, Sasol has a plant constructed to recover 50 000 tons of 1-pentene and 1-hexene by extractive distillation from Fischer-Tropsch hydrocarbons produced from the coal derived synthesis gas. In India, the Gujarat-Godrej Innovative Chemicals Company began the production of α-olefins from the dehydration of fatty alcohols. These α-olefins are used to produce α-olefin sulfonate which is used in the surfactant market in India. **[6]**.

1.2.2 Uses of C_6 olefins

The demand for olefins, both branched and linear has increased over the years with ~2.3 million tons per annum of linear α-olefins produced world-wide by different commercial processes. Commercially, higher olefins (C_6 and above) are important intermediates for a number of important industrial and consumer products. C_6 olefins have a wide range of industrial application, including its use in the production of polymers. These olefins are intermediates in the production of plasticizers which have superior volatility and cold weather flexibility characteristics, making these suitable to use for automobile interiors.

1-Hexene is one of the principal co-monomers used in the production of linear low-density polyethylene (LDPE) and high-density polyethylene (HDPE). Each year the detergent industry consumes a large quantity of α-olefins through numerous processes. Although use is made mostly of C_{10} – C_{16} olefins, the lighter C_6 α-olefins are converted to fatty acids and then used to produce alkenylbenzenesulfonic acid products. These products are used in the United States

and in Europe as perborate bleach activators in heavy duty laundry detergents. Another area where C_6 α-olefins are beneficial is in the production of hindered esters which are used as lubricants for jet engines and other high performance applications **[6]**.

1.3 C_6 oxygenated type compounds

1.3.1 Manufacture of C_6 oxygenated compounds

Alcohols are useful derivatives of saturated hydrocarbons. Alcohols with a C_6 and longer hydrocarbon chain are referred to as higher alcohols.

On a commercial scale, only methanol is produced from synthesis gas, but the IFP process uses highly activated catalysts under low pressure methanol synthesis conditions to produce higher alcohols. The catalyst is composed of copper or cobalt oxides together with at least one other metal *viz*, Al, Ce, Cr, Fe, La, Mn, Pr, Nd, Y or Zn and one Group I or II metal compound. By changing the catalyst composition, the higher alcohol content can be varied by 20 – 50 wt%. Unwanted products such as hydrocarbons, esters and ketones are also formed **[11]**.

C_3 to C_{20} alcohols can be synthesised by the oxo–synthesis. In this process, alcohols are reacted with synthesis gas to form aldehydes which are then hydrogenated (Scheme 1.6). Shell uses a catalyst that has strong hydrogenating activity which leads to the direct hydrogenation in the oxo reactor of the initially formed aldehyde. The alcohol mixture formed consists of about 80% linear compounds **[12]**.

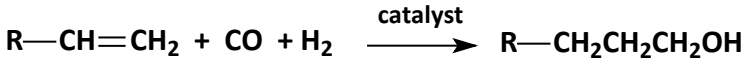

Scheme 1.6 Oxo-synthesis **[10, 11]**

Another process that leads to the formation of alcohols is the hydrogenation of aldehydes, carboxylic acids and esters in the presence of homogeneous or heterogeneous catalysts **[13]**. One of the processes that use this reaction is the hydrogenation of 2-ethyl-2-hexenal. The reaction is carried out using a nickel catalyst in a single step **[14]**.

Aldol condensation uses aldehydes formed during the oxo synthesis which are then subjected to aldol condensation in the oxo reactor. It is used for synthesis of 2-ethylhexanol, 2-methylpentanol and some highly branched isomeric C_{16} and C_{18} alcohols **[13]**.

Other methods that can be used to produce alcohols include: oxidation of saturated hydrocarbons, hydration of olefins, homologation of alcohols, hydrocarbonylation by the Reppe process, hydroxymethylation and fermentation **[13]**.

The dominant sources of 1-hexanol are either the Zeigler process using ethylene (Conoco or Ethyl Corporation) or its synthesis from natural products derived from coconut or palm oils (Henkel). In the Zeigler process, ethylene adds to triethylaluminum to form a mixture of trialkylaluminum products which are then oxidized with air to the corresponding aluminium alkoxides. The alkoxides are then hydrolysed to a mixture of linear primary alcohols (Scheme 1.7) **[13, 15]**. These have the same carbon atoms as the alkyl groups of the trialkylaluminum components.

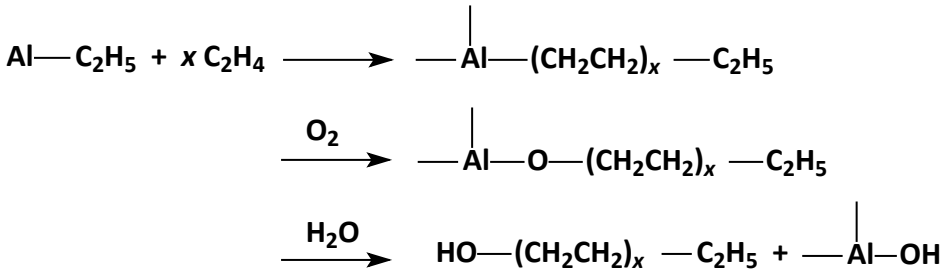

Scheme 1.7 Oxidation of trialkylaluminum compounds **[13]**

This process is a variant of the Ziegler process which was used to synthesise linear olefins as described in Section 1.2.1. Using this reaction, two commercial processes were developed by Conoco and Ethyl Corporation. The processes differ in chain-length distribution and the linearity of the alcohols produced, as well as the processes for the generation and control of distribution. In the Alfol alcohol process (Conoco process) a broad range of alcohols are produced (C_2 – C_{28}), whereas the Ethyl Corporation developed a process for mainly C_{12} and C_{14} alcohols **[13]**.

Other useful C_6 oxygenated compounds are C_6 aldehydes (hexanal, 2-methylpentanal, 2-ethylbutanal and 3-methylpentanal) which are almost exclusively prepared by hydroformylation or aldol condensation. Hexanal is prepared by hydroformylation of 1-pentene **[16]**.

1.3.2 Uses of C_6 oxygenated compounds

For commercial products the alcohol group is usually preferred in the primary position. The uses of higher alcohols are classified according to their carbon number. Those with a hydrocarbon chain length of C_{12} and above are used in the detergent industry, while those from C_6 to C_{11} are used as plasticizers. No dominance exists from C_6 to C_{11} linear alcohols with each being equally important. In 1996 the price of *n*-hexanol was 2.09 US dollars/kg with only the price of *n*-octanol being higher from the plasticizer alcohols. The alcohols for plasticizer production are chosen based on their different physical properties. The branched chain alcohols are cheaper than the linear alcohols primarily due to the propylene feedstock being cheaper than the ethylene feedstock used for linear alcohols. Although the primary use of C_6 alcohols is as plasticizers it can also be used as surfactants, lube additives and as a basic material for the perfume industry. Hexanols have superiority over pentanols in many applications with one of them being as flow improvers. This is due to their lower volatility and higher viscosity. Mixtures of 1-hexanol and 1-octanol are used as frothing agents in flotation of coal. Large quantities of these mixtures are added to aqueous drilling muds to prevent frothing that occurs during drilling for oil and gas **[13, 17].**

Hexanal can be hydrogenated or oxidised to the corresponding alcohols (hexanol) or carboxylic acids (hexanoic acid) respectively. The C_6 aldehydes are used as starting materials for tranquilisers and in the manufacture of agrochemicals, perfumes and catalysts for cross-linking polyesters **[16]**.

1.4 Oxidation of hydrocarbons

The demand for C_6 olefins and oxygenated products is increasing and existing methods mentioned may not be adequate to meet current demands. The activation of paraffins is more difficult than that of olefins, but the direct use of paraffins generates an economic interest as these are readily available as raw materials. Due to the very large scale capacity of these processes, an economically viable oxidant is necessary. The use of molecular oxygen coupled with a heterogeneous catalyst may offer an answer to an easy route to the functionalisation of saturated hydrocarbons through oxidation. Heterogeneous catalysis has found a direct impact on the global economy with approximately nine-out-of-ten processes utilising heterogeneous catalysts. A large portion of materials and commodities are produced by heterogeneous catalysis and more than 20% of industrial organic chemicals are obtained by either catalytic oxidation or ammoxidation of hydrocarbons **[18-21]**. The only process of selective paraffin oxidation that has been commercialised is the oxidation of *n*-butane to maleic anhydride using a vanadium phosphorus oxide (VPO) catalyst **[22, 23]**.

Hydrocarbon oxidation occurs by consecutive abstraction of hydrogen atoms and addition of oxygen atoms. Should consecutive hydrogen abstractions take place and desorption of water molecules occur, a new C–C bond may be formed and this is referred to as oxidative dehydrogenation. There are two types of oxidative dehydrogenation; intramolecular and intermolecular oxidative dehydrogenation. Intramolecular oxidative dehydrogenation occurs when hydrogen abstraction occurs on the same hydrocarbon molecule with the formation of a π C–C bond (Scheme 1.8 a), whereas intermolecular oxidation occurs as a result of hydrogen abstraction on different hydrocarbon molecules which then undergo dimerisation through formation of a new C–C bond (Scheme 1.8 b). To form an oxygenated hydrocarbon derivative the first abstraction of a hydrogen atom is followed by oxygen insertion **[18]**.

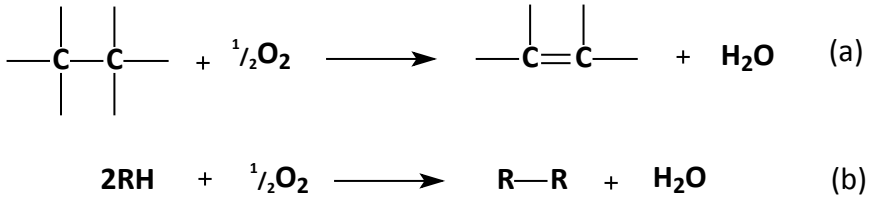

Scheme 1.8 Intramolecular (a) and intermolecular (b) oxidative dehydrogenation **[18]**

1.4.1 Electrophilic oxidation

Molecular oxygen reacts with a hydrocarbon molecule either through electrophilic or nucleophilic oxidation. At the solid surface dioxygen is adsorbed and is either present as a superoxide ion or a peroxide ion. At high temperatures the species are unstable and decompose to form the radical species, $O^{\cdot}$. The activated oxygen forms either the neutral singlet O_2, the ionic O_2^{-} or $O^{\cdot}$ which are strongly electrophilic reactants. These species attack the π bonds of the organic molecule i.e. the region of its highest electron density. Under heterogeneous catalytic conditions the peroxy and epoxy complexes formed as the result of an electrophilic attack of O_2^{-} or $O^{\cdot}$ species on the π bonds of the hydrocarbon molecules at the surface of an oxide lead to the degradation of the carbon skeleton **[18]**.

1.4.2 Nucleophilic oxidation

Nucleophilic oxidation of hydrocarbons occurs with lattice oxide ions, O^{2-}. These have no oxidising properties but can be inserted into the activated hydrocarbon molecule to form an oxygenated product. Here, the organic molecules are activated first during the process which renders them accessible to attack by nucleophiles. A series of consecutive steps of hydrogen abstraction and nucleophilic oxygen addition occurs. The surface of the catalyst requires different active centers for each of these steps to occur, as a result this type of mechanism requires a catalyst which contains a redox couple i.e. transition metal ions. Hence, this process needs to favour electron transfer and have high lattice oxygen anion mobility within the

material to ensure the re-oxidation of the reduced catalyst. The majority of the catalysts that are used correspond to metallic oxides with vanadium and molybdenum as one of the key elements, but also cations of variable oxidation states as Fe^{3+}/Fe^{2+}, V^{5+}/V^{3+}, Mo^{6+}/Mo^{5+}, Cr^{6+}/Cr^{3+}, Cu^{2+}/Cu^{+} etc. The cations of the catalyst act as oxidising agents in some of the consecutive steps forming the activated hydrocarbon species. Subsequently, this hydrocarbon species can undergo a nucleophilic attack by lattice oxygen ions and the oxygenated product is desorbed. This leaves oxygen vacancies which are then filled with oxygen from the gas phase simultaneously re-oxidising the reduced cations. Incorporation of oxygen from the gas phase into the oxide surface may not take place at the same site from which the surface oxygen is inserted into the hydrocarbon molecule but could occur at a different site, implying that oxygen ions are being transported through the lattice. This redox mechanism was postulated by Mars and van Krevelen to explain the kinetics of the oxidation of aromatics over V_2O_5 catalysts (Scheme 1.9) **[18, 24-26]**.

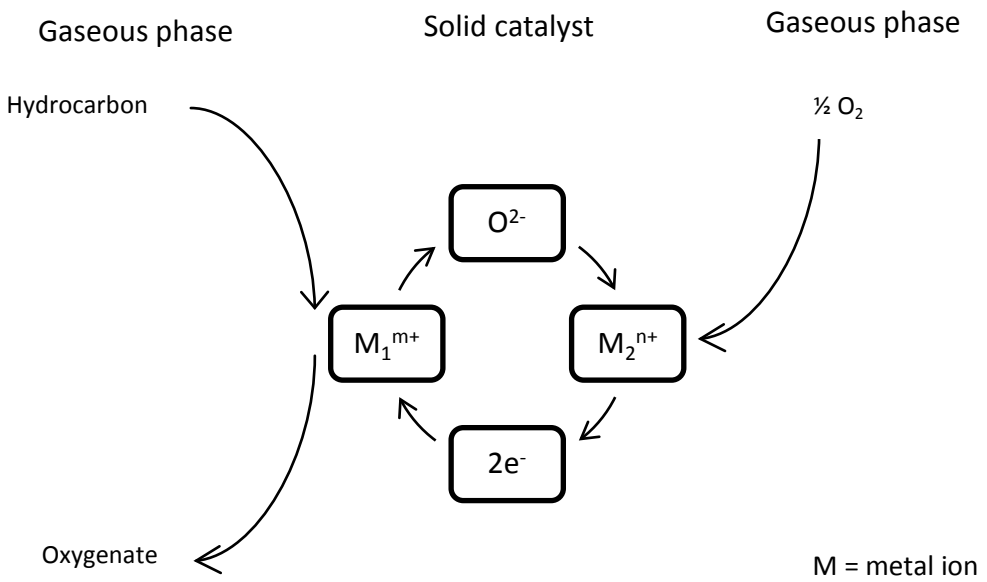

Scheme 1.9 Oxidation-reduction cycles postulated by Mars and van Krevelen **[18, 24, 26]**

1.4.3 Oxidation of *n*-hexane

Literature reports of very few catalytic systems for the conversion of *n*-hexane to terminal oxygenated products or olefins. However there are reports for the conversion of *n*-hexane to benzene over varying catalysts.

The conversion of *n*-hexane to benzene over tellurium loaded NaX and KX zeolites was found to occur at conversions as high as 80% with selectivities to benzene higher than 90%. Other products that were obtained were C_{1-5} cracked products and coke **[27]**.

In 1988, Centi *et al*. **[28]** reported on the oxidation of n-hexane over a VPO catalyst. The products that were obtained were maleic anhydride, phthalic anhydride, benzoic acid, cracked products and carbon oxides. The conversion was reported to be 50% with a selectivity of 23% to maleic anhydride.

Skotak *et al*. **[29]** reported on the conversion *n*-hexane in excess hydrogen in air over Pd/Al_2O_3 and Pt/Al_2O_3 catalysts. The major products were reported to be methylpentanes, methylcyclopentane and hydrogenolysis products. Benzene and cyclohexane were minor products.

The partial oxidation of *n*-hexane and cyclohexane using Rh-coated alumina monoliths was reported by Schimdt *et al.* **[30]**. This study was carried out in order to determine whether higher alkanes can be successfully converted to H_2 and CO in short contact time reactors. The conversion was reported to be ~100% for C/O ratios near syngas stoichiometry and decreased as the C/O ratio was increased.

The conversion of *n*-hexane has also been studied over magnesium orthovanadate ($Mg_3V_2O_8$). This study investigated void spaces as well as products formed *via* gas phase homogeneous

reactions. Benzene was also found to form in both empty steel and glass reactors. This showed that its formation was, in part, non-catalytic. The results implied that benzene production below 400 °C was catalytically driven, whilst production above 400 °C was thermodynamically driven **[31]**.

As has been explained above in Section 1.4.2, the reactions that occur between the hydrocarbon molecules and the oxygen species occur along many different pathways in a network of competing parallel and consecutive reactions. The literature reports from above show that a large range of products can form and achieving product selectivity remains the challenge. Thus the catalyst should be able to control the rate of product formation i.e. accelerate the sequence of steps leading to the desired products and hinder those leading to unwanted by products **[32]**.

1.5 References

1. K. Griesbaum, A. Behr, D. Biedenkapp, H-Z. Voges, D. Garbe, C. Paetz, G. Collin, D. Mayer and H. Höke, Hydrocarbons, Ullmann's Encyclopedia of Industrial Chemistry, 7th Edition, 2005 Electronic release, pp 1-60.
2. Kirk-Othmer Encyclopedia of Chemical Technology, Hydrocarbons, C_1-C_6, pp 1-22.
3. G. Centi, F. Cavani and T. Trifirò, in Fundamental and Applied Catalysis (M. V. Twigg and M. S. Spencer, eds.), Kluwer Academic/Plenum Publishers, New York, 2001.
4. R. Stöbele, Chem. Ing. Tech., 36 (1964) 858.
5. K. Ziegler, Angew. Chem., 64 (1952) 323.
6. Kirk-Othmer Encyclopedia of Chemical Technology, Olefins, Higher, pp 709-728.
7. Gulf Res. Dev. Co., DE 1 443 927, 1961.
8. Ethyl Corp., US 3 906 053, 1975.
9. J. C. Mol, J. Mol. Catal. A: Chem., 213 (2004) 39.
10. Y. Shiraki, S. Kawanno and K. Takeuchi, US Patent 4 783 573, 1988.
11. Institut Francas de Petrole, US 4 122 110, 1978.
12. A. Lundeen, R. Poe, Encycl. Chem. Process. Des., (1977) 465.
13. J. Falbe, H. Bahrmann, W. Lipps and D. Mayer, Alcohols, Aliphatic, Ullmann's Encyclopedia of Industrial Chemistry, 7th Edition, 2005 Electronic release.
14. BASF, DE 1 269 605, 1966.
15. K. Ziegler, Justus Liebigs Ann. Chem., 629 (1960) 1.
16. C. Kohlpaintner, M. Schulte, J. Falbe, P. Lappe and J. Weber, Aldehydes, Aliphatic, Ullmann's Encyclopedia of Industrial Chemistry, 7th Edition, 2007 Electronic release, pp 1-34.
17. Kirk-Othmer Encyclopedia of Chemical Technology, Alcohols, higher aliphatic, survey, pp 1-26.
18. J. Haber, in Oxidation of hydrocarbons (G. Ertl, H. Knözinger and J. Weitkamp, eds.), Vol 5, VCH, Weinheim, 1997.
19. M. M. Bhasin, J. H. McCain, B. V. Vora, T. Imai and P. R. Pujadó, Appl. Catal. A: Gen., 221 (2001) 397.
20. S. Albonetti, F. Cavani and F. Trifirò, Catal. Rev. Sci. Eng., (1996) 414.
21. F. Cavani and F. Trifirò, Catal. Today, 36 (1997) 431.
22. F. Cavani and F. Trifirò, Chemtech., 24 (1994) 18.

23. L. M. Madeira and M. F. Portela, Catal. Rev. Sci. Eng., 44 (2002) 247.
24. P. Mars and D. W. van Krevelen, Chem. Eng. Sci. Suppl., 3 (1954) 41.
25. J. C. Vedrine, J. -M. M. Millet, J. -C. Volta, Catal. Today, 32 (1996) 115.
26. J. C. Vedrine, G. Coudurier, J. -M. M. Millet, Catal. Today, 33 (1997) 3.
27. R. J. Mikovsky, A. J. Silvestri, E. Dempsey and D. H. Olson, J. Catal., 22 (1971) 374.
28. G. Centi and T. Trifirò, Catal. Today, 3 (1988)a 155.
29. M. Skotak and Z. J. Karpiński, J. Chem. Eng., 90 (2002) 89.
30. L. D. Schmidt, E. J. Klein, C. A. Leclerc, J. J. Krummenacher and K. N. West, Chem. Eng. Sci., 58 (2003) 1037.
31. H. Frei, Science, 313 (2006) 309.
32. H. B. Friedrich, N. Govender and M. R. Mathebula, Appl. Catal. A: Gen., 297 (2006) 81.

CHAPTER TWO
INTRODUCTION TO ZEOLITES

2

2.1 Introduction

The global catalyst market is estimated to be around 15 – 20 billion US dollars annually. About fifty percent of the catalysts are required in the chemical industry with the rest divided between refinery and environmental applications. The annual combined worth of products obtained from these industrial processes was estimated to be in the multi trillion US dollar level which is three orders of magnitude higher than the amount invested in them and thus the value created from the use of catalysts greatly exceeds its production cost **[1]**.

The right choice of catalyst for the right process depends largely on the nature of the reactant, intermediates and the specific target products. Size and shape selectivity of all three of these will greatly influence the choice of catalyst. This is generally attained by utilising catalysts of nanoporous nature and in order to provide such a feature the catalyst should have uniform pores with molecular dimensions. One such catalyst that possesses these features is the zeolite **[1]**.

Zeolites are crystalline microporous materials consisting of a 3D-aluminosilicate framework where pores and channels make up the building blocks. Zeolites can be either found in nature or synthesised in a laboratory and were first discovered by the Swedish mineralogist Axel Frederick Cronstedt in 1756, who observed that a certain mineral began to bubble on strong heating. The name zeolite was coined from the Greek, zeo: to boil and lithos: stone i.e. boiling stones.

Two centuries later researchers at Union Carbide developed procedures for the first synthetic zeolites, Zeolite A, X and Y and its industrial usage. These zeolites gained entry into the refinery operations and resulted in a 30% increase in gasoline yield, thus resulting in more efficient use of petroleum feedstocks. Consequently, zeolites entered the industrial scene and gained significant industrial importance in petroleum processing.

Today, over 600 different zeolites are known with the SiO_4 and AlO_4 arranged in a number of ways to give the different zeolites and about 20 of these have been commercialised for utilisation in industrial processes. Table 2.1 contains structures and compositions of some industrially important synthetic zeolites. The worldwide consumption of synthetic zeolites is about 1.7 – 2 million metric tons per year, while for natural zeolites, the annual consumption is averaging 2.5 million metric tons. Zeolites have gained importance in various industries and have found use as ion-exchangers, adsorbents or desiccants and as catalysts in a number of important processes in the chemical and petrochemical industries. The advantage that is offered in catalysis is that the crystal structure is known and therefore can contain well defined pores in which the catalytically active sites are embedded **[1-5]**.

Table 2.1 Properties of some industrially important synthetic zeolites **[2-5]**

Name	Structure type	Window	Dimensionality of pore system	Pore aperture (nm)	SiO_2/Al_2O_3
A	LTA	8-ring	3	0.41	2.0 – 6.8
P	GIS	8-ring	3	0.31 x 0.45 0.28 x 0.48	2.0 – 5.0
ZSM-5	MFI	10-ring 10-ring	3	0.53 x 0.56 0.51 x 0.55	20 – ∞
X	FAU	12-ring	3	0.74	2.0 – 3.0
Y	FAU	12-ring	3	0.74	3.0 – 6.0
Mordenite	MOR	12-ring 8-ring	2	0.65 x 0.70 0.26 x 0.57	9.0 – 35

Table 2.1 also shows the pore dimensions of zeolites which are of the order of molecular dimensions so that only certain molecules fit into the pores. This ability to discriminate molecules endows them with size and shape selective properties **[6]**.

This shape selectivity property is illustrated in Figure 2.1.

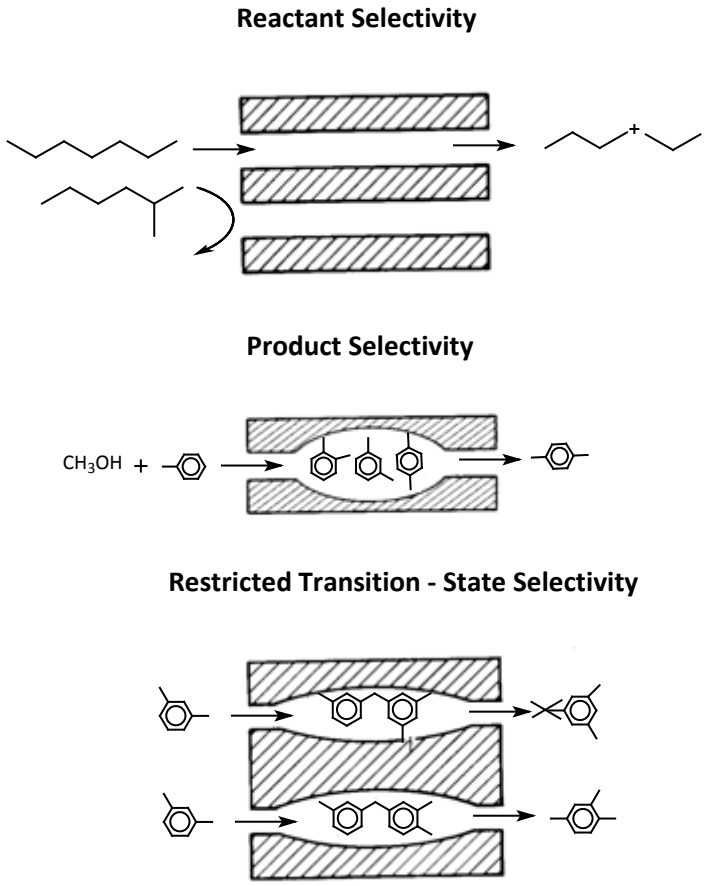

Figure 2.1 Examples of how zeolite pores affects the selectivity of reactions **[7]**

Reactant selectivity describes the phenomenon of zeolites acting as molecular sieves and excluding bulky molecules from entering the intra-crystalline void-structure while the smaller molecules enter. Product selectivity refers to the diffusivities of the reaction products formed in terms of microporous pore architecture and crystal size of the catalyst particles. Sterically

hindered products may stay much longer in the cavities, whereas the less hindered products may easily leave the microporous structure. The restricted transition state-type selectivity occurs when the spatial configuration around a transition state of a reaction intermediate situated in the intra-crystalline volume is such that only certain configurations are possible. Thus in this case, the formation of the reaction intermediates or transition states is sterically limited due to the shape and size of the microporous lattice allowing the access of the species formed to interact with the active sites **[7]**.

Considering Table 2.1, and from the point of view of catalysis, the most interesting zeolites have channel aperture rings of 8, 10 and 12 oxygen atoms rings. The table also shows the channel diameters, which range from 0.42 to 0.74 nm, which are comparable to the diameters of molecules of interest such as *n*-paraffins, isoparaffins, aromatics and their corresponding substitutes.

The adsorption capacity of the zeolite plays an important role because different molecules which enter the channels can be adsorbed differently. Factors that affect the adsorption behaviour are chain length, functional groups and molecular shape. Typically smaller molecules are able to pack more efficiently. These molecules also have access to areas in the zeolite that larger molecules find inaccessible. However, the packing of molecules in the pores depends on the architecture (dimensionality) of the zeolite. In a one dimensional zeolite, depending on the molecule size, the molecule is able to pack in a nose to tail arrangement. However, in zeolites mentioned in Table 2.1 e.g. ZSM-5 where intersecting channels occur, parts of the zeolite becomes inaccessible to long or bulky molecules **[8]**. Various studies on the adsorption of paraffins of different size on ZSM-5 have been done. Saturation adsorption capacities of $C_1 - C_{10}$ *n*-paraffins have been determined and show that adsorption capacity expressed in molecules adsorbed per unit cell decreases with carbon number with a steep drop between C_6 and C_8. The less efficient packing of C_7 and C_8 molecules could be explained by the observation that pentane and hexane have lengths less than the distance between the intersections and therefore fit nicely within the sinusoidal channel segment, while longer molecules protrude into the intersections and thus obstruct filling of adjacent sections **[8, 9]**.

The dimensions of ZSM-5, which affect the adsorption properties of ZSM-5 have made it an ideal example of a zeolite which has gained huge importance in heterogeneous catalysis, with its use industrially in the synthesis of ethylbenzene, the isomerisation of xylenes and the disproportionation of toluene **[10]**.

It is these features that make it the ideal zeolite to be studied for catalytic oxidation studies of medium chain linear paraffins i.e. *n*-hexane.

2.2 ZSM-5

2.2.1 Structure of ZSM-5

ZSM-5 is an abbreviation for Zeolite Socony-Mobil-5 who were the first to report it. ZSM-5 belongs to the pentasil group of zeolites because it is made up of ten 5-membered ring units (Figure 2.2). These units are joined together to form sheets which are linked together to form the three dimensional framework **[2]**.

The ZSM-5 unit cell comprises of 96 tetrahedral SiO_2 units that give rise to four straight channel sections and four zigzag channel intersections. The dimensions of the channels are shown in the Figure 2.2. The framework density is about 1.8 g/cm^3 and the micropore volume about 0.18 g/cm^3 **[11]**.

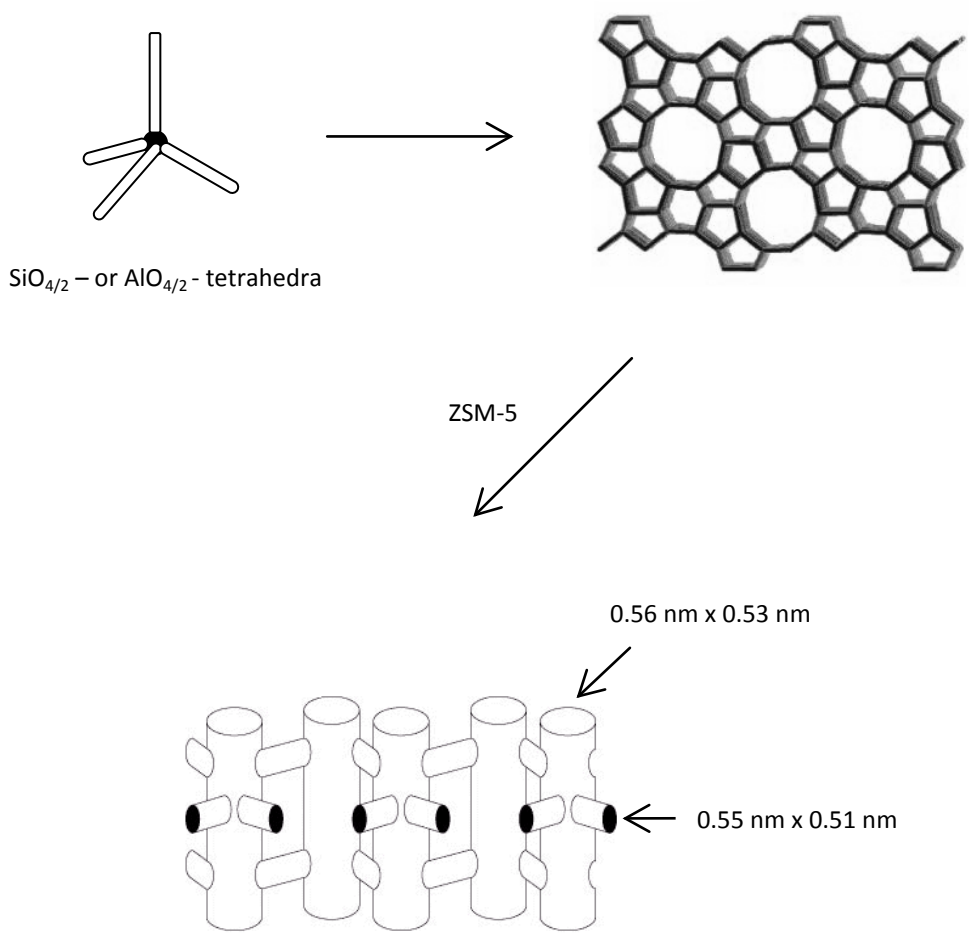

Figure 2.2 Structure of ZSM-5 zeolite showing the micropore system and dimensions **[5]**

In the ZSM-5 structure and similar zeolites, a lattice comprising of only tetrahedral Si-O is neutral (the 4^+ charge at the silicon is balanced by four oxygen atoms each with a 2^- charge, however, belonging to two tetrahedra). However, the replacement of some Si^{4+} atoms Al^{3+} causes a formal charge of 1^- on the tetrahedron which is then balanced by a proton or a metal cation forming an acid site. Therefore the structure is composed of tetrahedra of an Al^{3+} or Si^{4+} ion surrounded by four O^{2-} ions. The Al and Si atoms are generally referred to by the term "T-atoms" because of their tetrahedral coordination. The negatively charged tetrahedron is the corresponding base **[7]**. The Brønsted acid sites arise from 'bridging hydroxyl groups' within the pore structure of zeolites. The 'bridging hydroxyl groups' are usually formed either by

ammonium or polyvalent cation exchange which is followed by a calcination. The formation of the different acid sites is demonstrated in Scheme 2.1. An increase in temperature causes the protons to move and at 550°C can be lost as water molecules which results in the formation of Lewis acid sites **[7]**.

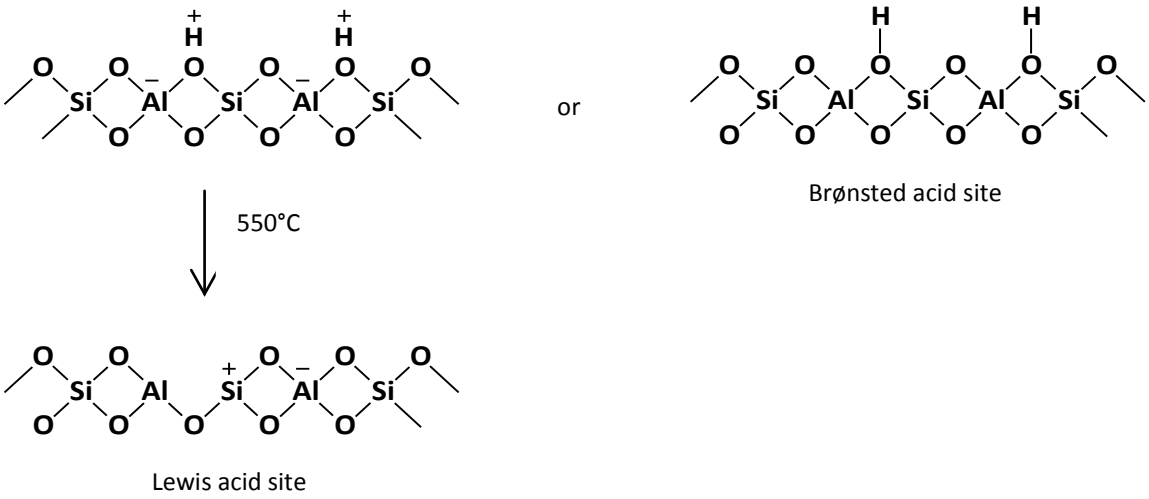

Scheme 2.1 Formation of Brønsted and Lewis sites **[7]**

This acidic property of zeolites, in particular ZSM-5, where the SiO_2/Al_2O_3 ratio can be varied from 20 to ∞, is the reason why this particular class of zeolites are generally referred to as solid acid catalysts. This acid character was the reason that these catalysts were developed for industrial applications in the fluid catalytic cracking industry **[12]**.

Catalytic cracking reaction of hydrocarbons can occur *via* three different pathways;

- classical cracking mechanism
- non-classical mechanism proposed by Haag-Dessau and
- oligomerisation cracking

The classical mechanism proceeds *via* the abstraction of hydride from a paraffin by a carbenium ion to form another carbenium ion, which cracks by scission forming an olefin. Large pore zeolites like Zeolite Y generally crack hydrocarbons *via* the classical cracking mechanism **[7]**. However, medium pore zeolites like ZSM-5 favour the non-classical Haag-Dessau mechanism. Haag and Dessau postulated that zeolites can protonate paraffins to give carbonium ions which are the transition states in cracking. The carbonium ions then decay into a paraffin and smaller carbenium ions which release protons to form the final cracking products **[13]**. This mechanism dominates at low conversions, high temperatures, low reactant pressures and with small and medium pore zeolites that have a low concentration of Brønsted acid sites. Oligomerisation cracking replaces the classical cracking mechanism at higher partial pressures. The chemistry of this mechanism is basically the same as that of the classical mechanism.

However, as aluminosilicalites, zeolites do not exhibit redox properties. The incorporation/confinement of redox metal ions in these channels and/or cavities can endow the catalyst with unique activity and properties because of strong electrostatic interactions between acidic and basic sites on the internal surface and the substrate. Fine tuning the size and hydrophobicity of the redox cavity can influence which molecules have access to the active site on the basis of their size or hydrophobicity/hydrophilic character. Therefore zeolites which contain these redox sites have an advantage over other redox catalysts in that the zeolites are able to influence the type of substrate molecules which interact with the active site **[14]**.

2.2.2 Characterisation of ZSM-5

The most important technique that is used for characterisation is X-ray diffraction (XRD). This technique is used to determine structure type and phase purity. It can be used to estimate the fraction of crystalline material in a mixture with amorphous materials in a zeolite sample by comparison with a standard material. This crystallinity is determined by comparing the intensities of reflections at $2\Theta = 27°$ **[15]**.

The elemental analysis can be done by wet chemical analyses, but physical methods such as X-ray fluorescence (XRF), atomic absorption spectrometry (AAS) and inductively coupled plasma (ICP) are preferred **[3]**.

The size of the apertures can be estimated by adsorption methods i.e. testing their accessibility to adsorptives of different kinetic diameters. Micropore volume measurements can be measured from the adsorption and desorption of nitrogen **[3]**.

The size and shape of the zeolite crystals or aggregates can be investigated by using electron microscopy **[3]**.

The nature, number and strength of the acid sites can be measured by using temperature programmed desorption of ammonia or pyridine, infrared spectroscopy (IR) in the region of OH stretching frequencies and the measurement of the catalytic activity of the zeolites in standard reactions **[3]**.

Although the SiO_2/Al_2O_3 ratio can be determined by elemental analyses, more detailed information can be obtained by high-resolution magic angle spinning-nuclear magnetic resonance (MAS-NMR) spectroscopy. Silicon (^{29}Si) and aluminium (^{27}Al) MAS-NMR spectroscopy can be used to give important information about the short range structural environment of the silicon and aluminium atoms **[3]**. ^{29}Si MAS-NMR can be used to distinguish all five possible Si(*n*Al) building units, where Si(*n*Al) represents a SiO_4 tetrahedron linked to *n*AlO_4 tetrahedra and to (4 – *n*) other SiO_4 tetrahedra. ^{27}Al MAS-NMR can be used to differentiate between tetrahedrally and octahedrally coordinated Al, even in non-crystalline material **[17]**.

Upon heating, zeolites may undergo different kinds of structural changes including: (i) cell volume contraction; (ii) displacive or reconstructive phase transformation; (iii) breaking and

formation of new bonds; (iv) negative thermal expansion; (v) structural collapse and (vi) structural breakdown. The thermal stability of zeolites is therefore an important parameter and can be determined by either XRD or differential thermal analysis (DTA) **[16]**.

2.3 Transition metal modified zeolites

Various transition metals have been used to modify zeolites **[18]**. Transition metals can be introduced into zeolites *via* various techniques; impregnation, direct synthesis, chemical vapour deposition and ion-exchange.

These methods introduce exchanged metal ions species in the cationic sites of the compound and occur as:

- bare cations coordinated exclusively to the framework oxygen atoms
- metal-oxo species coordinated to the framework and bearing extra-framework oxygen atoms
- metal oxide-like species supported in the zeolite inner volume or mostly at the outer surface of the crystals and
- metal cations positioned at framework positions (Figure 2.3) **[19]**

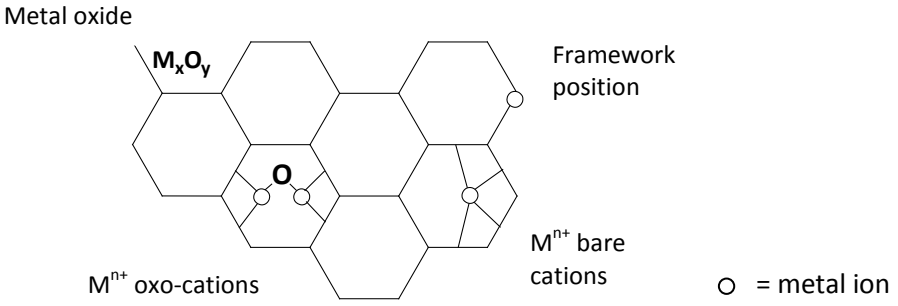

Figure 2.3 Illustraton showing the possible location of metal cation in zeolites **[19]**

2.3.1 Impregnation

This procedure requires the hydrated zeolite to be dried first then put into a warm cation solution. The mixture is then stirred for ~15 min, filtered (without washing) and then air dried. Cavani *et al*. **[20]** reported that vanadium zeolites prepared by the impregnation method showed a small decrease in sorption capacity after the preparation thus indicating that the vanadium ions probably are located inside the pores of the sample. X-ray diffraction studies of cobalt particles on ZSM-5 zeolites show that the cobalt particles contain a high concentration of basal plane stacking faults, thus suggesting that atoms of a particle lie at positions on the surface where intersection stacking faults exist **[21]**. The limitation is that other compounds are also incorporated i.e. an equivalent number of anions are also incorporated.

2.3.2 Direct synthesis

This technique involves the incorporation of the metal cation into the zeolite framework during the synthesis. The aluminium is replaced with the metal of choice at the stage of gel formation **[22, 23]**. In some cases a small amount of aluminium may be present. The metal ions may also exist in different oxidation states.

Studies in which vanadium-containing silicalites were prepared showed by ESR (electronic spin resonance) and NMR-spectroscopic data that V^{4+} or V^{5+} are not in tetrahedral positions of the silicalites. The authors speculate that the vanadium species are connected to the framework but at defect sites **[24]**. Another study reported that four different vanadium species were detected: (i) polynuclear vanadium oxide species containing reduced vanadium species, (ii) nearly octahedral vanadyl (VO^{2+}) species in the zeolitic channels, (iii) V^{5+} species in sites characterised by a nearly symmetric tetrahedral environment and (iv) after reduction a V^{4+} species in a nearly tetrahedral environment. The excess vanadium ions were found to remain as an amorphous oxide in pores or in internal positions **[25]**.

2.3.3 Chemical vapour deposition (CVD)

In this method the zeolite is first dehydrated in a vacuum within a sublimation reactor at 300°C for 1 h. The reactor valve is then closed and the reactor filled with nitrogen after which the liquid metal cation salt is added by syringe into the reactor. The zeolite and liquid are prevented from having direct contact. After the injection the reactor is evacuated and sealed to form an ampule. The ampule is cooled to -73°C during re-evacuation to prevent evaporative loss of the cation salt into the vacuum lines. The sealed ampule is then heated to 200°C for 5 h. The contents of the ampule (0.2 – 0.5 g batches) is transferred into a fritted quartz U-tube reactor and heated to 200°C in helium. The flow is then switched to a mixture of O_2 and H_2O with helium as the balance by passing a stream of O_2/He through a bubbler held at -73°C. After 2 h, the bubbler is bypassed and the reactor heated to 500°C for 1 h. Finally the samples are cooled to ambient temperatures and stored in a dry box **[26]**.

Reports using this method to prepare vanadium-containing ZSM-5 zeolite found that the CVD method leads to a stable compound. The formation of the metal oxide in this case VO_2^+ was found to proceed by the surface reaction of chloride ligands in the metal oxide salt ($VOCl_3$) with Si–OH–Al, followed by hydrolysis of residual chloride. Complete ion-exchange with Si–OH–Al can be achieved with a constant exchange stoichiometry for $V/Al \leq 1$. However, a second species begins to form with V/Al ratios above 0.5 **[26, 27]**.

2.3.4 Ion-exchange

Ion-exchange can be carried out in either the liquid phase or in a solid state reaction. Both methods lead to materials containing the metal cations on positions affiliated with the location of the Al^{3+} in the lattice.

In aqueous exchange, the zeolite is suspended in an aqueous solution of the soluble salt of the desired metal. This is performed at elevated temperatures (100°C) and under stirring. The

material is then filtered, washed until free of the salt ions and dried (100°C) **[28]**. Conventional aqueous ion-exchange is described in Equation 1 where a chloride ion is used as the dissolved salt of the ingoing cation M.

$$\mathbf{a[M(H_2O)_w]^{n+} + na\ Cl^- + bNaZ \leftrightarrow xMZ_n + (a\text{-}x)[M(H_2O)_w]^{n+}\ naCl^- + nxNa^+ + (b\text{-}z)NaZ} \qquad \mathbf{(1)}$$

where M = n-valent cation, Z = monovalent zeolite fragment and a, b, x, z = stoichiometric coefficients

The equilibrium of this reaction (Equation 1) does not lie heavily to the right, thus the partially exchanged solid and the solution has to be separated. In order to obtain a high degree of exchange this procedure needs to be repeated. This procedure has a number of limitations; due to the increase in effective size of the cations in aqueous solutions resulting from hydration, incomplete exchange or exchange only at positions close to pore openings may occur. Another limitation is when the cation in the desired valence state is unstable or insoluble in water.

These limitations are overcome when the solid state ion-exchange method is used. Here the zeolite and the compound containing the in-going cation are physically mixed and the mixture of solids is heated in an inert gas stream. This method also offers other advantages in that it does not require handling large volumes of salt solutions and avoids the problem of discarding waste salt solutions.

The solid state method may be described by Equations 2 and 3 depending on whether the starting material is a cation containing form of zeolites or a zeolite of the hydrogen form. In the case of Equation 2, equilibrium can be obtained similarly to conventional exchange. In order to obtain a high degree of exchange the solid chloride, in this case NaCl, has to be removed with washing with a small amount of solvent. If the hydrogen form of zeolite is used, continuous removal of the hydrogen halide in an inert gas stream or high vacuum can shift the equilibrium to the right resulting in 100% exchange **[29]**.

$$aMCl_n + bNaZ \leftrightarrow xMZ_n + (a-x)MCl_n + (b-nx)NaZ + nxNaCl \quad (2)$$

$$aMCl_n + bHZ \leftrightarrow xMZ_n + (a-x)MCl_n + (b-nx)HZ + nxHCl\uparrow \quad (3)$$

Co-containing zeolites (CoZSM-5 and CoY) prepared by the solid state ion-exchange procedure showed that complete exchange of all protons present can be achieved. On ZSM-5 only one proton was exchanged for each Co^{2+} cation while on faujasite two protons were exchanged with one cation. In the ZSM-5 zeolite the positions of the tetrahedrally coordinated Al^{3+} are spatially too separated. Thus only one Co^{2+} cation cannot balance the charge of two Al^{3+} cations in the zeolite lattice **[30]**. A previous study showed that ZSM-5 liquid phase ion-exchange led to an exchange of 20% of all protons but with a Co^{2+}/Al^{3+} ratio of 0.5 **[31]**.

Kucherov and Slinkin **[32]** reported on the introduction of Cr^{5+}, Mo^{5+} and V^{4+} ions in cationic positions of high-silica zeolites by the solid state reaction. The ions were found to be located in the H-ZSM-5 channels and the strong influence of O_2 adsorption on hyperfine structure of ESR spectra for Cr^{5+}, Mo^{5+} and V^{4+}confirmed the accessibility to gas phase molecules.

2.4 Applications of transition metal modified zeolites

As mentioned in Chapter One, the primary reason for the limited use of oxidation reactions is the difficulty in finding selective catalysts. A selective catalyst is supposed to perform a dual function: activate oxygen by generating oxygen species of proper reactivity and activating the paraffin to direct the oxidation in the desired way.

The presence of transition metals in the framework of a zeolite lattice can impart oxidation activity. This activity together with the shape selectivity property of the zeolite could lead to a highly active and selective catalyst. As mentioned earlier in this chapter the metal of choice needs to exhibit redox properties.

2.4.1 Transition metal modified zeolites and silicalites

Many studies show that transition metal modified zeolites or silicates can be used in oxidation reactions. The lower paraffins (ethane, propane and butane) can be converted to aromatics **[33-36]** (e.g. benzene, toluene and xylene) as well as being selectively converted to their corresponding olefins **[37-44]**. The medium to higher paraffins (hexane, heptane and octane) show a similar trend in product formation with aromatics formation, but studies also show that with certain metal ions the corresponding terminal oxygenated products can selectively be produced **[45-48]**.

There have been a few studies carried out with either modified zeolites or silicates that are able to activate the primary carbon atom of medium chained paraffins like *n*-hexane.

Reports using vanadium silicates (VS-2) with hexane and using H_2O_2 as an oxidant gave varying results. One study showed that a total terminal selectivity of 32% using VS-2 with a Si/V ratio = 58 **[47]** can be achieved, while another reported (Si/V = 78) much lower values of 11% **[45]**.

Vanadium and chromium silicates were tested in the liquid phase using TBHP (tert-butyl hydrogen peroxide) as an oxidant at 10°C. This study was one of the very few studies which reported on higher chain paraffin oxidation using vanadium containing zeolites. Both catalysts showed the same trend for substrate conversion (11%) as well as product distribution for hexane oxidation. The major products of the reaction included the corresponding ketones i.e. 2-hexanone and 3-hexanone (28.7 and 31.3%, respectively). With respect to terminal selectivity, a 4% yield was obtained to the corresponding aldehyde, whilst only a 0.1% yield was obtained to 1-hexanol **[46]**.

Recent studies on hexane oxidation were reported using Mn-exchanged zeolites prepared by the sublimation method. The effects of 8, 10 and 12 membered ring zeolites were compared. Oxidation was carried out in the liquid phase using a glass reactor and the products included

acids, alcohols, aldehydes and ketones. Initial terminal selectivity was found to reach a maximum for the 10-ring channels i.e. 24% selectivity (0.012% yield) and was found to be significantly higher than the reaction without a catalyst (8.2% selectivity) after 0.05% hexane conversion **[48]**.

2.4.2 Rationale for choice of transition metal modified zeolite for this study

As mentioned previously various transition metal ions have been used for paraffin oxidation studies and among these are Ga, Zn, V, Ti, Fe, Ni, Pt, Cu, Mn and Cr. However, of these metals, vanadium possesses certain superiority over these metals and its oxide is considered the most dominant transition metal oxide used in industrial catalytic processes. Vanadium oxide based catalysts are extensively used in a large number of catalytic processes involving selective oxidation reactions such as the conversion of butane to maleic anhydride, oxidation of *o*-xylene, 1,3 butadiene, methanol, CO, ammoxidation of hydrocarbons, selective catalytic reduction of NO and the partial oxidation of methane **[49-53]** and is the most important metal used in metal oxide catalysis **[54]**. An extensive open literature search in the period 1967 – 2000 showed that more than 28% of all papers published on supported metal oxide catalysis were on catalysts containing vanadium. This is twice the amount of the second most important metal, titanium **[53]**. However, titanium silicates were found to activate secondary and tertiary carbon atoms in paraffins, but are inactive in the oxidation of the primary C–H bonds **[55-59]**.

Supports like MgO, TiO_2, ZrO_2, Al_2O_3 and SiO_2 have been used to disperse vanadium over the surfaces **[60, 61]** and recently work in this laboratory reported on two studies using catalyst systems containing vanadium located on a support **[62-64]**. These studies showed promising results for the oxidative dehydrogenation of higher chain paraffins. The success of the various studies in our group and in many other research groups with the use of vanadium incorporated catalysts had led us to investigate the use of vanadium exchanged zeolites for the activation of a paraffin.

2.4.3 Silanisation

Zeolites have both an external and internal surface. ZSM-5 in particular is well known for its channel system, which has an important bearing on the shape selectivity properties. The term 'shape selectivity' implies that zeolites process only those molecules that have full access to their interior surface, as the exterior is considered to lack the structural definition **[6, 65]**. Smaller aromatic molecules that form in the channels of ZSM-5 can easily diffuse out and result in polyaromatic compounds, which could block access to the internal channels when coke formation on the external surface becomes predominant. This coverage of the external surface is the main cause of deactivation of H-ZSM-5 **[66, 67**. Inertisation or elimination of the external surface could therefore perhaps create a catalyst that only imparted shape selectivity.

The effects of depositing silica in the form of tetramethylorthosilicate ($Si(OCH_3)_4$) on HZSM-5 have been investigated by Hibino *et al.* **[68]** in an attempt to produce *para*-xylene selectively in alkylation and disproportion reactions. The results of the study showed that reactions carried out over the silicon deposited H-ZSM-5 (Si-HZSM-5) selectively produced more of the *para*-isomer. The enhancement of *para*-selectivity in the methylation of toluene using modified H-ZSM-5 with silicon compounds by the chemical vapour deposition (CVD) method was investigated by Kim and co-workers **[69].** Both studies found that deposited silica reduced the pore opening size and deactivated acid sites on the external surface, but the former was found to be the reason for high *para*-selectivity.

Further investigations into different methods of deposition were probed by Weber and co-workers **[70-72]**. The procedures investigated were chemical vapour deposition in a static vacuum system, a vapour phase flow system and chemical liquid deposition. A uniform coverage could be obtained by reducing the rate of deposition by using diluents at low temperatures (liquid deposition) or by reduction of contact times of tetraethylorthosilicate (TEOS) at relative high temperatures (vapour deposition). The authors also found that TEOS deposition occurs rapidly on zeolites with higher Al content due to the adsorption of water which catalyses the reaction. The adsorbed species resulting from TEOS deposition or diluents may occupy the pore opening. This consequently reduces the extent to which pore mouth

blocking occurs, and to obtain a more complete coverage, cyclic TEOS deposition should be used.

Further studies have been done on the use of different methods to eliminate the surface acidity and also into the kinetic rates and diffusion limitations **[73-77]**. The general conclusions from these studies reveal that the elimination of the exterior acidity by deposition of alkosilanes causes some pore narrowing and results in an increase in shape selectivity for zeolites.

2.5 Objectives of this study

The work presented in this dissertation was driven by the scarcity of literature on the activation of *n*-hexane using vanadium modified zeolites ZSM-5, especially in gas phase reactions.

The presented study was focused on;

- conversion of a medium chain feedstock i.e. *n*-hexane to more valuable products
- the design and construction of the reactor system required for catalytic testing
- the preparation of a catalyst using the solid state ion-exchange method, which is novel in its use in the oxidation of *n*-hexane
- characterisation of the prepared catalyst
- blank reactor testing under oxidative and non-oxidative conditions to ascertain the contribution of homogeneous gas phase reactions
- testing of precursor zeolites to determine the role of acidity in zeolite ZSM-5 catalysts
- catalytic testing of vanadium exchanged ZSM-5 zeolite by examining the effect of:
    - temperature
    - contact time
    - fuel-air ratio and

  - an increase of vanadium loading on Na-ZSM-5 on the formation of C_6 terminal products
- the possibility of regenerating Na-V-ZSM-5 and
- to establish if silanisation of the catalyst exterior surface is possible and if it can be used to enhance shape selectivity

2.6 References

1. B. Yilmaz and U. Müller, Top. Catal., 52 (2009) 888.
2. I. Chorkendorff and J. W. Niemantsverdriet, Concepts of modern catalysis and kinetics, Wiley-VCH, Weinheim, 2003, pp 199-205.
3. E. Roland and P. Kleinschmit, Zeolites, Ullmann's Encyclopaedia of Industrial Chemistry, 7th Edition, 2005 Electronic release, pp 1-31.
4. Kirk-Othmer Encyclopaedia of Chemical Technology, Vol 5, pp 200-245.
5. J. Weitkamp, Solid State Ionics, 131 (2000) 175.
6. P. B. Weis and V. J. Frilette, J. Phys. Chem., 64 (1960) 382.
7. M. Stöcker, Microporous and Mesoporous Mater., 82 (2005) 257.
8. K. M. A. De Meyer, S. Chempath, J. F. M. Denayer, J. A. Martens, R. Q. Snurr and G. V. Baron, J. Phys. Chem. B., 107 (2003) 10760.
9. J. F. M. Denayer, I. Daems and G. V. Baron, Oil and Gas Sci. Tech. -Rev. IFP, 61 (2006) 561.
10. H. Sato, Catal. Rev. -Sci. Eng., 39 (1997) 395.
11. B. Millot, A. Méthivier, H. Jobic, H. Moueddeb and J. A. Dalmon, Microporous and Mesoporous Mater., 38 (2000) 85.
12. Kirk-Othmer Encyclopaedia of Chemical Technology, Vol 11, pp 678-699.
13. W. O. Haag, R. M. Dessau, in: Proceedings of the 8th International Congress on Catalysis, DECHEMA, Frankfurt, 1984, 305.
14. R. A. Sheldon, 3rd World Congress on oxidation catalysis, R. K. Grasselli, S.T. Oyama, A. M. Goffrey and J. E. Lyons (eds), (1997) 151.
15. T. A. J. Hardenberg, L. Merten, P. Mesman, H. C. Muller, C. P. Nicolaides, Zeolites, 12 (1992) 685.
16. J. M. Thomas and W. J. Thomas, Principles and practice of heterogeneous catalysis, Wiley-VCH, Weinheim, 1997, pp 207-208.
17. G. Cruciani, J. Phys. Chem. Solids, 67 (2006) 1973.
18. W. M. H. Sachtler and Z. Zhang, Adv. in Catal., 39 (1993) 129.
19. B. Wichtelová, Z. Sobalik and J. Dědeček, Appl. Catal. B: Environ., 41 (2003) 97.
20. F. Cavani, F. Trifirò, P. Jirů, K. Habersberger and Z. Tvarůžková, Zeolites, 8 (1989) 12.
21. A. G. Dhere, R. J. De Angelis and P. J. Reucroft, J. Mol. Catal., 20 (1983) 301.

22. T. Inui, D. Medhanavyn, P. Praserthdam, K. Fukuda, T. Ukawa, A. Sakamoto and A. Miyamoto, Appl. Catal., 18 (1985) 311.
23. J. A. Rossin, C. Saldarriaga and M. E. Davis, Zeolites, 7 (1987) 295.
24. M. S. Rigutto, H. van Bekkum, Appl. Catal., 68 (1991) L1.
25. G. Centi, S. Perathoner, F. Trifiró, A. Aboukais, C. F. Aïssi and M. Guelton, J. Phys. Chem., 96 (1992) 2617.
26. H. S. Lacheen and E. Iglesia, J. Phys Chem. B., 110 (2006) 5462.
27. B. I. Whittington and J. R. Anderson, J. Phys. Chem., 95 (1991) 3306.
28. J. N. Armor, Stud. Sur. Sci. Catal., 92 (1994) 51.
29. H. G. Karge, Stud. Surf. Sci. Catal., 105 (1997) 1901.
30. A. Jentys, A. Lugstein and H. Vinek, J. Chem. Soc., Faraday Trans., 93 (1997) 4091.
31. A. Jentys, A. Lugstein, O. El-Dusouqui, H. Vinek, M. Englisch and J. A. Lercher, Stud. Surf. Sci. Catal., 100 (1995) 525.
32. A. V. Kucherov and A. A. Slinkin, Zeolites, 7 (1987) 38.
33. G. Centi and G. Golinelli, J. Catal., 115 (1989) 452.
34. Y. Ono, Catal. Rev. -Sci. Eng., 34 (1992) 179.
35. W. Schuster, J. P. M. Niederer and W. F. Hoelderich, Appl. Catal A; Gen., 209 (2001) 131.
36. K. Novoveská, R. Bulánek and B. Wichterlová, Catal. Today, 100 (2005) 315.
37. L. W. Zatorski, G. Centi, J. L. Nieto, F. Trifirò, G. Bellussi and V. Fattore, Zeolites: Facts, Figures, Future, (P. A. Jacobs and R. A. van Santen, eds.), Elsevier Science Publishers, Amsterdam, 1989, pp 1243-1252.
38. Y. -F. Chang, G. A. Somorjai and H. Heinemann, Appl. Catal. A: Gen., 96 (1993) 305.
39. Y. -F. Chang, G. A. Somorjai and H. Heinemann, J. Catal., 154 (1995) 24.
40. G. Centi and F. Trifirò, Appl. Catal. A: Gen., 143 (1996) 3.
41. K. Nowińska, A Waclaw and A. Izbińska, Appl. Catal. A: Gen., 243 (2003) 225.
42. A. Held, J. Kowalska and K. Nowińska, Appl. Catal. B: Environ., 64 (2006) 201.
43. G. J. Buckles and G. J. Hutchings, J. Catal., 151 (1995) 33.
44. R. Bulánek and K. Novoveská, Polish J. Chem., 78 (2004) 149.
45. P. R. Hari Prasad Rao and A. V. Ramaswamy, J. Chem. Soc., Chem. Commun., (1992) 1245.
46. A. P Singh and T. Selvam, J. Mol. Catal. A: Chem., 113 (1996) 489.

47. T. Tatsumi, Y. Watanabe, Y. Hirasawa and J. Tsuchiya, Res. Chem. Intermed., 24 (1998) 529.
48. B. -Z. Zhan, B. Modén, J. Dakka, J. G. Santiesteban and E. Iglesia, J. Catal., 245 (2007) 316.
49. I. E. Wachs and B. M. Weckhuysen, Appl. Catal. A: Gen., 157 (1997) 67.
50. F. Cavani and F. Trifirò, 3rd World congress on Oxidation Catalysis, Stud. Sur. Sci. Catal., (R. K. Grasselli, S.T. Oyama, A. M. Goffrey and J. E. Lyons, eds), 110 (1997) 19.
51. G. Deo, I. E. Wachs and J. Haber, Crit. Rev. Surf. Chem., 4 (1994) 141.
52. G. Bond and S. Flamerz Tahir, Appl. Catal., 71 (1991) 1.
53. E. A. Mamedov and V. Cortés Corberán, Appl. Catal. A: Gen., 127 (1995) 1.
54. B. M. Weckhuysen and D. E. Keller, Catal. Today, 78 (2003) 25.
55. T. Tatsumi, M. Nakamura, S. Negishi and H. Tominaga, J. Chem. Soc., Chem. Commun., (1990) 476.
56. D. R. C. Huybrechts, L. D. Bruyeker and P. A. Jacobs, Nature, 345 (1990) 240.
57. J. S. Reddy, S. Sivasanker and P. Ratnasamy, J. Mol. Catal., 70 (1991) 335.
58. D. R. C. Huybrechts, P. L. Buskens and P. A. Jacobs, J. Mol. Catal., 71 (1992) 129.
59. M. G. Clerici, Appl. Catal., 68 (1991) 249.
60. N. Steinfeldt, D. Müller and H. Berndt, Appl. Catal. A: Gen., 272 (2004) 201.
61. A. Khodakov, B. olthof, A. T. Bell and E. Iglesia, J. Catal., 181 (1999) 205.
62. E. A. Elkhalifa and H. B. Friedrich, Appl. Catal. A: Gen., 373 (2010) 122.
63. H. B. Friedrich and A. S. Mohamed, Appl. Catal. A: Gen., 347 (2008) 11.
64. N. Govender, H. B. Friedrich and M. J. van Vuuren, Catal. Today, 97 (2004) 315.
65. B. Smit and T. L. M. Maesen, Nature, 451 (2008) 671.
66. P. Magnoux, P. Cartraud, S. Mignard and M. Guisnet, J. Catal., 106 (1987) 242.
67. H. Schulz, Z. Siwei and W. Baumgartner, Stud. Surf. Sci. Catal., 34 (1987) 466.
68. T. Hibino, M. Niwa and Y. Murakami, J. Catal., 128 (1991) 551.
69. J. -H. Kim, A. Ishida, M. Okajima and M. Niwa, J. Catal., 161 (1996) 387.
70. R. W. Weber, H. P. Röger, K. P Möller and C. T. O' Connor, 12th International Zeolite conference, (1999) 2015.
71. R. W. Weber, K. P Möller, M. Unger and C. T. O' Connor, Microporous and Mesoporous Mater., 23 (1998) 179.
72. R. W. Weber, K. P Möller and C. T. O' Connor, Microporous and Mesoporous Mater., 35-36 (2000) 533.

73. H. P. Röger, K. P Möller, W. Böhringer and C. T. O' Connor, Stud. Surf. Sci. Catal., 130 (2000) 2909.
74. W. L. Duncan and K. P Möller, Adsorption, 11 (2005) 259.
75. H. Manstein, K. P Möller, W. Böhringer and C. T. O' Connor, Microporous and Mesoporous Mater., 51 (2002) 35.
76. A. Zampieri, A. Dubbe, W. Schweiger, A. Avhale and R. Moos, Microporous and Mesoporous Mater., 111 (2008) 530.
77. L. Mokrzycki, B. Sulikowski and Z. Olejniczak, Catal. Lett., 127 (2009) 296.

CHAPTER THREE
EXPERIMENTAL

3

3.1 Reactor Design

The reactor set up that was used in the catalytic testing is illustrated in Figure 3.1. The actual set up is given in Appendix A, A1.

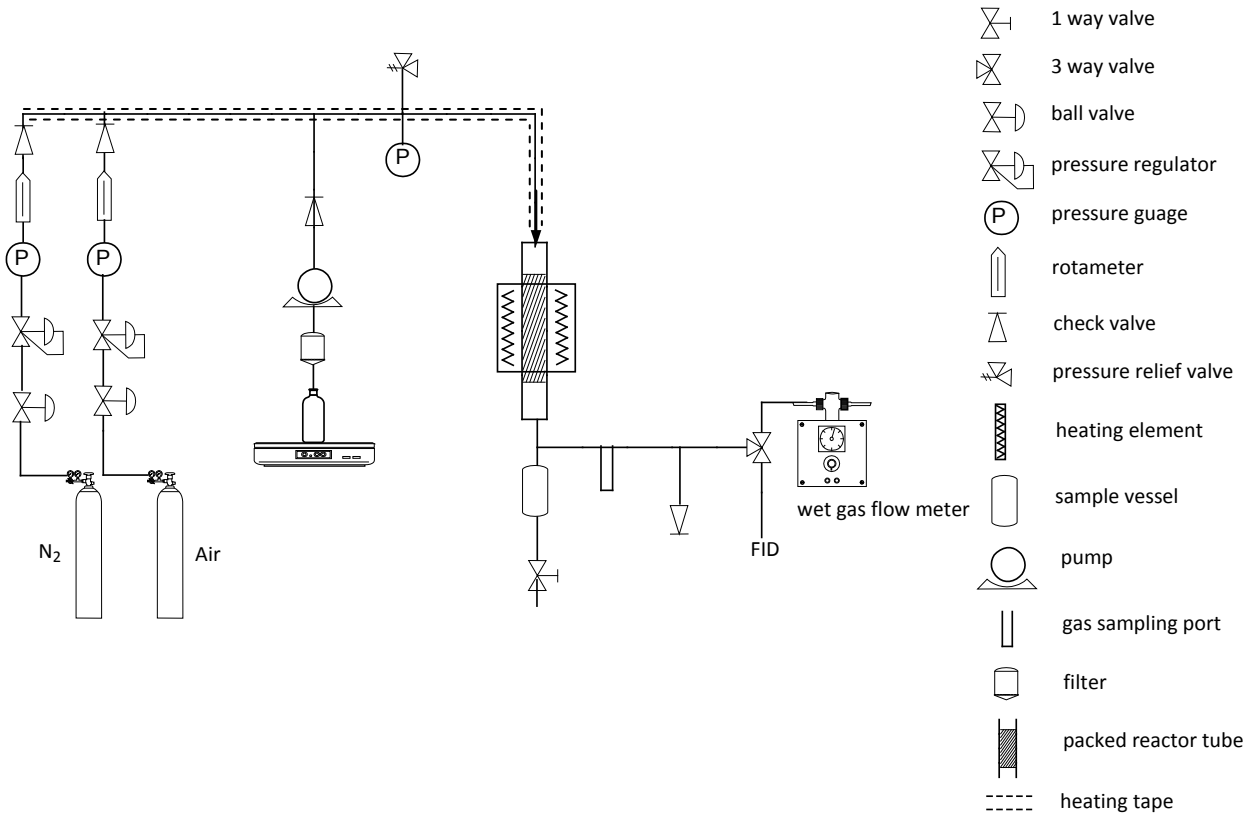

Figure 3.1 Reactor design

All copper and stainless tubing that was used for construction of the reactor set-up were obtained from East Coast Instruments (Durban, South Africa) and the fittings used were

purchased from Johannesburg Valve and fitting. Part names and codes are given in parentheses.

Copper tubing (¼ inch) was used for all gas delivery sections of the reactor preceding the heating tape. Air and nitrogen was fed into the system by means of gas cylinders supplied by Afrox. These were controlled using regulators specific to each gas (air or nitrogen multi stage gas regulators, Afrox). The flow of gases into the system was controlled by a ball valve (B-42S4, Swagelok) which was followed by mini regulators (¼ inch N_2 regulators, East coast Instrumentation) which were set at 100 kPa. The exact flow entering the system was controlled using rotameters specific to either gas (¼ inch stainless steel air or nitrogen rotameters (0-285 mL/min), East Coast Instrumentation). To prevent the back flow of gases at the end of each line a non-return check valve (B-4C-1/3, Swagelok) was fitted. At this stage stainless steel tubing was used. The feed hexane entered the system through $^{1}/_{16}$ inch stainless tubing with the aid of a HPLC pump (Lab Alliance Series II Isocratic pump, Anatech Instruments (PTY) Limited). The amount that entered was monitored using a top loading balance (Ohaus Adventurer electronic balance model Arc 120, Polychem Supplies c.c). A reducing union (SS-400-6-1, Swagelok) was fitted to the system to enable the change to ¼ inch tubing. Again a non-return check valve (SS-CHS4-1, Swagelok) was fitted in order to prevent a back flow of the feed. At a specific point the gas and the feed lines meet, with the aid of a tee-piece (SS-400-3, Swagelok), which facilitates mixing prior to entering the reactor tube. After the check valves on the gas and the feed lines, heating tape (400 watt, 240 volts, Darton Supplies) was placed in order to vaporise the feed. The heating tape was set to 180°C. Prior to entering the reactor tube a stainless steel union cross (SS-400-4, Swagelok) was attached to the line with a pressure relief valve (SS-4CPA2-3, Swagelok) and a pressure gauge (63 mm dial stainless steel pressure gauge-bottom entry, East Coast Instrumentation) was attached. This pressure relief valve was used for safety and monitor back pressure build-up in the system. The valve was set to 70 kPa.

The reactor tube for all experiments consisted of a stainless tube with ½ inch outer diameter and 30 cm length. The reactor tube was fitted with stainless steel reducing unions (SS-810-6-4) at the inlet and outlet. The reactor block/heating units (316 stainless steel heating unit with 6 cartridges of 230 volts and 250 watts, AMM Industries c.c.) supplied the system with the

required heat. The heating unit was 11 cm in length. Temperature control units were used to regulate temperature and K-type thermocouples were used to monitor the temperature. (Model: T99-400DMK9C-3 m PVC H110-K, H120-K, H140, Temperature Controls (Pty) Ltd) was placed into the block in order to get the required temperatures. A sliding thermocouple (Model: T99-450BK9C-3 m PVC H110-K, H120-K, H140, Temperature Controls (Pty) Ltd) was placed in a holder inside the reactor tube to monitor the internal temperature of the tube. The sliding thermocouple was made of $^{1}/_{16}$ inch tubing whilst the holder was made of ⅛ inch tubing, which was welded shut at the outlet.

Preceding the reactor tube, a stainless steel sample cylinder (304L-HDF4-150, Swagelok) set at 5°C was fitted to condense the gas products. The exit of the sample cylinder was fitted with a needle valve (SS-14DKM4, Swagelok) to collect the reaction products. These products were injected into a gas chromatograph using a 0.5 µL liquid syringe (0.5BNR-5/0.47-RA6, SGE).

The products which did not condense into the liquid phase were lead through ¼ inch stainless tubing which was attached to a stainless tee-piece (SS-400-3, Swagelok), fitted with a septum in order to withdraw a sample volume with a 1 mL gas tight syringe (1mdr-gt, SGE) to inject into the TCD equipped gas chromatograph. After the tee-piece, the ¼ inch stainless tubing led to a three-way ball valve (SS-83XKS4, Swagelok). The valve facilitated entry either to the gas chromatograph (FID) or to the wet gas flow meter (TG 1 Model 5, Poly-Test Instruments c.c.).

3.1.1 The reactor tube and catalyst packing

The reactor tube as mentioned above was made of stainless tubing of ½ inch outer diameter and 30 cm length. The catalyst was always packed in the hottest region of the reactor tube. In order to determine the hottest region the reactor tube was packed with carborundum (24 gritt, Promark Chemicals). First the thermocouple was tightened on to the reactor tube and glass wool was added. A known amount of carborundum was added to the whole tube and glass wool was used as a stopper. The heating unit was switched on and set at a specific temperature. The sliding thermocouple was moved at 1 cm intervals along the reactor tube

until the hottest region was determined. For the catalyst packing a similar procedure was followed. First the thermocouple fitting was added to the tube, then the glass wool and carborundum. The procedure deviated in that carborundum was only added until the hottest region of the tube. Glass wool was used to stopper the carborundum and a fixed volume of catalyst was added to the reactor tube. Again glass wool was added now to stopper the catalyst. After the glass wool glass beads (3 mm Soda-glass, Promark Chemicals) were added till the exit of the tube and glass wool was used as a stopper. An illustration of a packed reactor tube and the actual reactor tube used in this study can be seen in Appendix A, A1.

Prior to catalytic testing, the reactor tube was subjected to leak tests by first pressurising the reactor to 70 kPa with nitrogen. At the completion of an experiment the reactor tube was unpacked, washed with warm soap water, soaked in oxalic acid and again washed in warm water.

3.1.2 Gas chromatographs

Reaction products were analysed either using a Perkin Elmer Autosystem XL Gas chromatograph fitted with a CP-Sil 5CB (25 m x 0.15 mm x 0.2 µm) column equipped with a flame-ionization detector or a Perkin Elmer Clarus 600 fitted with a Fused Silica Carboxen 1006 porous layer plot column (30 m x 0.53 mm) equipped with a thermal conductivity detector. The gaseous organic sample entering the FID was analysed online using the sampling valve system, whilst the gaseous sample that entered the TCD was manually injected using a gas-tight syringe. All liquid samples were also manually injected. Product identification was performed by gas chromatography – mass spectroscopy on a Perkin Elmer Clarus 500 gas chromatograph coupled with a Clarus 560s mass spectrometer. The gas chromatograph was fitted with a CP-Sil 5CB (25 m x 0.15 mm x 0.2 µm) column.

3.2 Product quantification and analysis

The flow rate of feed that entered the reactor system was controlled by using a HPLC pump. The amount that entered for a given run time was calculated by difference and was determined using a weighing balance. The amount of gas (nitrogen and air) that entered the system was controlled by rotameters. The total amount of gas exiting the system was monitored using the wet gas flow meter.

The products that are formed during the catalytic testing can either exist in the vapour or liquid phase. The products from the vapour phase are analysed using a gas chromatograph equipped either a FID or a TCD detector. Products that are in the liquid phase were analysed using a gas chromatograph equipped with a FID detector.

The amount of each component in the injection volume was related to the total run time by using the total off-gas flow volume. Carbon dioxide and carbon monoxide that was obtained from the vapour phase was quantified using calibration curves. The calibration curves were obtained from injecting different volumes of a standard mixture of CO and CO_2 of known concentration and a graph of peak area versus number of moles was obtained. The organic components that were obtained in the vapour phase were determined by firstly obtaining a methane constant. The methane constant is obtained by dividing the response factor (R_f) of 1 given to methane by the volume of methane injected of known concentration. This value is used to calculate the quantity of ethane, ethene, propane, propene, butane and butene. The quantities of the other organic compounds are calculated using response factors.

The liquid phase contained in some cases both an organic layer and an aqueous layer. These were separated and analysed separately. The organic layer was injected into the GC and quantification was obtained using response factors. The aqueous layer was also injected in the FID and any organic products found in this layer were quantified using response factors. The amount of water present in each layer was obtained using a Karl Fischer titrator (KF Titrino

Plus, Metrohm). This value was then used to calculate, by difference, the mass of the organic portion of each liquid phase.

The values from the vapour and liquid phase were combined and used to calculate conversion, selectivity and yield. The total percent of carbon for each run was 100% and only a deviation of ± 5% was allowed. At each temperature four sequential runs were taken and only results obtained with a relative standard deviation of one was used. When time on-stream experiments were performed the experiments were repeated and again only results obtained with a relative standard deviation of one were used. The following equations show how each of the values were calculated:

$$\textbf{Conversion} = \left(1 - \frac{\textbf{moles of unreacted Hexane}}{\textbf{moles of hexane fed}}\right) \times 100\%$$

$$\textbf{Selectivity} = \left(\frac{\textbf{moles of specific product}}{\textbf{total moles of products}}\right) \times 100\%$$

$$\textbf{Yield} = (\textbf{Conversion} \times \textbf{Selectivity})$$

A sample calculation is shown in Appendix A, A3. For the sake of simplicity only a few products have been shown.

3.3 Catalyst synthesis and characterisation

Three precursor zeolites were examined; H-ZSM-5 with SiO_2/Al_2O_3 of 100 and 320 and Na-ZSM-5 with SiO_2/Al_2O_3 of 100. After initial reactor testing of the three precursor zeolites (Chapter Five, Section 5.2) only the precursor Na-ZSM-5 was exchanged with vanadium using the solid state ion-exchange method.

3.3.1 Synthesis of the solid state ion-exchanged Na-V-ZSM-5

Ten grams of Na-ZSM-5 (Süd Chemie, South Africa) was physically mixed in a mortar and pestle with 0.83 g of $VOSO_4.5H_2O$ (equimolar ratio of vanadium to aluminium). The mixture was then packed in a quartz tube and placed in the furnace under a nitrogen atmosphere for 24 hours. Thereafter the temperature was increased from room temperature to 500°C at 1.6°C/min. The compound was left at 500°C for 12 hours and thereafter cooled to room temperature. After cooling, the catalyst was washed with copious amounts of deionised water to remove the extraneous ions formed during synthesis, filtered and dried in the oven at 120°C overnight. Catalysts with different vanadium loadings were also prepared by varying the amount of $VOSO_4.5H_2O$ added **[1]**.

Prior to catalytic testing, the powdered catalysts were pelletized and sieved to a particle size of 300 μm to 500 μm.

3.3.2 Silanisation procedure

The deposition procedure was carried out in the liquid phase and achieved by first drying 2.5 g of the catalyst at 70°C for 3 h. Two approaches for the modification were used: (a) TEOS (20 mL) was added to the catalyst and this mixture was then stirred at room temperature for either 24, 48 and 36 hours and (b) a 5% volume mixture of TEOS in *n*-hexane was added to the catalyst and the mixture stirred at room temperature for 24 hours. The samples was subsequently washed with H_2O and dried at 100°C and thereafter calcined at 500°C **[2, 3]**.

3.3.3 Structural and chemical characterization of precursors and Na-V-ZSM-5

3.3.3.1 Inductively coupled plasma-optical emission spectroscopy (ICP-OES)

Catalyst dissolution was performed using 1 mL of water and thereafter adding 4 mL of hydrofluoric acid to 0.4 g of sample. Multi element standards were prepared and the elemental content was obtained by means of a Perkin Elmer, Optima 5300 DV ICP-OES **[4]**.

3.3.3.2 Fourier transform infrared (FT-IR) spectroscopy

Fourier transform infrared spectroscopy was obtained using attenuated total reflectance on a Perkin Elmer Spectrum 100.

3.3.3.3 X-ray diffraction (XRD)

Powder X-ray diffraction analysis was obtained on a Philips PW1050 diffractometer using monochromated Co Kα radiation, from 2^{o} to 90^{o} 2Θ with a scanning steps of 0.02^{o} at 1^{o} per minute. The diffraction data were captured by a Sietronics 122D automated micro-processor attached to the X-ray diffractometer.

3.3.3.4 Braunauer Emmet Teller (BET surface area) and porosity measurements

Nitrogen–BET surface area and porosity measurements were performed using a Micromeretics Gemini 2375 instrument. Before the measurements, samples weighing from 0.03 to 0.05 g were degassed from room temperature to 200°C at 1°C/min overnight. The surface area measurements were performed at a temperature of -196°C **[5-6]**.

3.3.3.5 Ammonia - temperature programmed desorption (NH_3-TPD)

The NH_3-TPD measurements were performed using a Micromeretics AutoChem II 2920 which incorporates a TCD detector. These measurements were carried out in a U-shaped quartz tube and heated from 25 – 900°C. The sample was then cooled to 120°C and a mixture of 4% NH_3 in helium was adsorbed. The NH_3-TPD of the samples was carried out by increasing the temperature linearly from 80 to 500°C with a heating rate of 10°C/min and a helium flow rate of 10 ml/min **[7]**.

3.3.3.6 Hydrogen - temperature programmed reduction (H_2-TPR)

The H_2-TPR measurements were performed using a Micromeretics AutoChem II 2920 which incorporates a TCD detector. These measurements were carried out in a U-shaped quartz tube. Prior to reduction the catalyst was preheated from 25 – 900°C under a stream of argon for 1 hour. The sample was then cooled under the stream of argon to 200°C. In the TPR measurements a mixture of 5% H_2 in argon was used as a reducing agent at a flow rate of 10 ml/min with a heating rate of 10°C/min **[8]**. In order to do quantitative analysis a calibration curve was established by passing hydrogen in argon with different hydrogen concentrations. The standard gas calibration method/experiment pertaining to the instrument was used. This calibration method is then affiliated to the TPR experiment being performed which allows the peak areas in the TPR experiment to be converted from arbitrary units to mL of hydrogen at standard temperature and pressure.

3.3.3.7 ^{27}Al and ^{29}Si magic angle spinning-nuclear magnetic resonance (MAS-NMR)

^{27}Al and ^{29}Si magic angle spinning nuclear magnetic resonance spectra were obtained using a Bruker Aviance 600 MHz. The samples were packed in a 4 mm zirconia rotor and 1024 scans were recorded at the spinning speed of 12 kHz **[6, 9]**.

3.3.3.8 Thermogravimetric analysis (TGA) and differential scanning calorimetry (DSC)

TGA and DSC analysis was performed on the samples under air atmosphere using the Thermal Analyser SDT Q600 analyzer. The temperature was increased from room temperature i.e. ~25°C to 900°C at a ramp rate of 10°C/min **[10]**.

3.3.3.9 Scanning electron microscopy (SEM)

Samples were mounted on an aluminium stub using double sided carbon tape and were subsequently coated with Au-Pd sputter coat using a Bio-Rad E5200 Auto sputter coater. The coated samples were then analysed using a Zeiss ULTRA 55 FEGSEM. The instrument has a field emission tungsten hairpin filament with a ZrO reserve, as an electron source.

3.3.4 Chemicals and reagents

The *n*-hexane used as the feed during catalytic testing was of ≥99.0% purity and acquired from Fluka. The gas chromatograph standards used to determine response factors were obtained from Sigma-Aldrich and were also of high purity.

All zeolites prior to exchange were obtained from Süd Chemie, Richards Bay. The vanadium source for the synthesis was vanadyl sulphate hydrate (Aldrich, 99.99%). The tetraethylorthosilicate that was used in the silanisation procedure was obtained from Fluka (≥99.0%).

For ICP-OES all standards were 1000 ppm and obtained from Polychem Supplies. Hydrofluoric acid (40%) was obtained from Riedel-de-Haën and used for digestion of the precursors and catalysts.

3.4 References

1. H. G. Karge, Stud. Surf. Sci. Catal., 105 (1997) 1901.
2. R. W. Weber, K. P Möller, M. Unger and C. T. O' Connor, Microporous and Mesoporous Mater., 23 (1998) 179.
3. R. W. Weber, K. P Möller and C. T. O' Connor, Microporous and Mesoporous Mater., 35-36 (2000) 533.
4. Method of ICP analysis, Süd Chemie, South Africa.
5. M. Volpe, G. Tonetto and H. de Lasa, Appl. Catal. A: Gen., 272 (2004) 69.
6. B. –Z. Zhan, B. Modén, J. Dakka, J. G. Santiesteban and E. Iglesia, J. Catal., 245 (2007) 316.
7. L. Rodríguez-González, F. Hermes, M. Bertmer, E. Rodríguez-Castellón, A. Jiménez-López and U. Simon, Appl. Catal. A: Gen., 328 (2007) 174.
8. A. A. Lemonidou, L. Nalbandian and I. A. Vasalos, Catal. Today, 61 (2000) 333.
9. H. S. Lacheen and E. Iglesia, J. Phys Chem. B., 110 (2006) 5462.
10. A. R. Pradhan, J. F. Wu, S. J. Jong, T. C. Tsai and S. B. Liu, Appl. Catal. A: Gen., 165 (1997) 489.

CHAPTER FOUR
CHARACTERISATION OF CATALYSTS

4

Catalyst characterisation is an important step in trying to understand the catalytic reactions that occur. Two different forms of ZSM-5 were investigated before the exchange procedure i.e. H-ZSM-5 (SiO_2/Al_2O_3 ratio = 100 and 320) and Na-ZSM-5 (SiO_2/Al_2O_3 ratio = 100) which were obtained from Süd-Chemie, South Africa. These zeolites although technically considered to be catalysts have been referred to throughout the text as precursor zeolites. These investigations led to the exchange of Na-ZSM-5 with the desired metal i.e. vanadium as outlined in the solid state ion-exchange procedure in Chapter Three, Section 3.3.1. The structure of the precursors and the structural modifications that took place prior to the exchange and after the exchange were examined using a combination of techniques and are described in this chapter. Lastly the vanadium exchanged zeolite underwent the silanisation procedure as described in Chapter Three, Section 3.3.2. This catalyst was also characterised and the results are also described in latter part of this chapter.

4.1 Precursor zeolites and vanadium exchanged catalysts

4.1.1 Inductively coupled plasma-optical emission spectroscopy (ICP-OES)

The precursors and vanadium exchanged zeolites were initially characterised by elemental analysis. As explained above only the Na-ZSM-5 was exchanged with vanadium. Table 4.1 shows the composition of the different compounds. The values obtained for the precursors match the data provided by the zeolite manufacturer.

The results also show that the exchange process was successful. After the exchange process the amount of sodium ions present in the catalyst was found to be lower. This implies that the vanadium ions replace the sodium ions and are in positions that were associated with the

sodium ions prior to exchange. Therefore the ions can be either on the external surface of the zeolite crystals or diffused inside its channels. Conceptually two sodium ions from the Si-OH-Al groups of the zeolite can be exchanged with one VO^{2+} species **[1]**. Thus complete exchange should be achieved at a VO^{2+}/Al^{3+} ratio of 0.5. However, complete Na^{+} exchange was only achieved at VO^{2+}/Al^{3+} ratios exceeding unity. Attempts to achieve a higher percentage of vanadium incorporation were unsuccessful and thus a 2.5 % loading of vanadium was the highest.

Table 4.1 Composition of precursors and vanadium exchanged zeolites

Sample	VO^{2+}/Al exchange ratio	Na (wt%)	Si (wt%)	Al (wt%)	V (wt%)	Si/Al
H-ZSM-5 (100)	-	-	48.5	0.99	-	50
H-ZSM-5 (320)	-	-	48.1	0.3	-	160
Na-ZSM-5 (100)	-	1.3	47.3	0.95	-	50
Na-V-ZSM-5	0.5	0.3	48.2	0.97	0.36	50
Na-V-ZSM-5	1.0	0.2	47.5	0.95	0.89	50
Na-V-ZSM-5	2.0	0.1	48.1	0.96	1.95	50
Na-V-ZSM-5	excess[a]	-	47.4	0.93	2.48	50

[a] all higher ratios that were attempted (mass of $VOSO_4.5H_2O$ from 2 – 6 g) yielded the same % of vanadium

Henceforth the precursors and catalysts shall be coded (in parentheses) according to the SiO_2/Al_2O_3 ratio or differentiated based on the percent vanadium exchanged, respectively.

4.1.2 Fourier transform infrared (FT-IR) spectroscopy

Infrared spectroscopy was used to gather information regarding the functional groups present in the compounds. The IR spectra of the three precursors were found to be similar to each other (Figure 4.1) and matched those obtained in literature for ZSM-5 zeolite **[2, 3]**. The framework absorption region in the 400 – 1400 cm^{-1} range shows the characteristic bands of

ZSM-5 zeolite **[2, 3].** The bands at 1221, 543 and 435 cm^{-1} confirm the presence of a 5-membered ring of the ZSM-5 zeolite **[3-5]**.

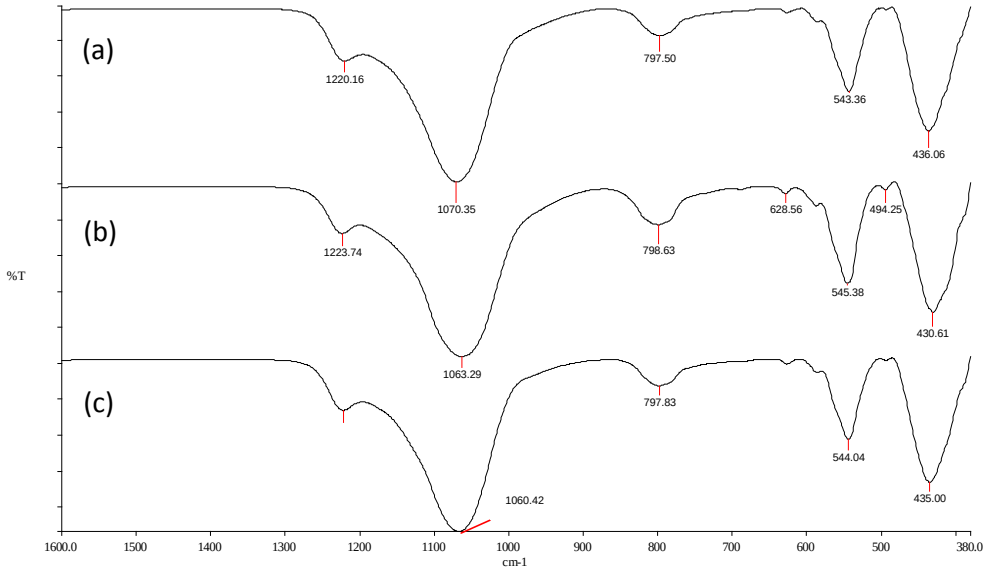

Figure 4.1 Infrared spectra of (a) H-ZSM-5 (100), (b) H-ZSM-5 (320) and (c) Na-ZSM-5 (100)

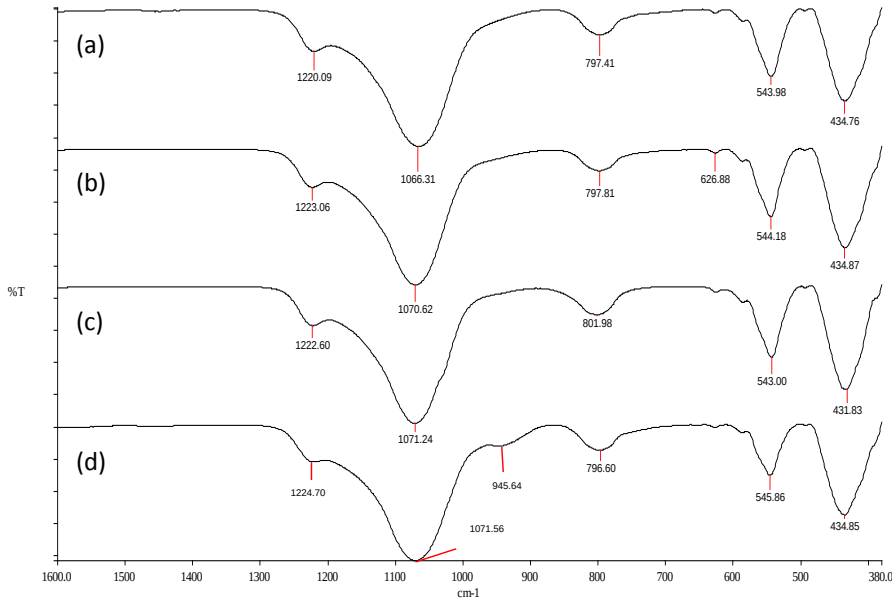

Figure 4.2 Infrared spectra of (a) Na-V-ZSM-5 (0.4%), (b) Na-V-ZSM-5 (0.9%), (c) Na-V-ZSM-5 (2.0%) and (d) Na-V-ZSM-5 (2.5%)

The band at 1220 cm^{-1} is assigned to the v_a(Si–O–SI) external asymmetric stretching, whilst the internal asymmetric stretching is found at 1070 cm^{-1}. The external symmetric stretching, v_s(Si–O–Si) is represented by the band at 790 cm^{-1} **[2]**.

The IR spectra of the vanadium exchanged zeolites are similar to that of the Na-ZSM-5 precursor (Figure 4.2). The characteristic bands associated with the zeolite structure are seen, but the IR band of the V=O stretching frequency at ~945 cm^{-1} is only seen upon introduction of the higher metal content (2.5% loading) **[6]**. The low loadings of vanadium present in the other catalysts are probably masked by the stronger absorption bands due to the precursor zeolite.

4.1.3 X-ray diffraction (XRD)

X-ray diffraction was used to determine the structure of the zeolite as well as the phase purity of the zeolite. The diffractogram shown in Appendix A, A4 shows that all the precursors were highly crystalline and the typical diffraction peaks at 2Θ = 26 – 28° can be seen.

The powder patterns after the exchange showed that all materials were highly crystalline and matched that of the precursor Na-ZSM-5 zeolite (Appendix A, A5). The results indicate that the framework of the Na-ZSM-5 was still retained and the absence of bulk phases in the XRD patterns implies that vanadium oxides are present in a nanocrystalline state or as small crystallites **[7]**. The relative crystallinity of the samples can be calculated using the sum of the intensities of the three major peaks in the region of 26 – 28 °2Θ **[8]**. It is calculated with the assumption that the parent zeolite, in this case Na-ZSM-5, is 100% crystalline. Table 4.2 shows that the relative crystallinity of the 2.0% loaded zeolite is slightly lower but with the 2.5% vanadium loading it decreased significantly. This indicates that for the lower loadings the vanadium species are well dispersed through the zeolite structure. The decrease in crystallinity observed for the 2.0% and 2.5% vanadium loaded zeolite could suggest the possibility of formation of metal oxide clusters which might locate outside the micropores of ZSM-5 zeolite.

Table 4.2 Relative crystallinities of the vanadium exchanged zeolites

Sample	Relative crystallinity (%)
Na-ZSM-5	100
Na-V-ZSM-5 (0.4%)	98
Na-V-ZSM-5 (0.9%)	97
Na-V-ZSM-5 (2.0%)	92
Na-V-ZSM-5 (2.5%)	77

There is a general consensus in literature that at low vanadium loadings vanadium oxide can remain as a highly dispersed monolayer **[9, 10]**. However, an increase in vanadium loading can result in (i) VO_x species forming chains of V-O-V **[10]**, (ii) the formation of $V_2O_4^{2+}$ dimers or (iii) polymeric VO_x clusters at external surfaces **[11]**. The ICP analysis for the catalysts at the higher loadings showed a decrease in sodium ions. The sodium ions can therefore play a role in determining the dispersion of the vanadium species and at the higher loadings lead to the formation of binuclear or multinuclear moieties bridging adjacent aluminium atoms. A similar phenomenon was noted by De Cola *et al.* in studies using ZSM-5 zeolites **[12]**.

4.1.4 Braunauer Emmet Teller (BET) surface area and porosity measurements

Adsorption and porosity characteristics of the parent and for the vanadium exchanged zeolites derived from nitrogen adsorption-desorption isotherms are given in Table 4.3. All precursor compounds were found to have high surface areas due to their porosity. The H-ZSM-5 (100) was found to have a higher surface area and pore volume than that of the Na-ZSM-5 with the same SiO_2/Al_2O_3. This is proposed to be because H^+ and Na^+ cations differ in ionic radius and therefore the pores are obstructed by Na^+ ions **[13]**.

Table 4.3 BET surface area measurements and porosity

Sample	BET (m^2/g)	V_T (cm^3/g)[a]	V_μ (cm^3/g)[b]
H-ZSM-5 (100)	408	0.67	0.26
H-ZSM-5 (320)	381	0.30	0.09
Na-ZSM-5 (100)	361	0.58	0.12
Na-V-ZSM-5 (0.4%)	381	0.69	0.13
Na-V-ZSM-5 (0.9%)	373	0.62	0.13
Na-V-ZSM-5 (2.0%)	369	0.64	0.12
Na-V-ZSM-5 (2.5%)	342	0.55	0.10

[a] V_T = Total pore volume
[b] V_μ = micropore volume

The total surface area and micropore volumes for the vanadium exchanged zeolites in Table 4.3 show that the lower vanadium loadings do not cause any significant change, suggesting that no pore blocking or plugging occurred as a result of the ion-exchange treatment **[14]**. These are also consistent with the above-mentioned result that the XRD crystallinity is almost the same as that of the precursor for the 0.5 and 0.9% vanadium loading. However, the surface area and pore volumes decrease at the highest loading of 2.5%, indicating a textural alteration which can be induced by the presence of oxide aggregates that partially block both the pore inside or at the entrance of channels of the zeolite **[7]**. These were consistent with the findings from XRD where the crystallinity was found to decrease for this catalyst.

4.1.5 Ammonia-temperature programmed desorption (NH_3-TPD)

The temperature programmed desorption of ammonia, NH_3-TPD, is one of the most commonly used methods for measuring surface acidity of zeolites. Two clear peaks were found by NH_3-TPD (Appendix A, A6 and A7). The first peak is labelled as the low temperature peak (*l*-peak) and is found between 140 and 280°C and is attributed to the desorption of weakly bound ammonia **[15-17]**. However, the concentration of these sites was reported to be of no catalytic importance **[18]**. The second peak is the high temperature peak (*h*-peak) and is found

in the temperature region between 260 and 440°C and it is usually attributed to the ammonia desorption from the Brønsted acid sites **[15, 16]**.

The amount of ammonia desorbed from the precursors and catalysts and the maximum temperature of desorption are summarised in Table 4.4.

Table 4.4 Quantitative analysis of acid sites using NH_3-TPD

	NH_3 desorption (°C)		**NH_3 desorbed (µmol/g)**	
Sample	***l*-peak**	***h*-peak**	***l*-peak**	***h*-peak**
H-ZSM-5 (100)	204	**413**	272.7	**462.6**
H-ZSM-5 (320)	172	**367**	86.9	**84.6**
Na-ZSM-5 (100)	216 & 240	-	517.4	-
Na-V-ZSM-5 (0.4%)	198	**387**	376.6	**89.9**
Na-V-ZSM-5 (0.9%)	195	**385**	161.7	**101.1**
Na-V-ZSM-5 (2.0%)	193	**383**	251.1	**110.6**
Na-V-ZSM-5 (2.5%)	196	**391**	119.3	**122.5**

As expected H-ZSM-5 (100) exhibits the highest concentration of the high temperature acid sites i.e. Brønsted acidity, as it is a well known fact the number and strength of acid sites is related to the amount of aluminium ions present in ZSM-5 zeolites. Also noteworthy among the H-form of the ZSM-5 zeolite is the shift of the peak position towards higher temperatures with the higher aluminium content. This shift is reported to not be an intrinsic one, but one that originates from the non-equilibrium phenomenon between adsorption and desorption of ammonia **[19]**. No high temperature peak is seen for the Na-ZSM-5, since most of the strong acid sites are neutralised by the alkaline ion. However, two merged peaks (Appendix A, A6) in the low temperature region are seen. The peak at 216°C possibly corresponds to the physisorbed ammonia or weakly bound ammonia and the second peak at 240°C also corresponds to the presence of very weak acidity, presumably originating from the Lewis

acidity on the Na^+ cation **[19]**. The exchange of the Na^+ ions with VO^{2+} ions results in an increase in acidity with the complete removal of all the Na^+ ions resulting in the highest acidity of 122.5 µmol/g.

4.1.6 Hydrogen-temperature programmed reduction (H_2-TPR)

H_2-TPR measurements were used to probe the reducibility of the catalysts but may also give information about the nature of the vanadium species. The TPR profiles of the catalysts are presented in Appendix A, A8. No H_2 was consumed in the presence of the precursors only, confirming that these are not reducible under these conditions. The TPR patterns of all catalysts consist of one peak with maximum in the range 560 – 620°C. The catalyst with the highest vanadium loading i.e. 2.5% showed a shift in the temperature of maximum H_2 consumption (T_{max}) to a lower value of 566°C. This decrease corresponds to a similar effect reported in literature and is ascribed to the very good dispersion of V species on the support which facilitates the reduction. It was also reported that the addition of alkali species to vanadium based mixed oxides hinders the reducibility **[20]**. This was found not to be case in this study as shown in Table 4.5. The reducibility was found to be similar in all catalysts. The TPR profile (Appendix A, A8) of the catalyst with the 2.5% loading showed the only asymmetrical reduction peak, which a literature report suggests to be surface 'bulk-like' vanadium species **[21]**.

Table 4.5 Results of H_2-TPR for vanadium exchanged zeolites

Sample	T_{max} (°C)	V (µmol/g)	H_2 consumed (µmol/g)	Degree of reducibility (%)	Average oxidation state of V
Na-V-ZSM-5 (0.4%)	614	78.5	46.8	60	2.8
Na-V-ZSM-5 (0.9%)	614	177.0	111.0	63	2.7
Na-V-ZSM-5 (2.0%)	615	389.0	233.0	60	2.8
Na-V-ZSM-5 (2.5%)	569	487.0	301.0	61	2.8

The presence of a single peak indicates that the reduction of vanadium dispersed on the zeolite proceeds *via* one step **[20]**. This is confirmed by the percent reducibility calculated as shown in Table 4.5. Even though quantification of TPR profiles does not give direct information about the V oxidation states, it can provide useful information. The average oxidation state for all catalysts was found to be similar. The vanadium species i.e. VO^{2+} has been exchanged with the sodium ions of the catalyst and therefore the average oxidation states were calculated based on the assumption that the initial oxidation state of the vanadium species is V^{4+}.

4.1.7 ^{27}Al and ^{29}Si magic angle spinning-nuclear magnetic resonance (MAS-NMR)

MAS-NMR was investigated to differentiate between the different chemical environments of the Si and Al species as described in Chapter Two, Section 2.2.2. The spectra of ^{29}Si and ^{27}Al MAS-NMR are presented in Figures 4.3 and 4.4 and are characteristic of the ZSM-5 zeolite structure. Figure 4.3 shows the ^{27}Al MAS-NMR of the precursors and the catalysts. The ^{27}Al spectra in all cases displayed a main peak at ~60 ppm and a weak peak at ~4 ppm corresponding to tetrahedral Al species within zeolite frameworks and octahedral non-framework Al species respectively **[7, 11, 22]**. According to findings **[18, 23]** the latter does not contribute to the acidity. In the case of the 2.5% loaded zeolite (Figure 4.3 (g)) the intensity of the peak at ~60 ppm decreased but the resonance signal at ~4 ppm sharply increased. This suggests that the VO^{2+} species distorted the coordination environments of the framework Al species and some of them might become NMR invisible due to their lower symmetry **[7, 24]**. It could also imply that with the higher loading more VO^{2+} species interacted with the framework Al species **[7]**.

The ^{29}Si MAS-NMR spectra (Figure 4.4) show a broad asymmetrical peak which are due to unequivalent SiO_4 tetrahedra in the ZSM-5 structure **[11, 22]**. In all cases the major peak is at –109 ppm with marked shoulders at –101 ppm and –111 ppm (Figure 4.3). The peaks at –109 and –111 ppm are assigned to Si (0Al) atoms, whilst the peak at –101 ppm is assigned to Si (1Al) atoms **[11, 22]**.

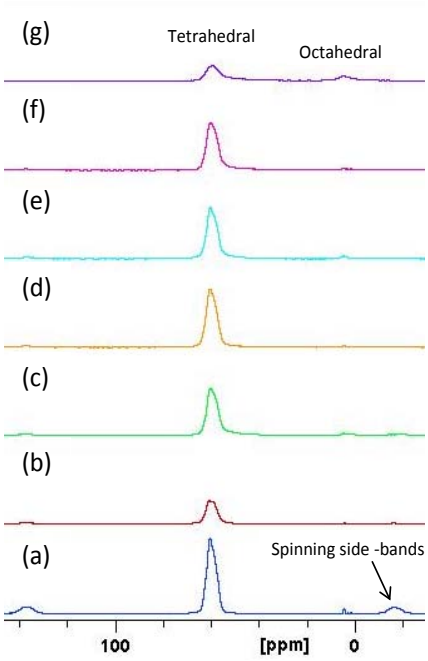

Figure 4.3 ^{27}Al MAS-NMR spectra of (a) H-ZSM-5 (100), (b) H-ZSM-5 (320), (c) Na-ZSM-5 (100), (d) Na-V-ZSM-5 (0.4%), (e) Na-V-ZSM-5 (0.9%), (f) Na-V-ZSM-5 (2.0%) and (g) Na-ZSM-5 (2.5%)

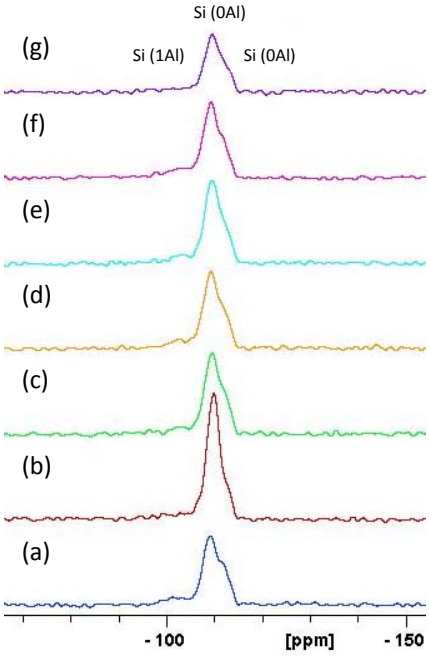

Figure 4.4 ^{29}Si MAS-NMR spectra of (a) H-ZSM-5 (100), (b) H-ZSM-5 (320), (c) Na-ZSM-5 (100), (d) Na-V-ZSM-5 (0.4%), (e) Na-V-ZSM-5 (0.9%), (f) Na-V-ZSM-5 (2.0%) and (g) Na-ZSM-5 (2.5%)

4.1.8 Thermogravimetric analysis (TGA) and differential scanning calorimetry (DSC)

Thermogravimetric analysis was performed in order to determine the stability of the precursors and catalysts and as shown in latter chapters, to determine the result of deactivation of the catalysts. The TGA–DSC curves are given in Appendix A, A9 and the calculated percentage losses are shown in Table 4.6 below.

Table 4.6 Weight loss (%) associated with the precursors and vanadium exchanged zeolites

	Weight loss (%)	
Sample	**Region A (25 – 350°C)**	**Region B (350 – 750°C)**
H-ZSM-5 (100)	8.9	0.45
H-ZSM-5 (320)	4.3	0.2
Na-ZSM-5 (100)	7.5	0.19
Na-V-ZSM-5 (0.4%)	7.0	0.65
Na-V-ZSM-5 (0.9%)	6.8	0.43
Na-V-ZSM-5 (2.0%)	6.8	0.61
Na-V-ZSM-5 (2.5%)	5.8	1.4

The weight loss curve was divided into two different regions, but both weight losses can be attributed to molecular water. Water can be present as either an intracrystalline fluid or as surface water and very weakly bound onto the surface of the compounds. It is well known that even at high temperatures water can be continuously removed from the zeolite species, however, it can be seen that the majority of water can be removed at 350°C. The weight loss for the H-ZSM-5 (100) is greater than that of the H-ZSM-5 (320) and Na-ZSM-5 (100) (Table 4.6). This is expected as zeolites with higher Si/Al ratios and sodium zeolites are known to be more hydrophobic. The Na-ZSM-5 (100) weight loss is similar to those of the vanadium exchanged zeolites. The DSC curve also shows that in the precursor the first weight loss is an endothermic process, whereas in the catalyst both weight losses are endothermic. This suggests that the water molecules are adsorbed on the surface of the precursors and catalysts.

The second endothermic peak is also for the removal of water species, as an increase in water content could have resulted from the exchange process. It is widely accepted that the thermal stability increases as the Si/Al ratio increases, as more energy is required to break the Si-O bond compared to the Al–O bond **[25]**. Zeolites' thermal stability have been taken as the temperature of the first exothermal peak on the DSC curve, however, it has been reported that some zeolites do not show this exothermal peak associated upon amorphisation and therefore parallel X-ray data is needed **[25]**. The DSC curves of the precursors and catalysts do not show this decomposition curve. However, the catalytic tests were carried out at temperatures well below 750°C and therefore determination of the point of zeolite structure collapse was not required.

4.1.9 Scanning electron microscopy (SEM)

Scanning electron microscopy can be used to gather information on the surface morphology of the compound. SEM images of the precursor zeolite i.e. Na-ZSM-5 and those of the vanadium exchanged can be found in Appendix A, A10. The images show irregularly shaped particles and no change in morphology was seen from the zeolite precursor and the vanadium exchanged zeolite. The images of both the precursor zeolite and the vanadium exchanged zeolites reflect morphologies of very crystalline zeolite materials **[26]**.

4.2 Silanised catalyst

The modification was attempted using the chemical liquid deposition method as outlined in Chapter Three, Section 3.3.2. After each modification, ICP analysis was performed and the percent silicon in each sample measured. Only in the sample that was mixed with TEOS and left to stir for 36 hours was there in change in percent composition of the sample. The characterisation of this catalyst is shown below, as is a comparison to the parent catalyst that was characterised above in Section 4.1. Therefore some of the results discussed above for the Na-V-ZSM-5 (0.9%) shall be repeated in the text below.

4.2.1 Inductively coupled plasma-optical emission spectroscopy (ICP-OES)

The compositions of the parent and silanised Na-V-ZSM-5 are shown in Table 4.7. The Si/Al ratios increased, confirming that a small amount of silicon was deposited on the sample during modification. Also there was a decrease in the V/Al ratio content which could imply that some of the vanadium species were removed during the deposition procedure. These results indicate that the silanisation process was successful but has altered the chemical composition of the catalyst.

Table 4.7 Composition of silanised Na-V-ZSM-5 and Na-V-ZSM-5 (0.9%)

Sample	Na (wt%)	Si (wt%)	Al (wt%)	V (wt%)	Si/Al
Na-V-ZSM-5 (0.9%)	0.2	47.5	0.95	0.89	50
Silanised Na-V-ZSM-5	0.1	49.5	0.60	0.40	83

4.2.2 Fourier transform infrared (FT-IR) spectroscopy

Figure 4.5 shows the unsilanised and silanised Na-V-ZSM-5 spectra. The spectra are similar to each other and the characteristic bands associated with ZSM-5 zeolite are seen and no new shoulder or peak was observed.

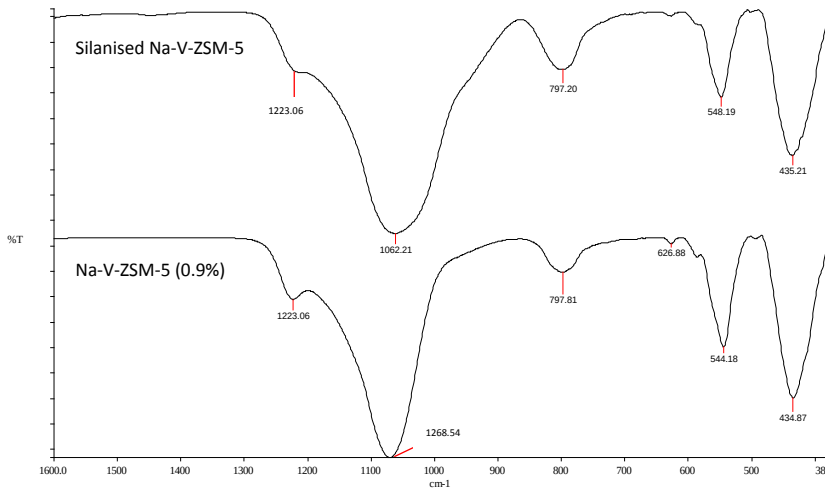

Figure 4.5 Infrared spectra of the silanised Na-V-ZSM-5 and Na-V-ZSM-5 (0.9%)

4.2.3 X-ray diffraction (XRD)

The diffractogram of the silanised catalyst can be found in Appendix A, A11. The pattern matched that of the unsilanised Na-V-ZSM-5 (0.9%) shown in Appendix A, A5 (b). Again the typical diffraction peaks at 2Θ = 26 – 28° can be seen. The relative crystallinity of the samples was calculated **[8].** However, in this case it was calculated with the assumption that the parent catalyst is Na-ZSM-5 (0.9%). Table 4.8 shows that the relative crystallinity of the silanised catalyst has decreased drastically.

Table 4.8 Relative crystallinity of the silanised Na-V-ZSM-5

Sample	Relative crystallinity (%)
Na-V-ZSM-5 (0.9%)	100
Silanised Na-V-ZSM-5	39

This severe decrease in crystallinity could imply the possibility of silicon oxide clusters deposited on the surface of the catalyst, as well as outside the micropores, and that the silanisation process has not only chemical altered the catalyst but structurally as well. These results are inconsistent with those reported in literature **[27, 28]**. The authors only observed significant decreases in the relative crystallinity values for mordenite and beta samples modified in liquid phase and vapour phase flow systems.

4.2.4 Braunauer Emmet Teller (BET) surface area and porosity measurements

The BET surface area and porosity measurements are presented in Table 4.9. The results show a decrease in surface area and pore volumes, thus implying some pore blocking and plugging has occurred. These results confirmed the findings from the XRD analysis. The micropore volumes is slightly lower than that of the parent catalyst, which could possibly mean that the oxide aggregates block the entrance of the channels of the zeolite rather than plug the inside of the pore.

Table 4.9 BET surface area and porosity measurements of silanised Na-V-ZSM-5

Sample	BET (m^2/g)	V_T (cm^3/g)[a]	V_μ (cm^3/g)[b]
Na-V-ZSM-5 (0.9%)	373	0.62	0.13
Silanised Na-V-ZSM-5	62	0.06	0.09

[a] V_T = Total pore volume
[b] V_μ = micropore volume

4.2.5 Ammonia-temperature programmed desorption (NH_3-TPD)

Temperature programmed desorption was used to probe the acidity of the silanised catalyst. The profile for the silanised catalyst is shown in Appendix A, A12, whilst the table below compares the results of the parent and silanised catalyst. Again two types of acid sites are seen and the quantitative analyses of these peaks are given in Table 4.10. The results obtained

from inductively coupled plasma spectroscopy (ICP) and the strength and numbers of the acid sites measured are in good agreement indicating the strong mutual consistency previously seen of these results. These are also in good agreement with literature where it was reported that samples modified by chemical liquid deposition showed a slight decrease in acidity **[27, 28]**.

Table 4.10 Quantitative analysis of acid sites using NH_3-TPD for silanised Na-V-ZSM-5

	NH_3 desorption (°C)		**NH_3 desorbed (µmol/g)**	
Sample	***l*-peak**	***h*-peak**	***l*-peak**	***h*-peak**
Na-V-ZSM-5 (0.9%)	195	385	161.7	**101.1**
Silanised Na-V-ZSM-5	202	386	68	**76**

4.2.6 Hydrogen-temperature programmed reduction (H_2-TPR)

Temperature programmed reduction was used to determine the degree of reducibility of silanised catalyst. The H_2-TPR profile (Appendix A, A13) shows two peaks as opposed to the single peak seen in the Appendix A, A8 (b) in the unsilanised material. This implies that two types of reductions are occurring and possibly reduction from some surface oxide like species (Table 4.11).

Table 4.11 Results of H_2-TPR of silanised Na-V-ZSM-5

Sample	**T_{max} (°C)**	**V (µmol)**	**H_2 consumed (µmol)**	**Degree of reducibility (%)**	**Average oxidation state of V**
Na-V-ZSM-5 (0.9%)	614	5.56	3.51	63	2.7
Silanised Na-V-ZSM-5	575	5.44	2.27	41	2.8
	666	5.44	0.26	4	3.1

4.2.7 ^{27}Al and ^{29}Si magic angle spinning-nuclear magnetic resonance (MAS-NMR)

The MAS-NMR spectra of the Al and Si species of the silanised catalyst and the unsilanised catalyst are shown in Figures 4.6 and 4.7 and are similar to that obtained for ZSM-5. The ^{27}Al spectrum for the silanised catalyst is of lower intensity than that of the parent catalyst. This is expected as the ICP results showed that the aluminium content decreased. The ^{29}Si spectrum of the silanised catalyst is similar to that of the parent catalyst, but does show that the there is a slight modification of the framework which is consistent with the increase in silicon species as noted from ICP analysis.

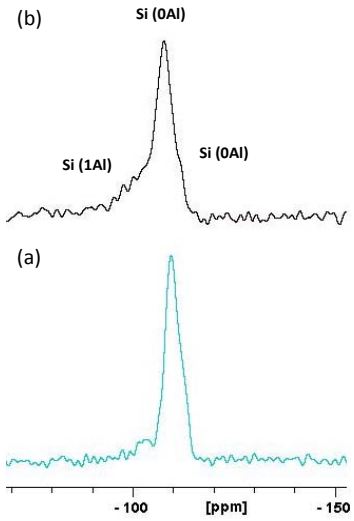

Figure 4.6 ^{27}Al MAS-NMR spectra of (a) silanised Na-V-ZSM-5 and (b) Na-V-ZSM-5 (0.9%)

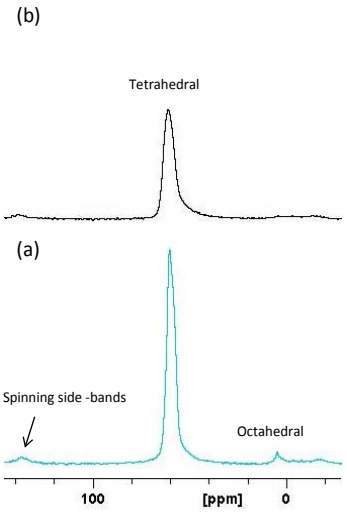

Figure 4.7 ^{29}Si MAS-NMR spectra of (a) silanised Na-V-ZSM-5 and (b) Na-V-ZSM-5 (0.9%)

4.2.8 Thermogravimetric analysis (TGA) and differential scanning calorimetry (DSC)

The TGA and DSC curves of the silanised catalyst are given in Appendix A, A14 and the percent weight loss in Table 4.12 below.

Table 4.12 Weight loss (%) associated with silanised Na-V-ZSM-5 and Na-V-ZSM-5 (0.9%)

	Weight loss (%)	
Sample	**Region A (25 – 350°C)**	**Region B (350 – 750°C)**
Na-V-ZSM-5 (0.9%)	6.8	0.43
Silanised Na-V-ZSM-5	6.2	1.1

Again both weight losses can be attributed to the loss of water adsorbed on the catalyst surface. The percent loss for the silanised and parent catalyst does not show any significant difference. Again the DSC curves show that both weight losses are endothermic processes.

4.2.9 Scanning electron microscopy (SEM)

The SEM image of the silanised catalyst can be seen in Appendix A, A15. The morphology of the catalyst when compared to the Na-V-ZSM-5 (0.9%) seems to indicate that the crystallinity has decreased. This evidence correlates with the results of the XRD analysis which showed a severe decrease in relative crystallinity for the silanised catalyst.

4.3 References

1. A. Jentys, A. Lugstein and H. Vinek, J. Chem. Soc., Faraday Trans., 93 (1997) 4091.
2. F. J. van der Gaag, J. C. Hansen and H. van Bekkum, Zeolites, 4 (1984) 369.
3. F. Cavani, F. Trifiro, P. Jirû, K. Habersberger and Z. Tvaržková, Zeolites, 8 (1988) 12.
4. M. S. Rigutto and H. van Bekkum, Appl. Catal., 68 (1991) L1G.
5. L. W. Zatorski, G. Centi, J. L. Nieto, F. Trifiro, G. Bellussi and V. Fattore, Zeolites, (1989) 1243.
6. I. E. Wachs, Catal. Today, 27 (1996) 437.
7. M. Mhamdi, A. Ghorbel and G. Delahay, Catal. Today, 142 (2009) 239.
8. T. A. J. Hardenberg, L. Merten, P. Mesman, H. C. Muller, C. P. Nicolaides, Zeolites, 12 (1992) 685.
9. A. A. Lemonidou, L. Nalbandian, I. A. Vasalos, Catal. Today, 61 (2000) 333.
10. B. Grzybowska-Świerkosz, Appl. Catal.: Gen., 157 (1997) 409.
11. H. S. Lacheen and E. Iglesia, J. Phys Chem. B., 110 (2006) 5462.
12. P. L. De Cola, R. Gläser and J. Weitkamp, Appl. Catal.: Gen., 306 (2006) 85.
13. R. H. Petrucci and W. S. Harwood, General chemistry, principles and modern applications, 7th Ed, Prentice hall, New Jersey, 1997.
14. Y. -F. Chang, G. A. Somorjai and H. Heinemann, J. Catal., 154 (1995) 24.
15. A. Held, J. Kowalska and K. Nowińska, Appl. Catal. B: Environ., 64 (2006) 201.
16. L. W. Zatorski, G. Centi, J. L. Nieto, F. Trifirò, G. Bellussi and V. Fattore, Zeolites: Facts, Figures, Future, (P. A. Jacobs and R. A. van Santen, eds.), Elsevier Science Publishers, Amsterdam, 1989, pp 1243-1252.
17. R. R. Pinto, P. Borges, M. A. N. D. A. Lemos, F. Lemos, J. C. Vedrine, E. G. Derouane, F. R. Ribeiro, Appl. Catal. A: Gen., 284 (2005) 39.
18. L. Rodríguez-González, F. Hermes, M. Bertmer, E. Rodríguez-Castellón, A. Jiménez-López and U. Simon, Appl. Catal. A: Gen., 328 (2007) 174.
19. H. Sato, Catal. Rev. – Sci. Eng., 39 (1997) 395.
20. A. A. Lemonidou, L. Nalbandian and I. A. Vasalos, Catal. Today, 61 (2000) 333.
21. H. Berndt, A. Martin, A. Brükner, E. Schreier, D. Müller, H. Kosslick, G. –U. Wolf and B. Lücke, J. Catal, 191 (2000) 384.
22. J. Komorek, T. Romotowski, E. M. Serwicka and V. M. Mastikhin, Zeolites, 14 (1994) 629.

23. K. S. Triantafyllidis, L. Nalbandia, P. N. Trikalitis, A. K. Ladavos, T. Mavromoustakos and C. P. Nicolaides, Microporous and Mesoporous Mater., 75 (2004) 89.
24. D. Ma, Y. Lu, L. Su, Z. Xu, Z. Tian, Y. Xu, L. Lin, X. Bao, J. Phys. Chem. B, 106 (2002) 8524.
25. G. Cruciani, J. Phys. Chem. Solids, 67 (2006) 1973.
26. V. S. R. Rajasekhar Pullabhotla and S. B. Jonnalagadda, Ind. Eng. Chem. Res., 48 (2009) 9097.
27. R. W. Weber, K. P Möller, M. Unger and C. T. O' Connor, Microporous and Mesoporous Mater., 23 (1998) 179.
28. R. W. Weber, K. P Möller and C. T. O' Connor, Microporous and Mesoporous Mater., 35-36 (2000) 533.

CHAPTER FIVE
RESULTS AND DISCUSSION

5

Different forms of ZSM-5 i.e. H and Na (precursor zeolites) were investigated under oxidative and non-oxidative conditions. The oxidation of *n*-hexane was investigated using a vanadium exchanged zeolite synthesised using the solid state ion-exchange method. This chapter details the investigation into optimising conditions for the formation of the desired terminal products using the vanadium exchanged zeolite.

5.1 The investigation of *n*-hexane using a carborundum packed reactor

5.1.1 Non-oxidative conditions

Non-catalytic evaluation of *n*-hexane, under non-oxidative conditions (N_2 atmosphere) was initially performed using the same stainless steel, fixed-bed reactor, packed with carborundum, which was subsequently used for catalytic evaluation. The temperature was varied from 300 to 500°C and the flow rates of *n*-hexane and nitrogen are illustrated in Table 5.1.

Table 5.1 Flow rates for the carborundum packed reactor under non-oxidative conditions

Hexane (mmol.h^{-1})	N_2 (mmol.h^{-1})	Hexane in total flow (%)
45.97	200.78	16.63

No conversion was found to occur under these conditions, which show that oxygen species are required to activate the *n*-hexane molecule.

5.1.2 Oxidative conditions

The same carborundum packed reactor was treated under oxidative conditions as described in Table 5.2. Again the temperature was varied from 300 – 500°C.

Table 5.2 Flow rates for the carborundum packed reactor under oxidative conditions

Hexane (mmol.h^{-1})	O_2 (mmol.h^{-1})	N_2 (mmol.h^{-1})	Hexane in air (%)	Hexane in total flow (%)
45.97	34.48	166.30	28	16.63

The results, given in Table 5.3, show that no conversion occurred below 450°C, but above 450°C conversion showed an increasing trend up to 500°C (8%). The major product of non-catalytic transformation was COx (mainly CO_2), with minor selectivities to cracked products, hexene isomers, tetrahydrofuran (THF) and benzene.

Table 5.3 Results for the carborundum packed reactor experiment

		Selectivity (C mol. %)							
Temp. (°C)	Conv. (C mol. %)	Cracked Prods. [a]	1-ene[b]	2-ene[b]	3-ene[b]	THF	Benzene	CO	CO_2
300	0	0	0	0	0	0	0	0	0
350	0	0	0	0	0	0	0	0	0
400	0	0	0	0	0	0	0	0	0
450	5.9	0	1.9	3.5	1.8	0	0	0	91
500	7.7	1.6	1.8	2.8	1.4	0.3	1.1	1.4	87

[a] cracked prods. = C_1 – C_5 products
[b] 1-ene = 1-hexene, 2-ene = 2-hexene and 3-ene = 3-hexene

A comparative assessment of the product profile to a previous study using a carborundum packed reactor for *n*-hexane oxidation provided a contrast in results **[1]**. The study reported conversion increased from 350°C reaching 45% at 500°C. The product profile did not include cracked products, but benzene, whose selectivity increased with temperature, and hexene isomers. However, the difference in the results obtained may be attributed to the difference in percent *n*-hexane in air (7.8% in the previous study compared to 28% in the current study) and the difference in reactor setups i.e. a shorter heating element was used in this study in order to minimize further free radical reactions that may have occurred with the use of a longer heating element.

n-Hexane oxidation in air over Pt monoliths shows that cracking products are favoured at low C_6H_{14}/O_2 ratios, whilst the dehydrogenated parent is formed at high C_6H_{14}/O_2 ratios **[2]**. *n*-Hexane oxidation in a single gauze Pt/Rh reactor at very short contact times shows that the reactors can be tuned to produce high selectivities to either olefins (60% selectivity for a ratio of $C_6H_{14}/O_2 \approx 1.0$) or oxygenates (70% selectivity for a ratio of $C_6H_{14}/O_2 \approx 2.5$) **[3]**. No benzene formation was noted with either of these systems. The mechanism suggested from this study shows that initial hydrogen abstraction is not preferred as it led to low product selectivity. Abstraction of the secondary hydrogen led to the products obtained in their study and can be used to explain the surface assisted homogeneous pathways to the hexene isomer products obtained from the study described in this thesis (Figure 5.1).

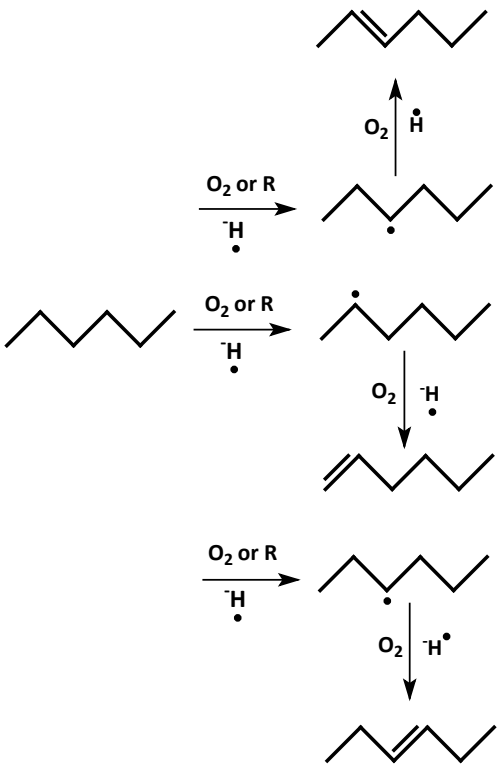

Scheme 5.1 Suggested homogenous reaction pathways for *n*-hexane partial oxidation

5.2 Evaluation of precursor zeolites under non-oxidative and oxidative conditions

5.2.1 Non-oxidative conditions

H-ZSM-5 with SiO_2/Al_2O_3 ratios of 100 and 320 and Na-ZSM-5 (SiO_2/Al_2O_3 ratio = 100) were investigated under non-oxidative conditions. A volume of 1.5 mL of precursor zeolite was packed in the hottest region of the reactor tube as described in Chapter Three, Section 3.1.1 and illustrated in Appendix A, A2. *n*-Hexane and nitrogen were passed over the zeolite using flow rates described in Table 5.1. Due to the presence of deactivation phenomena all the reported data refer to the catalytic behaviour exhibited after one hour on-stream for the precursor zeolites.

H-ZSM-5 (100) and H-ZSM-5 (320) produced almost exclusively C_1 – C_5 products (cracking products). Conversion was found to increase with an elevation of the temperature (Figure 5.1). H-ZSM-5 with higher of SiO_2/Al_2O_3 ratio, i.e. lower aluminium content, showed a lower selectivity and yield to cracked products (yield decrease of 40% for H-ZSM-5 (100) to 9% for H-ZSM-5 (320) at 500°C). In contrast, Na-ZSM-5 gave no conversion of *n*-hexane and hence no cracked products.

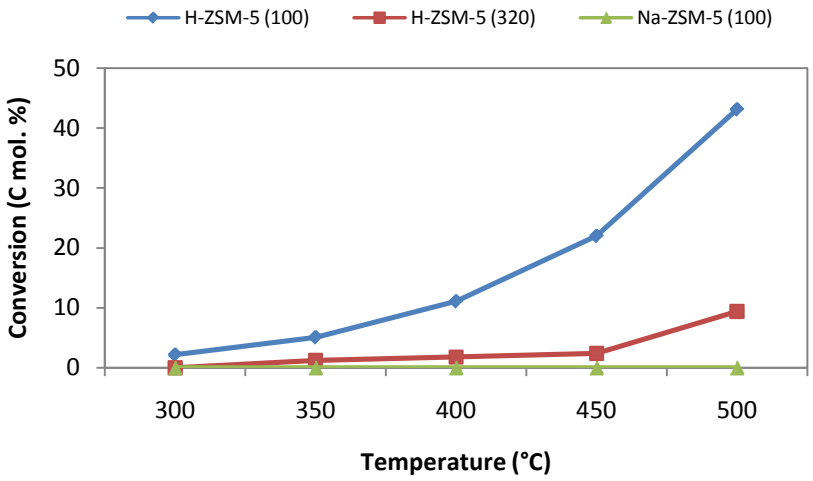

Figure 5.1 Conversion under non-oxidative conditions for H-ZSM-5 with SiO_2/Al_2O_3 = 100 and 320 respectively and Na-ZSM-5 (100)

Table 5.4 Selectivity to products from the non-oxidative reaction of *n*-hexane over H-ZSM-5 (100)

		Selectivity (C mol. %)[a]								
Temp. (°C)	**Conv. (C mol. %)**	**C_1**	**C_2**	**$C_2^{=b}$**	**C_3**	**$C_3^{=b}$**	**C_4**	**$C_4^{=b}$**	**C_5**	**Cyclic**
300	2.2	-	-	-	32.7	13.0	20.7	1.0	2.3	-
350	5.1		2.6	3.5	33.1	14.5	16.3	3.7	1.1	1.2
400	11.1	0.6	5.2	6.1	35.8	22.3	12.1	2.0	0.5	1.5
450	22	1.0	7.7	8.5	29.9	25.6	8.1	1.2	0.2	1.7
500	43.1	1.5	9.8	11.4	22.9	27.0	5.6	-	-	3.6

[a] products not included in the table are other cracking products i.e. 2-butene, 1-pentene, 2-pentene
[b] $C_2^=$ = ethene, $C_3^=$ = propene and $C_4^=$ = butene

The formation of these $C_1 – C_5$ products is attributed to the cracking of *n*-hexane and depends on many factors. The cracking is caused by the high temperature acid sites *via* the mechanisms mentioned in Chapter Two, Section 2.2.1. These mechanisms are complicated due to the occurrence of many sequential and parallel reaction steps such as primary cracking, secondary cracking, dealkylation and hydrogen transfer reactions. The number and strength of the acid sites present in the catalyst, dictated by the distribution and number of aluminium ions in the ZSM-5 crystal lattice, are important parameters that influence the activity and product selectivity. The strong acid sites, which are seats for hydrogen transfer reactions, can accelerate the formation of cyclic compounds and aromatics **[4]**. The concentration of the strong acid sites was calculated in Chapter Four, Section 4.1.5. H-ZSM-5 (100) was found to have the highest concentration and correspondingly showed the highest conversion and consequently selectivity and yield to cracking products. Na-ZSM-5 did not possess the high temperature acid sites and as expected did not show any formation of cracked products. Literature also reports that H-ZSM-5 exchanged with potassium, in order to inhibit surface acidity of the zeolite, showed no trace of cracking activity under non-oxidative conditions **[5]**.

Apart from the differing conversions, the product distribution for the H-ZSM-5 with varying SiO_2/Al_2O_3 ratios was also different (Table 5.4 and 5.5). With increasing aluminium content the selectivities and yields of cyclic compounds increase, indicating increased participation of the oligomerisation and hydrogen transfer reaction. The product distribution shows that different reaction cracking pathways are occurring as mentioned in Chapter Two, Section 2.2.1. The results suggest that in the case of H-ZSM-5 (320) at lower temperatures the route to the dominant C_3 olefinic product occurs *via* carbenium ion formation and then beta scission to form propene. With the H-ZSM-5 (100), the possible route to propane formation could result when the zeolite protonates the paraffin resulting in the formation of a carbonium ion which, due to protolytic cracking, forms propane **[6]**. In both cases sequential and parallel reaction steps occur with increasing temperature.

Table 5.5 Selectivity to products from non-oxidative reaction of *n*-hexane over H-ZSM-5 (320)

		Selectivity (C mol. %)[a]								
Temp. (°C)	**Conv. (C mol. %)**	**C_1**	**C_2**	**$C_2^{=b}$**	**C_3**	**$C_3^{=b}$**	**C_4**	**$C_4^{=b}$**	**C_5**	**Cyclic**
300	-	-	-	-	-	-	-	-	-	-
350	1.3	-	17.9	-	30.1	52.0	-	-	-	-
400	1.8	-	16.1	4.3	23.3	38.4	-	17.0	-	-
450	2.4	2.0	14.4	5.0	18.9	34.5	5.5	15.0	-	-
500	9.4	2.1	13.2	6.6	17.1	33.9	5.4	14.0	-	0.1

[a] products not included in the table are other cracking products i.e. 2-butene, 1-pentene, 2-pentene etc
[b] $C_2^{=}$ = ethene, $C_3^{=}$ = propene and $C_4^{=}$ = butene

5.2.2 Oxidative conditions

The H- and Na- form precursor zeolites were investigated under oxidative conditions as outlined in Table 5.2. Conversion was found to increase with temperature and then decrease at higher temperatures for H-ZSM-5 (320) and Na-ZSM-5 (100). Selectivities to products for each precursor zeolite are given in Tables 5.6 – 5.8. H-ZSM-5 (100) was found to be more active than the other two precursor zeolites (Figure 5.2), which is consistent with literature in which in it was stated that the oxidative activity of zeolites is correlated to surface acidity **[6]**. Total oxidation was found to be lower when surface acidity was inhibited by the use of Na-ZSM-5. These observations suggest that the formation of carbon oxides may be ascribed to the reaction of gaseous oxygen with the activated molecules formed in the interaction of the hydrocarbons with the acid centers of the zeolite. A literature report on the oxydehydrogenation of ethane showed that more methane was produced over H-ZSM-5 than over Na-ZSM-5. This suggested that the strong Brønsted acid sites of H-ZSM-5 were capable of activating oxygen and facilitating reactions between ethane and oxygen which lead almost exclusively to the formation of carbon dioxide and cracking products **[7]**. Other studies of the oxydehydrogenation of ethane and propane **[8, 9]** also concluded that the strong Brønsted acid sites are responsible for non-selective oxidation to carbon oxides and for cracking activity. Removal of these strong Brønsted acid sites by Na^+ ion-exchange was found to result in much lower activity, but the selectivity to hydrocarbons was found to improve

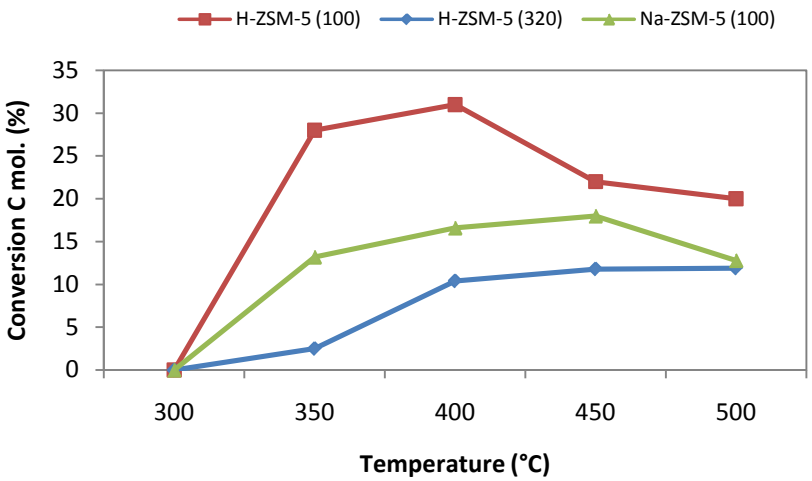

Figure 5.2 Conversion under oxidative conditions for H-ZSM-5 (SiO_2/Al_2O_3 = 100 and 320 respectively and Na-ZSM-5 (100)

Table 5.6 Selectivity to products from the oxidation reaction of *n*-hexane over H-ZSM-5 (100)

		Selectivity (C mol. %)						
Temp. (°C)	**Conv. (C mol. %)**	**Cracked prods.**	**1-Hexanol**	**Hexanal**	**Hexanoic acid**	**1-Hexene**	**Cyclics & aromatics**	**COx**
300	-	-	-	-	-	-	-	-
350	2.8	18.9	0.02	0.2	0.1	2.2	50.2	3.4
400	31	19.4	0.02	0.1	0.1	3.3	20.4	12.9
450	22	26.9	0.1	0.0	0.8	1.1	9.7	34.1
500	20	49.5	0.0	0.0	0.3	0.6	2.4	36.9

When compared to the results of the non-oxidation study, it was seen that a significant modification of the catalytic activity was noted in the presence of gaseous oxygen. In addition to the formation of carbon oxides, the formation of cyclic and aromatic compounds also increases significantly, while lower quantities of cracked products are observed. Some of the cyclic and aromatic products included in the product profile are cyclopentanone, cyclohexane, benzene, tetrahydrofuran, *cis* and *trans*-2,5-dimethyltetrahydrofuran, 2,5-dimethylfuran, 2-

methyl-1-hexene as well as toluene, ethylbenzene, xylene, *n*-propylbenzene, 2-methyltetrahydropyran, 3,5-dimethylcyclopentene, 1-ethyl-4-methyl-benzene, 1, 2, 4-trimethylbenzene etc. It is generally proposed that this category of products are formed through the protolysis of paraffin, the cracking of the carbonium ion to paraffin and olefin, oligomerisation of olefins, cyclisation of oligomerised products and formation of aromatics from cyclic rings by hydrogen transfer.

Table 5.7 Selectivity to products from the oxidation reaction of *n*-hexane over H-ZSM-5 (320)

		Selectivity (C mol. %)						
Temp. (°C)	**Conv. (C mol. %)**	**Cracked prods.**	**1-hexanol**	**Hexanal**	**Hexanoic acid**	**1-hexene**	**Cyclics & aromatics**	**COx**
300	0.0	-	-	-	-	-	-	-
350	2.5	5.8	0.03	-	-	-	57.2	22.8
400	10.4	9.9	0.05	-	0.8	1.6	28.1	31.7
450	11.8	19.6	0.2	-	0.2	1.8	12.9	45.5
500	11.9	22.2	0.1	-	0.1	2.3	0.9	58.2

Table 5.8 Selectivity to products from the oxidation reaction of *n*-hexane over Na-ZSM-5 (100)

		Selectivity (C mol. %)						
Temp. (°C)	**Conv. (C mol. %)**	**Cracked prods.**	**1-hexanol**	**Hexanal**	**Hexanoic acid**	**1-hexene**	**Cyclics & aromatics**	**COx**
300	0.0	-	-	-	-	-	-	-
350	13.2	13.1	0.1	-	0.2	-	11.9	19.3
400	16.6	19.1	0.1	-	0.1	0.5	43.0	21.4
450	18.0	25.1	0.02	-	0.1	1.1	0.8	43.2
500	12.8	27.2	0.0	-	0.0	0.9	0.0	37.3

Although the increase in aromatics and cyclics is seen, the activity of the catalyst decreases with increasing time on-stream and temperature in the presence of gaseous oxygen. This suggests that although there was a higher rate of formation of cyclic and aromatics, these can also block active sites for oxygen activation, and therefore this carbonaceous material inhibits the activity of the catalyst. However, deactivation of zeolites is a complex process. The compounds responsible for zeolite deactivation (coke) are too weakly basic to be retained on the active sites. Therefore the deactivation cannot result from poisoning of the active sites, but from limitation or blockage of the access of the reactant to these sites. The coke species can be situated inside the micropores and/or on the outer surface. Coking and deactivation are dependent on various factors: operating conditions, reaction time, temperature, pressure and the nature of the reactant. Various techniques (FT-IR, UV-vis, ^{13}C (Cross Polarisation)/MAS-NMR) are available for the characterisation of the chemical nature of coke **[10]**. However, this study was not aimed at reviewing this but rather to ascertain evidence of coke formation and to investigate to a certain extent the degree of coking. BET surface area and porosity measurements were performed on the spent precursor zeolite (Table 5.9). When compared to the precursor zeolite data shown in Chapter Four, Section 4.1.4, Table 4.3, it is evident that there is a decrease in surface area and as well as some pore blockage. This is consistent with the findings that there is some species blocking the active sites in the pores.

Table 5.9 Spent precursor zeolite data under oxidative conditions

Sample	BET (m^2/g)	V_T (cm^3/g)[a]	V_μ (cm^3/g)[b]
H-ZSM-5 (100)	257	0.44	0.07
H-ZSM-5 (320)	284	0.26	0.09
Na-ZSM-5 (100)	311	0.49	0.11

[a] V_T = Total pore volume
[b] V_μ = micropore volume

TGA analysis was performed on the spent catalysts to determine the mass loss due to carbon deposits, which is believed to be formed during the reaction and consist of a variety of different compounds having a wide distribution of boiling points. The weight loss in the second temperature region i.e. 350 – 750°C is believed to be responsible for the mass loss due to carbon deposits **[11, 12]**. The weight loss in this region for the fresh precursor zeolites was

minimal (Chapter Four, Section 4.1.8). The results are presented in Table 5.10 and the TGA and DSC curves in Appendix A, A16. As expected the H-ZSM-5 (100) shows the largest weight loss due to carbon deposits.

Table 5.10 TGA analysis for spent precursor zeolites

	Weight loss (%)	
Sample	**Region A (25 – 350°C)**	**Region B (350 – 750°C)**
H-ZSM-5 (100)	7.3	19.3
H-ZSM-5 (320)	7.0	5.8
Na-ZSM-5 (100)	7.4	0.8

The results from the oxidative study showed that very small amounts of terminally activated hexane compounds were also produced under oxidative conditions using the precursor ZSM-5 zeolites. However, it was anticipated that the introduction of vanadium will favour higher production of these products. The results obtained from the non-oxidative and oxidative study of the precursor zeolites, together with the reports from literature, led to the decision to investigate vanadium exchanged Na-ZSM-5 zeolites for the oxidation of *n*-hexane.

5.3 Evaluation of vanadium exchanged zeolites under oxidative conditions

Na-ZSM-5 (100) was loaded with vanadium using the solid state ion-exchange method. The results of the catalyst characterisation, presented in Chapter Four, prompted the investigation and optimisation of the formation of terminal products using the Na-V-ZSM-5 with a ~1% vanadium loading. Thereafter the different vanadium loadings were examined under these optimised conditions.

The process of *n*-hexane oxidation may result in many different products such as: oxygen bearing compounds of C_6 (oxidation process), hexenes (from oxidative dehydrogenation), C_1 –

C_5 compounds (from cracking process), COx (total oxidation) and finally higher hydrocarbons, which result from oligomerisation. Apart from the effect of catalyst composition the distribution of these products depends on the reaction temperature, contact time and fuel-air ratio. These different parameters were examined and discussed in the following sections.

5.3.1 Effect of temperature on *n*-hexane activation

Initial catalytic testing that was performed involved sampling continuously while ramping the temperature from 300 to 450°C at 50°C increments at a contact time of 0.8 s. Results showed that no conversion occurred at 300°C. Subsequently fresh catalysts were tested at 350, 400 and 450°C at a contact time of 0.8 s and fuel-air ratio of 1.3 (conditions outlined in Table 5.2). Sampling was performed at the first hour and thereafter every 1.5 hours for a period of 24 hours.

Na-V-ZSM-5 (0.9%) under oxidative conditions gave superior conversion and selectivities to terminally functionalised products when compared to non-catalytic conditions as well as non-oxidative and oxidative conditions of the precursor zeolites. Variation in temperature was shown to influence conversion, selectivity, as well as the formation of terminal carbon products (Figure 5.3 – 5.6). Other products not included in the product profiles are shown in Appendix A, A17.

At each temperature, the highest conversion was observed at the initial sampling time of 1 hour. A decrease in conversion was noted with an increase in time on-stream at each temperature setting. The highest conversion of 27% was observed at 400°C at 1 h on-stream, which then decreased and stabilised at 18%. At 450°C *n*-hexane conversion decreased from 25% (1 h on-stream) to 10% (24 h on-stream).

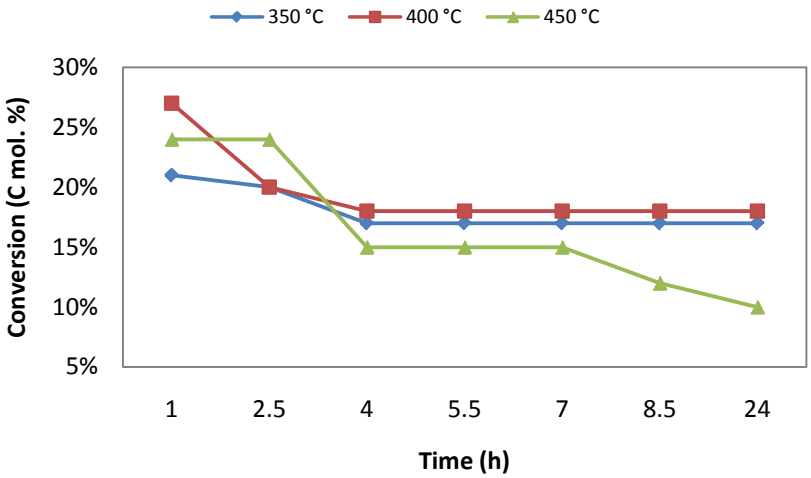

Figure 5.3 Effect of temperature on the conversion of *n*-hexane over Na-V-ZSM-5 (0.9%)

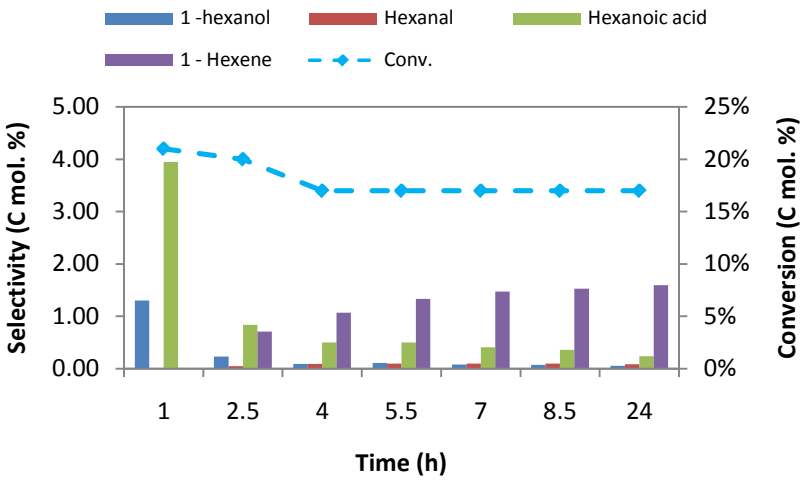

Figure 5.4 Selectivity to terminal products in *n*-hexane oxidation over Na-V-ZSM-5 (0.9%) at 350°C and 0.8 s contact time

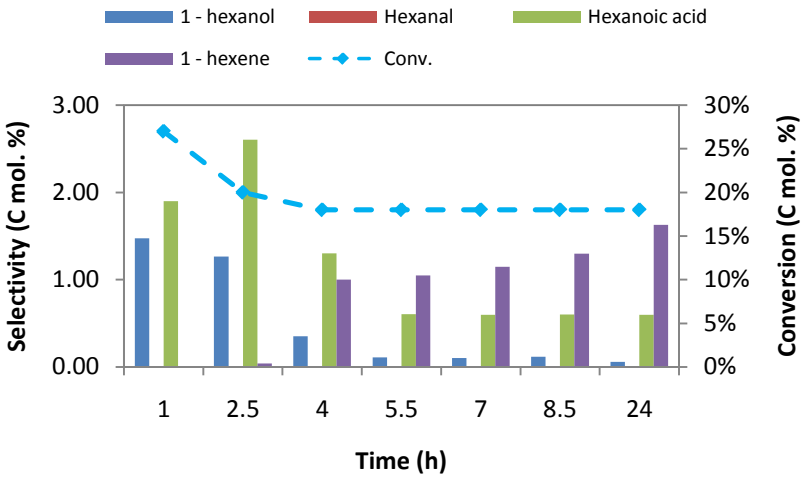

Figure 5.5 Selectivity to terminal products in *n*-hexane oxidation over Na-V-ZSM-5 (0.9%) at 400°C and 0.8 s contact time

At all three temperatures, the product profile was found to be similar, with 1-hexanol and hexanoic acid forming at the initial times on-stream and subsequently decreasing in preference to 1-hexene as time on-stream increases. However, the selectivity and yields to these three products varies at each temperature. At 450°C, the selectivity to COx increases (Appendix A, A17). This alludes to the possibility of the primary and secondary products reacting further to eventually form CO_2.

The formation of 1-hexene could follow direct oxidative dehydrogenation of *n*-hexane or the dehydration of 1-hexanol pathways. The selectivity to 1-hexanol decreases as the formation of 1-hexene increases which implied that 1-hexene is a secondary product. 1-Hexene is thus possibly formed through the interaction of *n*-hexane with oxygen species to form 1-hexanol which is subsequently dehydrated over the acidic centres. The optimum temperature for the formation of 1-hexanol was found to be 400°C.

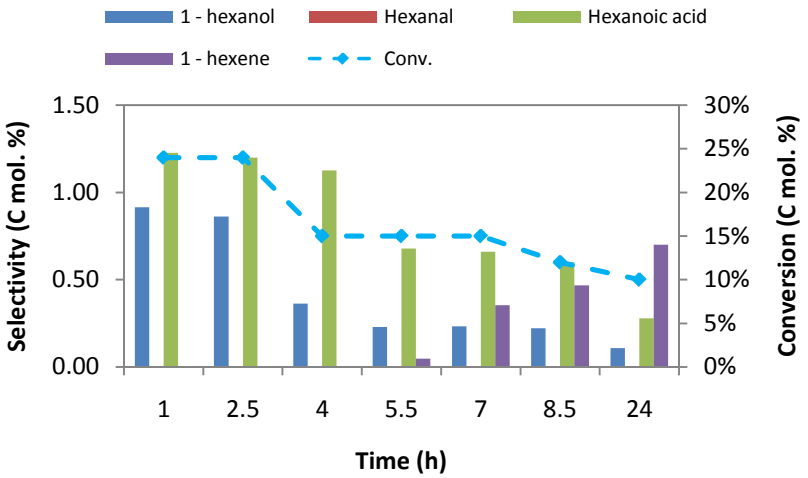

Figure 5.6 Selectivity to terminal products in *n*-hexane oxidation over Na-V-ZSM-5 (0.9%) at 450°C and 0.8 s contact time

5.3.2 Effect of contact time on *n*-hexane activation

Variation of the contact time at 0.5, 0.8, 1.1 and 1.5 s, at the same temperature of 400°C, suggested that the 1.1 s contact time was the best for *n*-hexane conversion (Figs. 5.7). Selectivities to terminal oxygenated products are shown in Figures 5.6 and Figures 5.8 – 5.10.

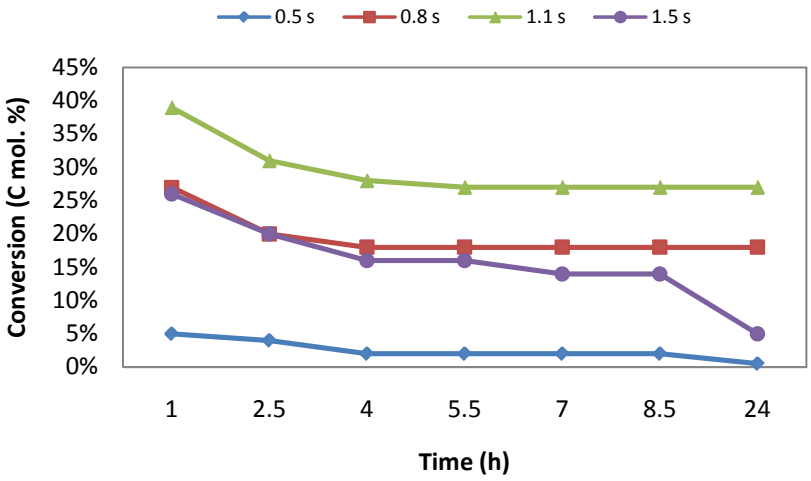

Figure 5.7 Effect of contact time on the conversion of *n*-hexane over Na-V-ZSM-5 (0.9%)

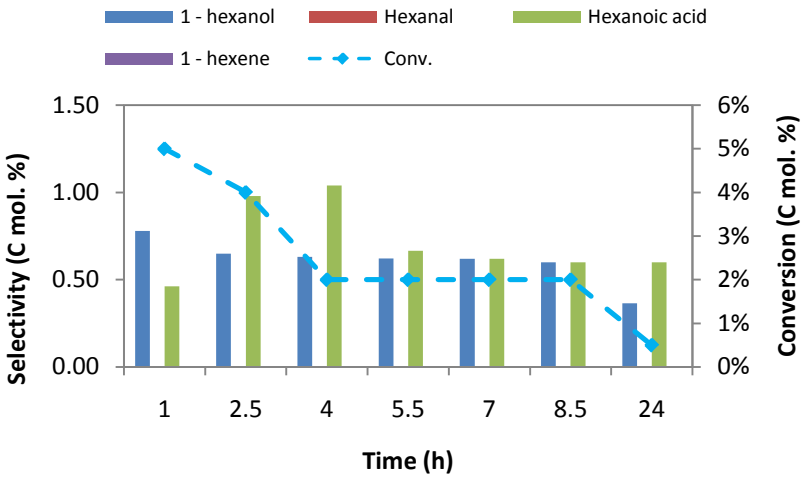

Figure 5.8 Selectivity to terminal products in *n*-hexane oxidation over Na-V-ZSM-5 (0.9%) at 400°C and 0.5 s contact time

At a contact time of 0.5 s, the conversion is the lowest as compared to 1.1 and 1.5 s, which suggests that most of the feed does not have sufficient time to penetrate within the pores of the zeolite and therefore does not encounter the active metal centers. Therefore it is assumed that the conversion of *n*-hexane at this contact time could be predominantly attributed to the reactions occurring at the active sites on the exterior surface of the zeolite.

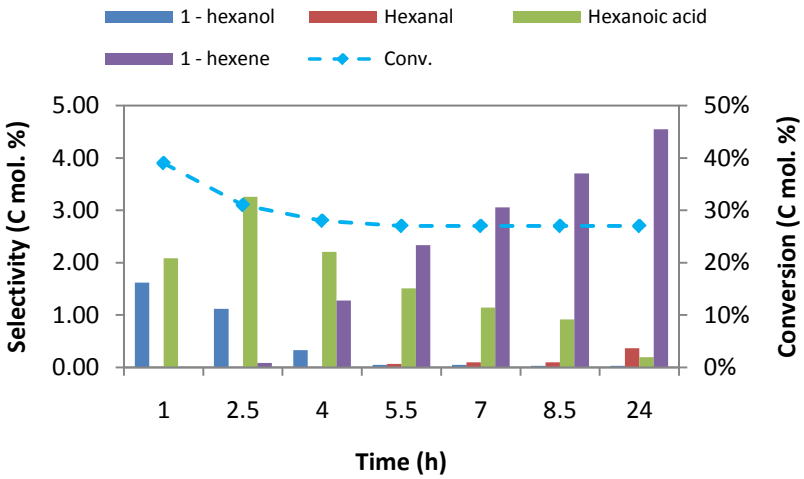

Figure 5.9 Selectivity to terminal products in *n*-hexane oxidation over Na-V-ZSM-5 (0.9%) at 400°C and 1.1 s contact time

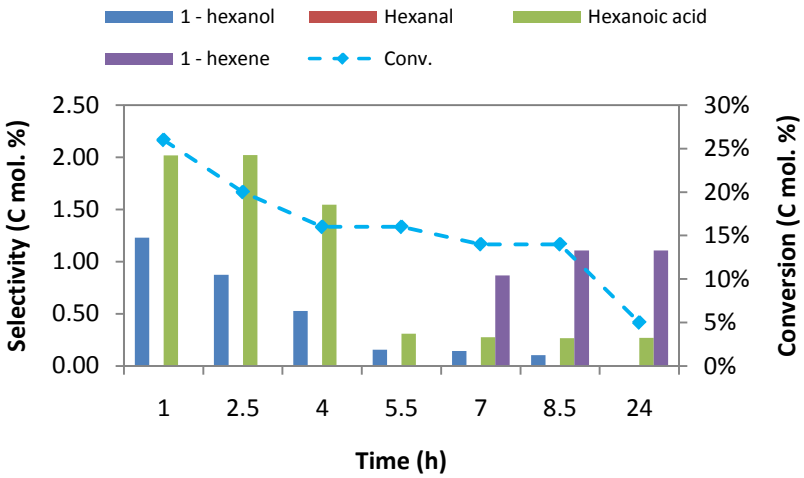

Figure 5.10 Selectivity to terminal products in *n*-hexane oxidation over Na-V-ZSM-5 (0.9%) at 400°C and 1.5 s contact time

At the longest contact time of 1.5 s, the conversion is initially high at 25% before steadily decreasing up to 24 h on-stream. It is assumed that the feed enters the pores and reacts with the active centers and forms a fairly bulky terminal product molecule, which will then have difficulty exiting the pore due to the relatively low gas flow rates associated with longer contact times. This could lead to parallel and consecutive secondary reactions **[13]** culminating in the formation of COx which can then leave the pores. This is evident from the COx formation after 24 hours on-stream (Appendix A, A17).

The formation of coke or carbonaceous deposits could steadily increase under different conditions and in this case it is contact time. As mentioned in Section 5.2.2 above, the formation of coke or carbonaceous deposits in the pores or on surface of the catalyst results in deactivation of the catalyst with time **[10]**. The formation could increase the pore blockage and render the pores and active sites inaccessible **[9, 10]**. Coking or deactivation was first observed from the change in colour of the catalysts. All spent catalysts were found to be black after the completion of the reaction under all the experimental conditions. BET surface area and porosity measurements of the spent catalysts are shown in Table 5.11 below. In all cases, the results conclude to a decreasing surface area and pore volume. The spent catalyst data for the 0.5 s contact time shows minimal pore blockage, which is consistent with the catalytic

findings in which it was reported that the higher flow volumes prevent the feed molecules from having sufficient time to react with the active centers. The spent catalyst results for the 1.5 s contact time also agree with the postulation that parallel and secondary reactions result in COx, which is removed from the catalyst and therefore also results in a lower degree of pore blockage. For the 0.8 and 1.1 s contact times the feed molecules have sufficient time to react with the active centers, thereby resulting in higher activities and this will also result in higher blockage of pores.

Table 5.11 Physical data for spent Na-V-ZSM-5 (0.9%) under varying contact times

Spent catalyst contact time (s)	BET (m^2/g)	V_T (cm^3/g)[a]	V_μ (cm^3/g)[b]
Fresh catalyst	373	0.62	0.13
0.5	253	0.58	0.09
0.8	108	0.52	0.01
1.1	111	0.43	0.02
1.5	189	0.46	0.06

[a] V_T = Total pore volume
[b] V_μ = micropore volume

TGA weight loss analysis is shown in Table 5.12 with the TGA and DSC curves found in Appendix A, A18. Again the second weight loss was analysed for the weight loss due to the carbonaceous compounds. For all spent catalysts the weight loss was higher than the fresh catalyst (Chapter Four, Section 4.1.8) in this region and, as expected, smaller weight losses are for the catalysts used at the lowest and highest contact times.

The investigation of varying contact times at constant temperature of 400°C showed that a 1.1 s contact time seems to be ideal both for the diffusion of the feed within the pore and the diffusion of the products out of the pore. This contact time resulted in the highest yield of 1-hexanol as compared to the other contact times, and it was therefore decided to investigate what effect fuel-air ratio would have on the production of 1-hexanol and other terminal products at this contact time.

Table 5.12 TGA analysis of spent Na-V-ZSM-5 (0.9%) data under varying contact times

	Weight loss (%)	
Spent catalyst contact time (s)	**Region A (25 – 350°C)**	**Region B (350 – 750°C)**
0.5	6.5	7.1
0.8	5.1	17.2
1.1	4.9	17.3
1.5	5.0	6.0

5.3.3 Effect of fuel-air ratio on *n*-hexane activation

At optimum conditions of 400°C and contact time of 1.1 s, the effect of the fuel-air ratio was investigated at 0.7, 1.3 and 2.0.

The highest conversion was obtained at the 1.3 ratio (Fig. 5.11). Under oxygen rich conditions (0.7 ratio) the formation of oxygenates was favoured (Figs. 5.9, 5.12 & 5.13). The formation of hexanal was also favoured. A higher selectivity to COx was also recorded for this ratio (Appendix A, A17). Using oxygen lean (2.0 ratio) conditions, there was an increase in the cyclic and aromatic products, with a similar trend noted for the non-oxidative investigation. The optimum fuel-air ratio was found to be 1.3, which is in excess of the stoichiometric requirements for an oxidation or oxidative dehydrogenation reaction to occur according to the Mars and Van Krevelen mechanism **[14]**. Under this condition, conversion and yield to 1-hexanol were optimum and the COx production was moderate.

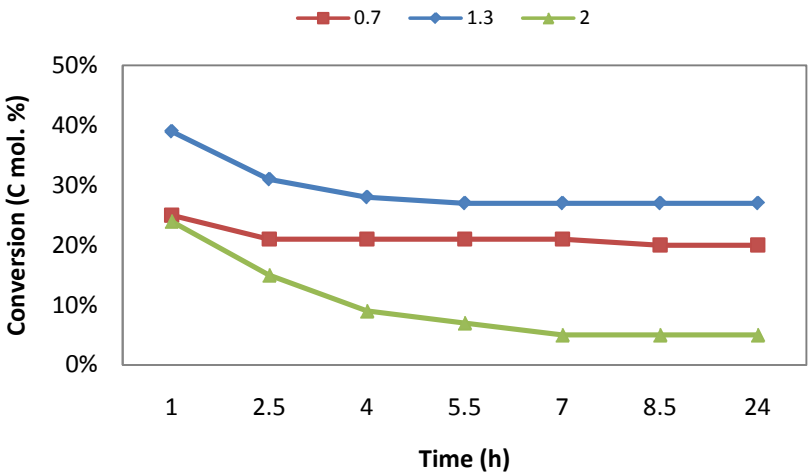

Figure 5.11 Effect of fuel-air ratio on the conversion of *n*-hexane

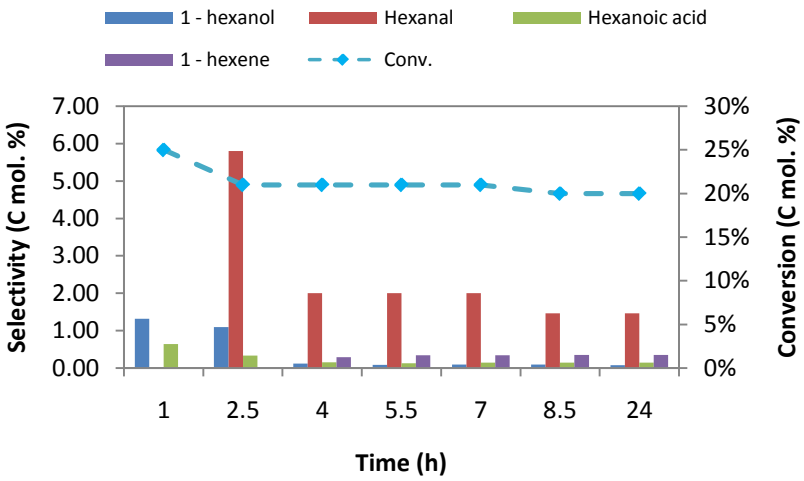

Figure 5.12 Selectivity to terminal products in *n*-hexane oxidation over Na-V-ZSM-5 (0.9%) at 400°C, 1.1 s contact time and fuel-air ratio of 0.7

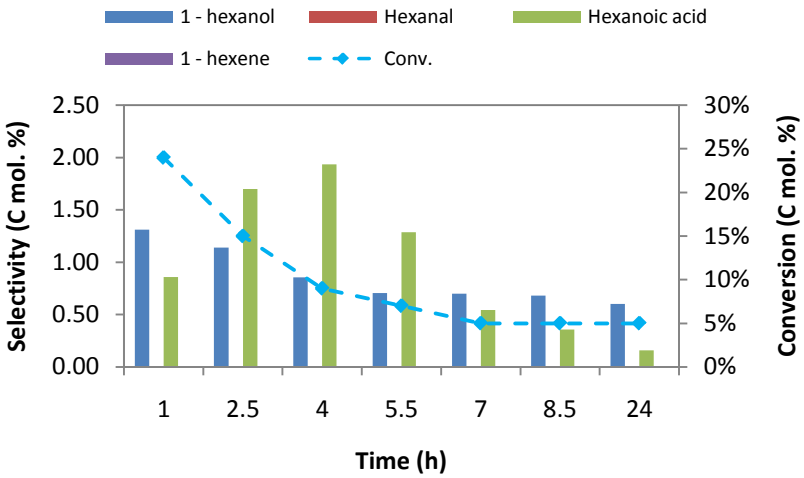

Figure 5.13 Selectivity to terminal products in *n*-hexane oxidation over Na-V-ZSM-5 (0.9%) at 400°C, 1.1 s contact time and fuel-air ratio of 0.2

5.3.4 Effect of vanadium loading on the activation of *n*-hexane

The results of the catalytic evaluation of the 0.9% vanadium exchanged zeolite provided the conditions for the optimal formation of terminal products. These conditions were (temperature of 400°C, contact time of 1.1 s and fuel-air ratio of 1.3) were subsequently used for the evaluation of the catalysts with differing vanadium loadings that were characterised in Chapter Four.

The conversion profile, Figure 5.14, shows that conversion decreases with an increase in vanadium loading above 0.9%. The product profiles are depicted in Figures 5.9, 5.15 – 5.17. It was found that the selectivity to the desired product 1-hexanol decreases with an increase in vanadium loading. It was also noted that with the higher vanadium loadings there was an increase in COx formation (Appendix A, A17). The NH_3-temperature programmed desorption results from the catalyst characterisation (Chapter Four, Section 4.1.6) showed that as the vanadium loading increased, the Brønsted acidity of the catalysts increased. This would imply that more cracking products should be seen with an increase in vanadium loading. However, this was not seen, but an increase in COx formation was seen. This leads to the possibility that

the cracked products are oxidised rapidly to COx. XRD crystallinity and BET surface area and micropore volume measurements for the catalysts with the higher loadings showed that the vanadium species affected the structure of the catalysts. The results indicated that some vanadium species could be located outside the zeolite pores for these catalysts. Therefore these species can block the feed molecules from entering the pores, as well as oxidise the feed molecules rapidly to form COx as seen for the higher loadings.

A report in literature pertaining to the oxidative dehydrogenation of propane to propene, has shown that addition of alkali species to vanadium based mixed oxides hinders the reducibility of the V_2O_5 species, which in turn decreases the catalytic activity. Further conclusions suggested that the electronic promoting effect of the alkali metals (irrespective of the alkali used) was significant for propene selectivity **[15]**. In the study presented in this thesis the H_2-TPR results (Chapter Four, Section 4.1.6) showed that the reducibility of the Na-V-ZSM-5 catalysts was similar irrespective of whether sodium was present. However, the promoting effect of sodium may be responsible for the higher activity and selectivity to 1-hexene seen with the 0.5 and 0.9% loaded Na-V-ZSM-5 since these catalysts have a higher sodium content.

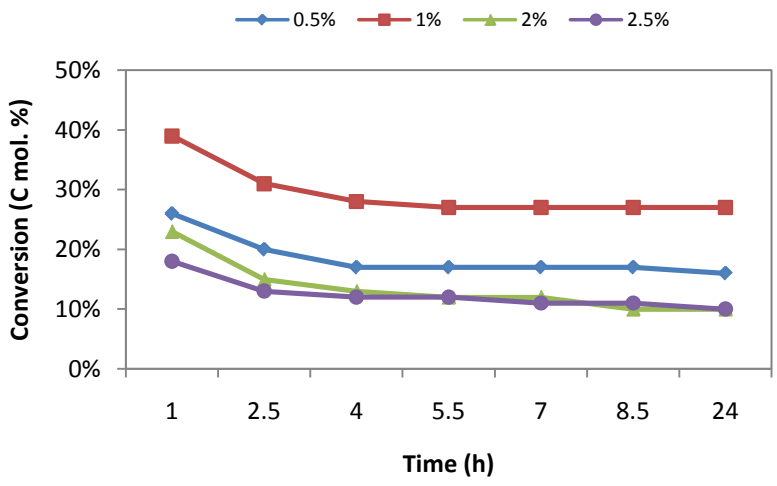

Figure 5.14 Effect of vanadium loading on the conversion of *n*-hexane

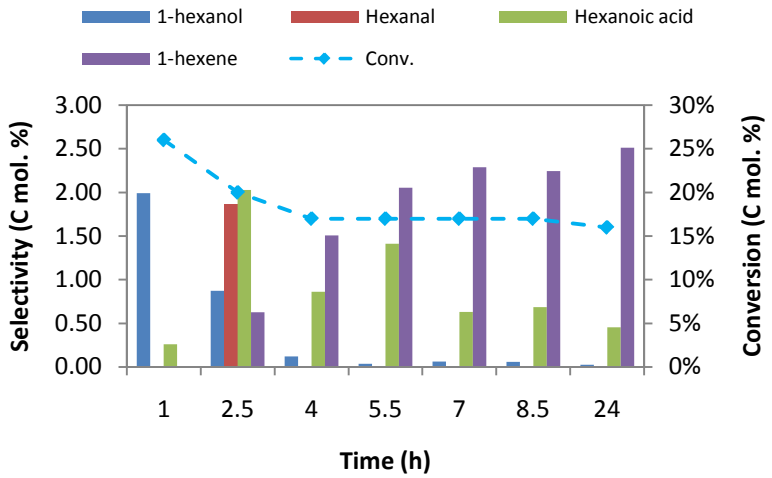

Figure 5.15 Selectivity to terminal products in *n*-hexane oxidation over Na-V-ZSM-5 (0.5%) at 400°C, 1.1 s contact time and fuel-air ratio of 1.3

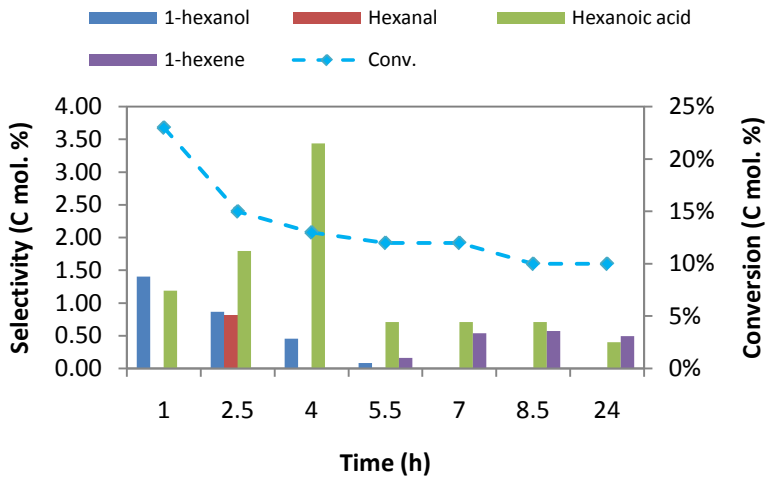

Figure 5.16 Selectivity to terminal products in *n*-hexane oxidation over Na-V-ZSM-5 (2.0%) at 400°C, 1.1 s contact time and fuel-air ratio of 1.3

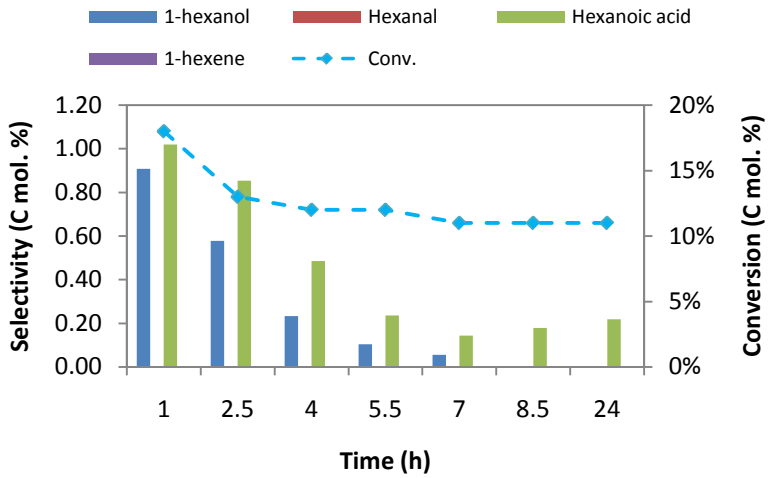

Figure 5.17 Selectivity to terminal products in *n*-hexane oxidation over Na-V-ZSM-5 (2.5%) at 400°C, 1.1 s contact time and fuel-air ratio of 1.3

The results show that in terms of terminal products the highest selectivity to 1-hexanol was obtained using a vanadium loading of 0.9%. The production of cracked and COx products was also minimal with this loading.

5.3.5 Regeneration

Various types of catalyst deactivation are known; poisoning, fouling, mechanical deactivation, leaching and sintering. The method of deactivation of zeolites, as mentioned in above in Section 5.2.2, does not occur from poisoning of the active sites but from limitation or blockage of the access of the reactant to these sites i.e. fouling. The coke species is usually situated inside the micropores and/or on the outer surface. This type of catalyst deactivation is usually a regenerable process **[10, 16]**. A catalyst that offers high activity and selectivity to desired products and that can be regenerated is an important component to industrial processes.

This part of the study involved investigating whether the Na-V-ZSM-5 catalyst can be regenerated. Earlier TGA/DSC studies to liberate the coke species involved treatment of the

catalyst in air up to 900°C and showed that the postulated coke molecules were removed up to 750°C. The regeneration study involved using the Na-V-ZSM-5 (2.5%), which showed a minimal amount of coke formation. The reaction conditions were those that were optimised; 400°C, contact time of 1.1s and fuel-ratio of 1.3. Almost identical results (Figure 5.18 and Appendix A, A17) to those reported in Figure 5.17 above for the Na-V-ZSM-5 (2.5% were obtained). The reaction was terminated after 24 hours on-stream and then the catalyst was treated in the reactor under air at 650°C for 24 hours. Following this, the initial experimental conditions were resumed and the activity of the catalyst was monitored until stable activity was attained at 7 h on-stream.

The results show that the catalyst activity and selectivity to products were the same as obtained with the fresh catalyst within experimental error. The Na-V-ZSM-5 zeolites with different vanadium loadings are believed to behave in a similar manner and therefore prove that it is possible to regenerate catalysts synthesised by the solid state ion-exchange procedure.

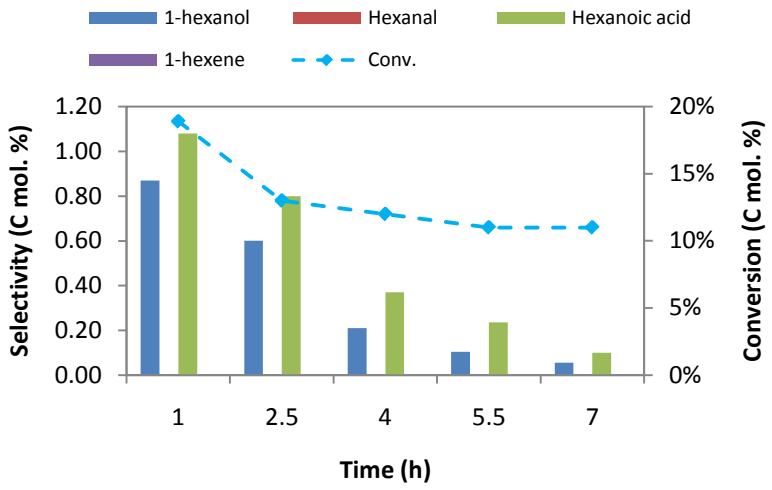

Figure 5.18 Selectivity to terminal products in *n*-hexane oxidation over regenerated Na-V-ZSM-5 (2.5%) at 400°C, 1.1 s contact time and fuel-air ratio of 1.3

5.3.6 Silanisation

Silanisation of the exterior surface of the catalyst was found to result in some pore narrowing and an increase in shape selectivity as explained in Chapter Two, Section 2.4.2. The Na-V-ZSM-5 (0.9%) was found to show the highest activity and provided the highest yield and selectivity to 1-hexanol. This prompted the idea of silanising the Na-V-ZSM-5 using the chemical liquid deposition procedure. Characterisation results of the resulting catalyst were discussed in Chapter Four, Section 4.2. The characterisation results proved that this method of depositing silicon on the zeolite was successful. However, this deposition has chemically and structurally altered the composition of the catalyst. This catalyst was then subjected to the optimum catalytic conditions found for the Na-V-ZSM-5 (0.9%) i.e. 400°C, 1.1 s contact time and 1.3 fuel-air ratio. The results for the terminal products are shown below in Figure 5.19.

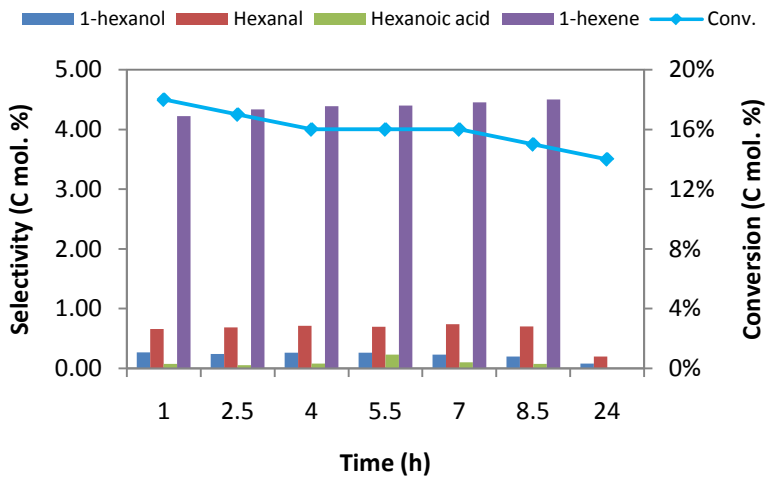

Figure 5.19 Selectivity to terminal products in *n*-hexane oxidation over silanised Na-V-ZSM-5 at 400°C, 1.1 s contact time and fuel-air ratio of 1.3

The activity of the catalyst was found to be much lower than the unsilanised catalyst (Figure 5.10) and deactivation was found to occur at a much slower rate. This could be due to the feed molecules not being able to penetrate the pores due to the narrower pores seen by the BET surface area and pore volume measurements in Chapter Four, Section 4.2.4. Chapter

Four, Section 4.2.5 showed that the acidity of the catalyst was reduced. The selectivity to the C_6 terminal products is shown in Figure 5.19. The selectivities and yields, when compared to the parent catalyst, are much lower, except for the 1-hexene which seems to maintain the selectivity but decreases in yield. Part reason for this could be that there was a reduction in vanadium species (decrease in V/Al ratio) which was a result of the silanisation procedure. The higher selectivity to aromatics and cyclics seen with time on stream could be due to the higher formation of olefins (1-hexene) as these are known to be precursors of aromatics. These reactions are believed to occur in the pores of the zeolites as the exterior surface has been altered by the deposition of silicon species **[17]**.

The aim was to increase in the selectivity to 1-hexanol, but by reducing the surface acidity, the vanadium content, surface area and pore volumes were reduced. It was therefore found that by trying to fine tune certain aspects there is a loss in another.

5.3.7 Possible mechanism of *n*-hexane partial oxidation

These studies showed that in the absence of vanadium i.e. the precursor zeolite Na-ZSM-5 formed mainly cracked products and COx with a very small amount of C_6 oxygenated products. The conversion was also found to be higher in the presence of vanadium. These results suggest that the vanadium species plays a role in the partial oxidation of the hexane molecule. The mechanistic role of the vanadium species under conditions used in this study has not been proposed before in literature. However, from the literature reports on other similar systems the following has been proposed as a possible route to the products from this study.

As mentioned in Chapter One a selective catalyst is supposed to perform a dual function: activate oxygen by generating oxygen species of proper reactivity, and activate the starting material to direct the oxidation in the desired way.

Oxygen activation on the catalyst surface is a necessary stage for the heterogeneous partial oxidation reaction. Adsorbed oxygen on oxide surfaces can exist in a number of forms, molecular or atomic, neutral or charged. It is assumed that during the adsorption on the reduced surface, oxygen can accept electrons one by one going in succession all the way to the fully reduced form, i.e. O^{2-} , which may differ only slightly from the lattice oxygen ions as illustrated in Scheme 5.2. These species of oxygen have been known to be generated on vanadium containing catalysts **[18]**.

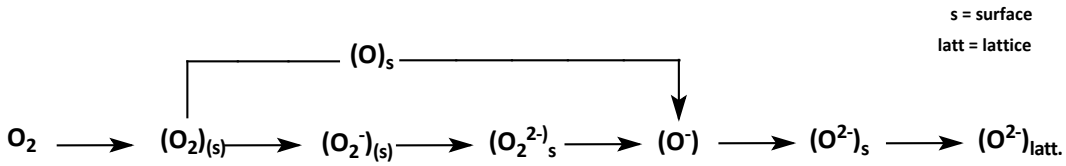

Scheme 5.2 Generation of active oxygen species

Theoretically, both adsorbed and lattice oxygen can take part in the oxidation. It is widely agreed that the lattice oxygen plays an important role in selective oxidation. It is shown in a number of works **[19-21]** that partial oxidation catalysts can serve by themselves as a source of active oxygen and for some time perform the oxidation in the absence of O_2 in the gas phase. The amount of consumed oxygen could correspond to several monolayers. Subsequent re-oxidation restores the depleted oxygen. Vanadium incorporated in ZSM-5 is likely to co-ordinate at specific sites on the zeolite framework. Literature suggests that the vanadium exists as $(VO_2)^+$ species which are co-ordinated to one Al site. It also can exist as $V_2O_4^{2+}$ dimers (which co-exist with $(VO_2)^+$) and $VO(OH)_2^+$ at higher vanadium loadings **[22]**.

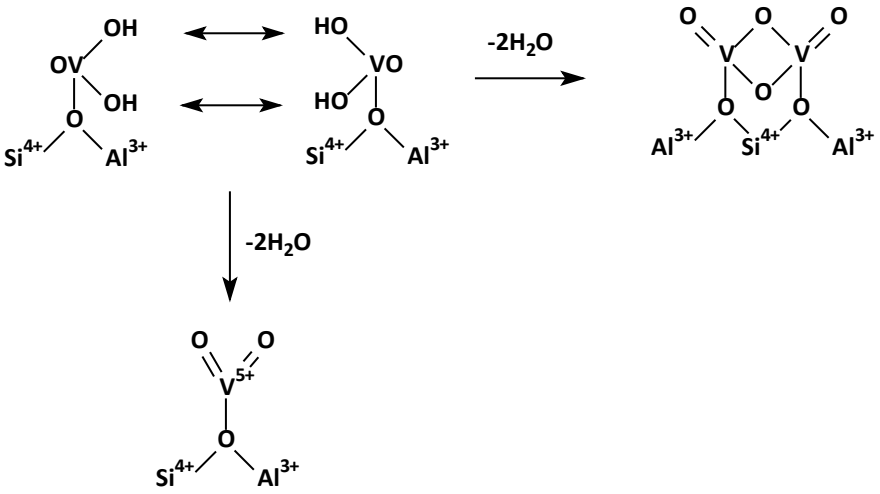

Scheme 5.3 P**o**ssible interaction of vanadium species with the zeolite support

Vanadium containing catalysts that possess a metal-oxygen double bond, as shown above (Scheme 5.3), are known both for the oxygen insertion function as well as oxidative dehydrogenation behaviour. The redox cycle that can be described by these types of species is generally considered to proceed *via* the following pathway **[23]**:

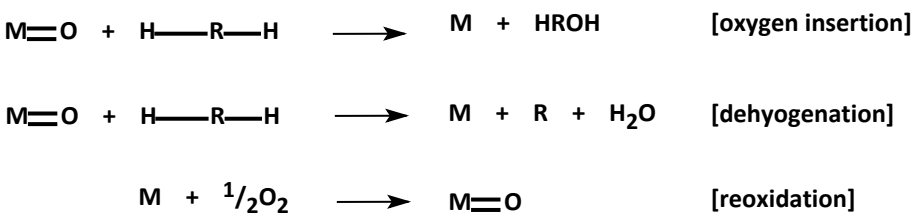

Scheme 5.4 Redox cycle for a metal containing complex

Both of the above pathways occur *via* a Mars and van Krevelen redox mechanism. To mechanistically show the formation of hexene occurs via a Mars and van Krevelen redox mechanism, the first step uses lattice oxygen atoms to abstract hydrogen atoms from C_6H_{14}, in an irreversible C-H bond activation step **[24]**. Hexane ODH to hexene is envisaged to occur via the following sequence:

1. The weak associative adsorption of hexane on lattice oxygen (O*)

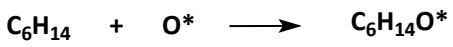

2. C-H cleavage *via* H-abstraction from hexane using neighbouring lattice oxygen

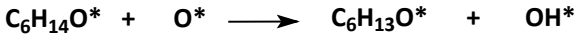

3. Desorption of hexene by hydride elimination from adsorbed alkoxide species

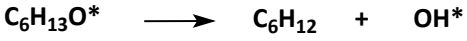

4. Recombination of OH groups to form water and a reduced metal center (*)

5. Re-oxidation of reduced M-centers *via* dissociative chemisorption of O_2

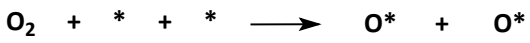

The detection of water as part of the product spectrum as a by product alludes to fact that the above mentioned mechanisms for the formation of 1-hexanol and 1-hexene is prevalent. Similarly other isomers of these two products can also be formed. Thermodynamics suggest a preferable activation of *n*-hexane to activate hexane at the C_2 and C_3 positions. However, the formation of terminal functionality products, such as 1-hexene and 1-hexanol suggest that desired shape selectivity that is created by incorporating vanadium in a zeolite matrix has indeed achieved the aims of this work.

5.3.8 Other products

Experiments to investigate the effect of temperature, contact time and fuel-air ratio in this work have conclusively shown the optimum conditions for the conversion of *n*-hexane and the selectivity to terminal functionalized products.

Under oxidative conditions, higher temperatures and a redox-metal active catalyst, oxidative dehydrogenation reactions are known to occur. Water is a "by-product" of this reaction and could be responsible for a modification of the catalyst. Under reaction conditions, the water formed is in the gas phase and this steaming effect on zeolites is well documented in literature, whereby de-alumination of the zeolite could occur **[4, 6, 25]**. XRD analysis of the spent catalyst revealed an unchanged structure, suggesting that the de-alumination effect was not prevalent in this work. Aside from the de-alumination effect, the presence of water within or on the surface of the zeolite provides an environment for the exchange of Na^+ cations with H^+ ions, which in turn will modify the acidity of the zeolite and contribute to the acid cracking mechanisms mentioned previously **[6, 26]**. An increase in the production of cracking products was seen under certain conditions and this could be due to the modification of the catalyst due to the presence of water.

However, the formation of cracked and aromatic products prevailed under all oxidative experimental conditions in this study. This is in stark contrast to the results obtained under non-oxidative conditions where there was no conversion of *n*-hexane, which supports the theory that the presence of oxygen is conducive to the formation of cracked and aromatic products. As mentioned in Chapter Two, Section 2.2.1, the initial step in the cracking mechanism comprises of the formation of a carbonium ion on the Brønsted acid sites and a subsequent step where the species concomitantly decomposes to an adsorbed carbenium ion and lower paraffins or hydrogen. The mechanism of formation of the cracked products is shown in Scheme 5.2 **[27]**. The acidity that is required for this mechanism can be generated from either the vanadium ions or from H^+ ions that can arise in the presence of water.

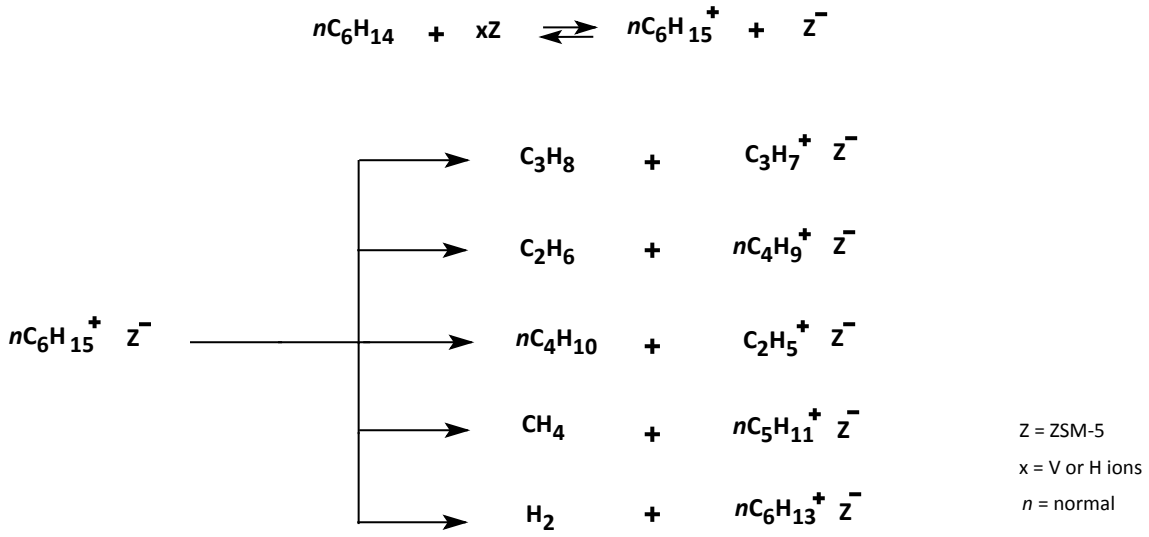

Scheme 5.5 Suggested mechanism for *n*-hexane cracking **[27]**

The absorbed carbenium ion, as shown in Scheme 5.3 and mentioned in Section 5.2.2, in turn can undergo dehydrogenation, hydride transfer, isomerisation, β-scission and other reactions to form other products, including the cyclic and aromatics that were seen in the product profile. The cyclic and aromatic products that formed were similar to those found for the precursor zeolites and are listed as part of Appendix A, A17. Other than these products, linear C_6 products (Total selectivity varied from 3 to 22%) can also be formed and among those that were seen are *cis* and *trans*-2-hexene, *trans*-3-hexene, 1,3-hexadiene, 1,5-hexadiene, 2,3-hexadione, 2,5-hexadione, 3-methyl-2-pentene , 2-hexanol, 5-hexen-1-ol and cis-4-hexen-1-ol. Selectivities to these products are reported in Appendix A, A20.

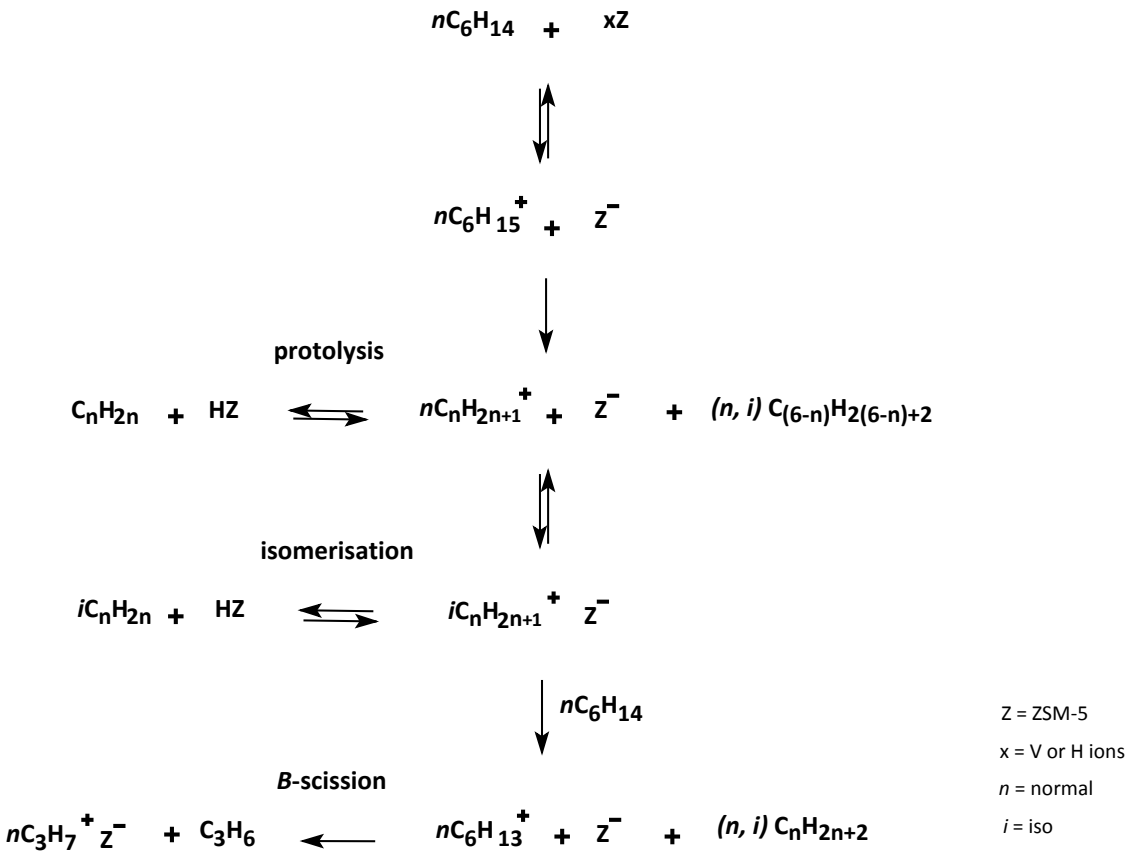

Scheme 5.6 Suggested mechanism for other products formed **[27]**

Appendix A, A19, shows the distribution of cracking products for the different reaction conditions that were employed in this study. Results indicate that olefins are preferred over paraffins, and ethene, propene and butene are the main cracked products formed. Theoretically bond breakage would result in pairs of products i.e. $C_1 + C_5^=$ (terminal bond breakage), $C_2^= + C_4$ and $C_2 + C_4^=$ (intermediate C–C bond breaking), $C_3 + C_3^=$ (central bond breakage) and $H_2 + C_6^=$ (terminal C–H bond breaking). Jolly *et al*. showed that the central bond is more reactive (57.1%) than the intermediate C–C bond (17.3%) which, in turn, is more reactive than the terminal C–C bond (2.9%) **[27]**. However, depending on the Si/Al ratio of the zeolite, the C–H bond may be more reactive than the terminal C–C bond. Nevertheless the central bond was found to be most reactive in both cases. This is consistent with the data obtained under the different conditions investigated in this study as shown in Appendix A, A17, where the major cracked product, propene, formed as a result of central bond breakage and

then ethene and butane resulting from in the intermediate bond breakage. If a monomolecular mechanism was the predominant reaction path, the same selectivity to the paraffin and the olefin molecules should be expected for each of the pairs: C_1-$C_5^=$, $C_2^=$-C_4, C_2-$C_4^=$ and C_3-$C_3^=$. However, Appendix A, A19, shows some discrepancies in most of the results under various conditions of this study and thus indicates that due to the occurrence of many sequential and parallel reaction steps, different pathways are occurring as seen for the precursor zeolites earlier.

Of the cracked products formed, ethene and propene are preferred **[28]**. These are highly in demand as a major feedstock in polymer and alkylbenzene production. The highest combined yields that were achieved in this study were ~8% under conditions which are also the optimum conditions for C_6 terminal yields. However, a higher combined selectivity of ~32% was achieved with the Na-V-ZSM-5 at 0.5 s contact time (400°C and fuel-air ratio of 1.3). Another product of value is methanol, which can later be converted to hydrocarbons. Again the optimum conditions for C_6 terminal products showed the best yield of methanol i.e. 2.7%, but the best selectivity to methanol (12%) was seen at 24 h on-stream with the reaction at 350°C at a contact time of 0.8 s (fuel-air ratio of 1.3). The formation of methane and ethene has been postulated to be attributed to the further cracking of propane **[29].** These studies show that propane selectivity decreases to zero with time on-stream, but only at the higher temperature of 450°C does methane and ethene selectivity increase. These results suggest that the partial oxidation products can be easily oxidised to COx and indeed used in total oxidation or combustion as fuel to generate heat **[30]**. C_6 mono-olefins were also part of the products formed and again the highest yield (3.6%) was achieved at optimum conditions for C_6 terminal products. However, the highest selectivity that was obtained was 13% at 400°C at a contact time of 0.8 s (fuel-air ratio of 1.3).

5.3.9 Comparison to literature

The optimum conditions for *n*-hexane activation were compared to those found in the literature using redox metal ion-exchanged zeolites or silicalites. Iglesia *et al*. reported initial terminal selectivities of 24% at a 0.05% conversion with a Mn-ZSM-5 zeolite in the liquid phase

under pressure, giving a yield of terminal products of 0.012% **[31]**. Singh and Selvam used vanadium silicalites and achieved a 0.1% yield to 1-hexanol **[32]**. Besides the higher yields and conversions obtained under optimum conditions in the study reported in this thesis, air was used as an oxidant rather than more expensive oxidants like N_2O, O_2 and TBHP. Furthermore this study was carried out in the gas phase, which eliminates the problems of leaching, which is a common problem associated with liquid phase catalysis. In addition the catalysts also favoured other products of value i.e. ethene, propene, methanol and mono-olefins.

5.4 References

1. H. B. Friedrich, N. Govender and M. R. Mathebula, Appl. Catal. A: Gen., 297 (2006) 81.
2. A. G. Dietz III, A. F. Carlsson and L. D. Schmidt, J. Catal., 176 (1996) 459.
3. R. P. O'Connor and L. D. Schmidt, Chem. Eng. Sci., 55 (2000) 5693.
4. S.K. Sahoo, N. Viswanadham, N. Ray, J. K. Gupta, I. D. Singh, App. Catal. A: Gen., 205 (2001) 1.
5. G. Centi and G. Golinelli, J. Catal., 115 (1989) 452.
6. M. Stöcker, Microporous and Mesoporous Mater., 82 (2005) 257.
7. Y. -F. Chang, G. A. Somorjai and H. Heinemann, J. Catal., 154 (1995) 24.
8. Y. -F. Chang, G. A. Somorjai and H. Heinemann, Appl. Catal. A: Gen., 96 (1993) 305.
9. L. W. Zatorski, G. Centi, J. L. Nieto, F. Trifirò, G. Bellussi and V. Fattore, Zeolites: Facts, Figures, Future, (P. A. Jacobs and R. A. van Santen, eds.), Elsevier Science Publishers, Amsterdam, 1989, pp 1243-1252.
10. M. Guisnet and P. Magnoux, Appl. Catal. 54 (1989) 1.
11. A. R. Pradhan, J. F. Wu, S. J. Jong, T.C. Tsai and S. B. Liu, Appl. Catal. A: Gen., 165 (1997) 489.
12. X. Guo, Y. Zheng, B. Zhang and J. Chen, Biomass and Bioenergy, 33 (2009) 1469.
13. J. Weitkamp, Solid State Ionics, 131 (2000) 175-188.
14. P. Mars and D. W. van Krevelen, Chem. Eng. Sci. Suppl., 3 (1954) 41.
15. A. A. Lemonidou, L. Nalbandian and I. A. Vasalos, Catal. Today, 61 (2000) 333.
16. J. A. Moulijn, A.E. van Diepen and F. Kapteijn, Appl. Catal. A: Gen., 212 (2001) 3.
17. A. Smiešková, E. Rojasová, P. Hudec and L. Šabo, Appl. Catal. A: Gen., 268 (2004) 235.
18. G.I. Panov, A. K. Uriarte, M. A. Rodkin, V. I. Sobolev, Catal. Today, 41 (1998) 365.
19. V.D. Sokolowsky, Catal. Rev.: Sci. Eng., 32 (1990) 1.
20. T.V. Andrushkevich, Catal. Rev.: Sci. Eng., 35(2) (1993) 213.
21. Y. Schuurman, J.T. Gleaves, J.R. Ebner, M.J. Mummey, Stud. Surf. Sci. Catal., (1994) 203.
22. H. S. Lacheen, and E. Iglesia, J Phys. Chem. B., 110 (2006) 5462.
23. M. Ai, Catal. Today, 52 (1999) 65.
24. K. Chen, A. T. Bell, E. Iglesia, J. Phys. Chem., B, 104 (2000) 1292.

25. C. A. Trujillo, U. N. Uribe, P. – P. Knops-Gerrits, L. A. Oviedo. A, P. A. Jacobs, J. Catal., 168 (1997) 1.
26. W. O. Haag, R. M. Dessau, in: Proceedings from the 8th International Congress on Catalysis, DECHEMA, Frankfurt (1984) 305.
27. S. Jolly, J. Saussey, M. M. Bettahar, J. C. Lavalley and E. Benazzi, Appl. Catal. A: Gen., 156 (1997) 71.
28. O. Bortnovsky, P. Sazama and B. Wichterlova, Appl. Catal. A: Gen., 287 (2005) 203.
29. R. Bulanek, K. Novoveska, Polish J. Chem., 78 (2004) 149.
30. M. M. Lin, Appl. Catal. A: Gen., 207 (2001).
31. A. P. Singh and T. Selvam, J. Mol. Catal. A., 113 (1996) 489.
32. B. –Z. Zhan, B. Modén, J. Dakka, J. G. Santiesteban and E. Iglesia, J. Catal., 245 (2007) 316.

CHAPTER SIX
SUMMARY AND CONCLUSION

6

The abundance of longer chained paraffins from gas and coal to liquid plants has stimulated interest in producing more valuable products, such as oxygenates and olefins *via* selective oxidation processes to accomplish this. The work in this study focused on trying to activate *n*-hexane using zeolites exchanged with vanadium.

The initial part of this work was to design and construct a system to efficiently investigate the gas phase catalysis reactions. A stainless steel, fixed-bed reactor was constructed and tested for efficiency before being used for the study of the vanadium modified catalysts in this work.

Initial testing involved blank or carborundum packed reactor testing. The major product of non-catalytic transformation of *n*-hexane was COx (mainly CO_2) with minor selectivities to cracked products, hexene isomers, THF and benzene. The results of the blank reactor study showed that under reaction conditions contributions from the homogeneous gas phase reactions are minimal.

Zeolite precursors, H-ZSM-5 (100 and 320) and Na-ZSM-5 (100) were then investigated to determine the impact of acidity on the transformation of *n*-hexane. It was found that the Na-form of the ZSM-5 zeolite was able to minimize the formation of cracked products, which are known to be formed due to the high temperature acid sites. It was shown that the strong acid sites were responsible for the unselective oxidation and ultimately in the formation of larger amounts of COx.

The Na-ZSM-5 was exchanged with $VOSO_4.5H_2O$ using the solid state ion-exchange method. Different vanadium loadings were achieved by varying the vanadium in relation to aluminium. With an excess of $VOSO_4.5H_2O$ the highest loading of 2.5% was achieved. These catalysts were characterised using various techniques. Infrared spectroscopy showed the typical bands assigned to the framework vibrations of the ZSM-5 zeolite, with only the highest loading showing a V=O stretching band. XRD studies showed that the catalysts maintained the structure, but the crystallinity calculations showed that the higher loadings have affected the structure. These results were consistent with the BET surface area and porosity measurements, which showed that for the higher loadings some textural alteration and pore blockage had occurred. Ammonia-temperature programmed desorption was used to determine the acidity of the zeolites. As expected the H-ZSM-5 showed the highest acidity, whilst the Na-ZSM-5 showed no Brønsted acidity. These results were consistent with the results obtained with the non-oxidative testing of the precursor zeolites. Solid state NMR was used to determine the different chemical environments of the zeolites, which were relatively similar in all cases, except for the zeolite with the higher loading of 2.5%. The ^{27}Al spectrum of the 2.5% loaded zeolite showed that the VO^{2+} species possibly distorted the coordination environments of the framework aluminium species. Thermogravimetric analysis showed that the zeolite structure was very stable at high temperatures and only weight loss due to water was seen.

The catalytic conditions in using the 0.9% Na-V-ZSM-5 were then optimized. The effect of temperature was initially investigated. In each case conversion was the highest after 1 h on-stream and results were therefore all compared after 1 h on-stream. The results showed that 400°C was optimum for the production 1-hexanol. Contact time was then investigated by keeping the temperature constant at 400°C. Initial conversion values were found to increase with contact time until a contact time of 1.5 s. Here it was assumed that the feed entered the pores and reacted with the active centers forming a fairly bulky terminal product molecule, which then has difficulty in exiting the pore due to the relatively lower gas flow rates associated with higher contact times. This could lead to parallel and consecutive secondary reactions and ultimately in the formation of COx, which can then leave the pores. From these results a 1.1 s contact time seemed to be ideal both for the diffusion of the feed within the pore and the diffusion of the products out of the pore. Keeping the temperature and contact

time constant, the fuel-air ratio was varied. Using oxygen rich conditions the formation of oxygenated products was favoured, with a higher selectivity to COx. Under oxygen lean conditions more cyclic and aromatic products were formed. At a fuel-air ratio of 1.3, the conversion and selectivity to 1-hexanol was optimum with a moderate production of COx. The best yield to 1-hexanol was found to be 0.63% under these conditions.

When the optimum conditions found for the Na-V-ZSM-5 (0.9%) were used to test the catalysts with different vanadium loadings, the results showed that with an increase in vanadium loading the conversion increased up to a 0.9% loading. The subsequent decrease was possibly due to changes in structure that were observed for the higher vanadium loadings. The Na-V-ZSM-5 (2.0%) showed a slightly higher selectivity to 1-hexanol i.e. 2% at a lower initial conversion. However, these higher loadings, i.e. 2.0% and 2.5%, favoured the production of COx, implying that with the greater acidity generated by the vanadium species, and structural changes, the catalyst was much more oxidising.

During each reaction a large amount of different products are formed, which are also thought of as higher value products. In terms of cracked products, it was observed that olefins are preferred over paraffins and that ethene, propene and butene are the main products, with ethene and propene being preferred from a technical viewpoint. The highest yields that were achieved were ~8% under the same optimum conditions for C_6 terminal yields (1.5% to 1-hexanol and hexanoic acid). However, a higher combined selectivity of ~32% was achieved with the Na-V-ZSM-5 (0.9%) at 0.5 s contact time (400°C and fuel-air ratio of 1.3). Another product of value, methanol, also showed the best yield under optimum conditions for terminal C_6 production i.e. 2.7%, but the best selectivity (12%) was seen at 24 h on-stream with the reaction at 350°C at a contact time of 0.8 s (fuel-air ratio of 1.3). C_6 mono-olefins were also part of the products formed and again the highest yield (3.6%) was achieved at optimum conditions for C_6 terminal products. However, the highest selectivity that was obtained was 13% at 400°C at a contact time of 0.8 s (fuel-air ratio of 1.3).

Various industrial applications require catalysts that are able to be regenerated. The used Na-V-ZSM-5 was treated under air in the reactor at 650°C to combust the coke species. The catalyst was then tested and it was found that the initial activity and selectivity could again be achieved.

The last aspect investigated was whether silanisation, which is referred to as the removal of acidity associated with the exterior active surface, could be achieved. The catalyst was characterised and chemical and structural changes were observed. The catalyst was tested under the optimum conditions that were found for the Na-V-ZSM-5 (0.9%) and it was found to have lower activity. The surface acidity of the catalyst, as well as the pore volumes, was lower and this resulted in lowering of the activity, as well as selectivities to the desired terminal products.

Although this study did not achieve high selectivities to desired terminal products, the activity of the catalyst and the yields were much higher than those obtained from literature reports.

APPENDIX A

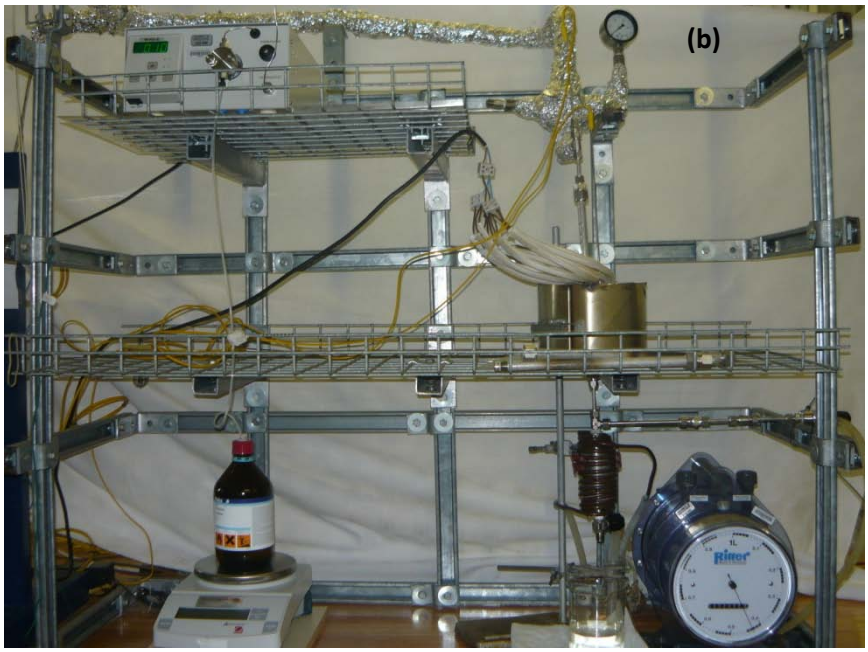

Appendix A1 Figures (a) and (b) showing actual reactor set up

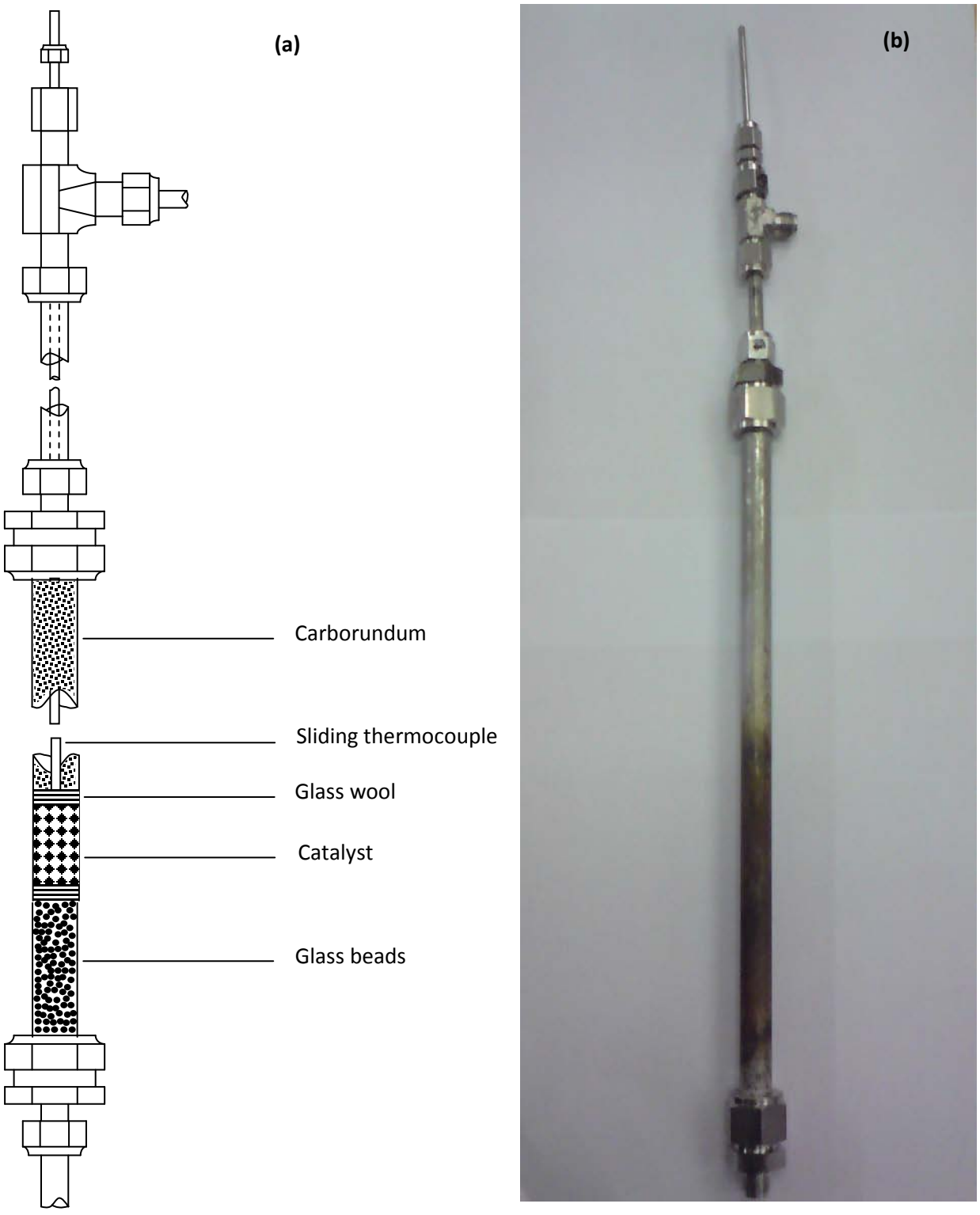

Appendix A2 Illustration of (a) packed reactor tube and (b) actual reactor tube

Reaction Name	Pack T							
Pressure (kPa)	101.325							
Temp. (K)	298							
Mw hexane (g/mol)	86.19							
Carbon no. hexane	6							
Density hexane (g/mL)	0.659							
Date	12-Aug	12-Aug	12-Aug	12-Aug	12-Aug	12-Aug	12-Aug	13-Aug
Time	07:00	08:00	09:30	11:00	12:30	14:00	15:30	07:00
Int. Temp (°C)	401	400	400	398	400	400	399	398
Gas reading (l)	15106.50	15109.10	15112.90	15116.70	15120.45	15124.20	15128.00	15166.90
Balance (g)	1033.36	1029.66	1024.28	1018.74	1013.38	1008.06	1002.59	946.73
Mass drained (g)		2.3402	3.925	4.1737	4.0519	4.115	4.3018	44.7705
Water phase (g)		0.17	0.29	0.18	0.17	0.12	0.25	2.92
Time online (h)		1.00	2.50	4.00	5.50	7.00	8.50	24.00
Time online (min)		60.00	150.00	240.00	330.00	420.00	510.00	1440.00
Time at T (min)		1.00	2.50	4.00	5.50	7.00	8.50	24.00
Karl Fischer		93%	94%	94%	94%	89%	89%	76%
Water phase		1.10E-02	1.70E-02	1.06E-02	1.12E-02	1.24E-02	2.69E-02	7.09E-01
Liquid in (g)		3.70	5.38	5.54	5.36	5.32	5.47	55.86
Liquid in (mL/min)		0.094	0.091	0.093	0.090	0.090	0.092	0.091
Liquid in (g/min)		3.70E+00	5.38E+00	5.54E+00	5.36E+00	5.32E+00	5.47E+00	5.59E+01
Liquid in (mol)		4.29E-02	6.24E-02	6.43E-02	6.22E-02	6.17E-02	6.35E-02	6.48E-01
Mol carbon in		2.58E-01	3.75E-01	3.86E-01	3.73E-01	3.70E-01	3.81E-01	3.89E+00
Liq. out (g/min)		2.34E+00	3.93E+00	4.17E+00	4.05E+00	4.12E+00	4.30E+00	4.48E+01
Organic phase out (g/min)		2.17E+00	3.63E+00	3.99E+00	3.88E+00	4.00E+00	4.05E+00	4.18E+01
Gas in (mL/min)		1049.67	1526.28	1571.67	1520.61	1509.26	1551.82	15847.24
Gas out (mL/min)		2600.00	3800.00	3800.00	3750.00	3750.00	3800.00	38900.00
Gas out (mol/min)		1.06E-01	1.55E-01	1.55E-01	1.53E-01	1.53E-01	1.55E-01	1.59E+00
Liquid mass balance		63%	73%	75%	76%	77%	79%	80%
Gas out in (mL/min)		43.33	42.22	42.22	41.67	41.67	42.22	41.99

Appendix A3 Sample spreadsheet to illustrate method of calculation (readings)

Time		08:00	9:30	11:00	12:30	14:00	15:30	07:00
Gas flow (mL/min)		2600.00	3800.00	3800.00	3750.00	3750.00	3800.00	38900.00
Temp. (°C)		400	400	398	400	400	399	398
Vol. injected		2.50E-01	2.50E-01	2.50E-01	2.50E-01	2.50E-01	2.50E-01	2.50E-01
Area								
ethylene		104022.70	40914.28	19133.80	10591.55	4483.35	2190.80	1104.68
propene		262929.40	100534.11	50565.70	40216.23	28785.22	8286.51	5733.22
hexane		393471.26	408551.45	408718.30	408391.17	390004.91	417775.81	410525.33
methane		1098.77	485.83	334.48	0.00	0.00	0.00	0.00
Total		761522.13	550485.67	478751.28	459198.95	423273.48	428253.12	417363.23
Corrected area	**Rf**							
ethylene	1.0	104022.70	40914.28	19132.80	10591.55	4483.35	2190.80	1104.68
propene	1.0	262929.40	100534.11	50565.70	40216.23	28785.22	8286.51	5733.22
hexane	1.0	393471.26	408551.45	408718.30	408391.17	390004.91	417775.81	410525.33
methane	1.0	1098.77	484.83	334.48	0.00	0.00	0.00	0.00
Total		761522.13	550484.67	478751.28	459198.95	423273.48	428253.12	417363.23
Mol (%) (or Vol.%)[a]	**Mw**							
ethylene	28.05	6.52%	2.57%	1.20%	0.66%	0.28%	0.14%	0.07%
propene	42.08	10.99%	4.20%	2.11%	1.68%	1.20%	0.35%	0.24%
hexane	86.19	8.02%	8.32%	8.33%	8.32%	7.95%	8.51%	8.36%
methane	16.04	0.12%	0.05%	0.04%	0.00%	0.00%	0.00%	0.00%
Total		25.65%	15.15%	11.68%	10.67%	9.43%	9.00%	8.67%
Vol. out (mL/min)[b]								
ethylene		169.61	97.50	45.60	24.91	10.54	5.22	26.95
propene		285.81	159.72	80.34	63.05	45.13	13.17	93.24
hexane		208.42	316.29	316.42	312.01	297.96	323.44	3253.51
methane		3.14	2.02	1.39	0.00	0.00	0.00	0.00
Total		666.99	575.54	443.75	399.97	353.64	341.82	3373.70
Mol out (mol/min)[c]								
ethylene		6.94E-03	3.99E-03	1.86E-03	1.02E-03	4.31E-04	2.14E-04	1.10E-03
propene		1.17E-02	6.53E-03	3.29E-03	2.58E-03	1.85E-03	5.38E-04	3.81E-03
hexane		8.52E-03	1.29E-02	1.29E-02	1.28E-02	1.22E-02	1.32E-02	1.33E-01
methane		1.28E-04	8.27E-05	5.70E-05	0.00E+00	0.00E+00	0.00E+00	0.00E+00
Total		2.73E-02	2.35E-02	1.81E-02	1.64E-02	1.45E-02	1.40E-02	1.38E-01
Mol Carbon	**Carbon no.**							
ethylene	**2**	1.39E-02	7.98E-03	3.73E-03	2.04E-03	8.62E-04	4.27E-04	2.20E-03
propene	**3**	3.51E-02	1.96E-02	9.86E-03	7.74E-03	5.54E-03	1.62E-03	1.14E-02
hexane	**6**	5.11E-02	7.76E-02	7.76E-02	7.66E-02	7.31E-02	7.94E-02	7.98E-01
methane	**1**	1.28E-04	8.27E-05	5.70E-05	0.00E+00	0.00E+00	0.00E+00	0.00E+00
Total Mol Carbon		1.00E-01	1.05E-01	9.13E-02	8.63E-02	7.95E-02	8.14E-02	8.12E-01

[a]corrected Area x constant x Mr[methane]/Mr[component], [b]Mol(%) x Gas out, [c] n=pV/RT

Appendix A3 Sample spreadsheet to illustrate method of calculation (gaseous products/lights)

Time	08:00	9:30	11:00	12:30	14:00	15:30	07:00
Gas flow (mL/min)	2600.00	3800.00	3800.00	3750.00	3750.00	3800.00	38900.0
Temp (°C)	400	400	398	400	400	399	398
Peak Areas							
CO	26580.14	29565.12	29849.47	29015.86	26402.57	25485.31	29015.86
CO_2	48592.89	56735.72	61038.96	58625.49	52874.71	50388.36	58625.49
Vol. (%)							
CO	5.47E-08	6.08E-08	6.14E-08	5.97E-08	5.43E-08	5.24E-08	5.97E-08
CO_2	8.57E-08	1.00E-07	1.08E-07	1.03E-07	9.33E-08	8.89E-08	1.03E-07
Vol. (mL/min)							
CO	1.42E-03	2.31E-03	2.33E-03	2.24E-03	2.04E-03	1.99E-03	2.32E-02
CO_2	2.23E-03	3.80E-03	4.09E-03	3.88E-03	3.50E-03	3.38E-03	4.02E-02
Mol/min=(mol carbon no.)							
CO	**1.42E-03**	**2.31E-03**	**2.33E-03**	**2.24E-03**	**2.04E-03**	**1.99E-03**	**2.32E-02**
CO_2	**2.23E-03**	**3.80E-03**	**4.09E-03**	**3.88E-03**	**3.50E-03**	**3.38E-03**	**4.02E-02**
Total Mol Carbon	**3.65E-03**	**6.11E-03**	**6.42E-03**	**6.12E-03**	**5.53E-03**	**5.37E-03**	**6.34E-02**

Appendix A3 Sample spreadsheet to illustrate method of calculation (gaseous COx)

Time		08:00	9:30	11:00	12:30	14:00	15:30	07:00
Water out (g/min)		0.01	0.02	0.01	0.01	0.01	0.03	0.71
Temp. (°C)		400	400	398	400	400	399	398
Area								
methanol		569.06	2738.78	8581.68	31717.68	41738.78	68581.68	731717.68
1-hexanol		0.00	0.00	0.00	464.04	1534.89	4121.67	10726.18
Total		569.06	2738.78	8581.68	32181.72	43273.67	72703.35	742443.86
Corrected area[d]	**Rf**							
Methanol	0.34	1673.71	8055.24	25240.24	93287.29	122761.12	201710.82	2152110.82
1-hexanol	1.2	0.00	0.00	0.00	386.70	1279.08	3434.73	8938.48
Total		1673.71	8055.24	25240.24	93673.99	124040.19	205145.55	2161049.31
Corrected area %								
Methanol		0.00%	0.00%	0.00%	6.79%	23.17%	27.51%	28.81%
1-hexanol		0.00%	0.00%	0.00%	0.41%	1.03%	1.67%	0.41%
Total		100.00%	100.00%	100.00%	100.00%	100.00%	100.00%	100.00%
Mass out(g/min)[e]								
methanol		0.00E+00	0.00E+00	0.00E+00	7.58E-04	2.88E-03	7.39E-03	2.04E-01
1-hexanol		0.00E+00	0.00E+00	0.00E+00	4.61E-05	1.28E-04	4.50E-04	2.93E-03
Total		1.10E-02	1.70E-02	1.06E-02	1.12E-02	1.24E-02	2.69E-02	7.09E-01
Mol out (mol/min)	**Mw**							
methanol	32	0.00E+00	0.00E+00	0.00E+00	2.37E-05	8.99E-05	2.31E-04	6.39E-03
1-hexanol	102.2	0.00E+00	0.00E+00	0.00E+00	4.51E-07	1.25E-06	4.40E-06	2.87E-05
Total		1.28E-04	1.88E-04	1.10E-04	1.39E-04	1.86E-04	4.49E-04	1.34E-02
Mol Carbon	**Carbon no.**							
methanol	1	0.00E+00	0.00E+00	0.00E+00	2.37E-05	8.99E-05	2.31E-04	6.39E-03
1-hexanol	6	0.00E+00	0.00E+00	0.00E+00	2.70E-06	7.52E-06	2.64E-05	1.72E-04
Total Mol Carbon		7.66E-04	1.13E-03	6.61E-04	6.75E-04	6.69E-04	1.51E-03	3.79E-02

[d]corrected Area /total corrected area, [e]Mass % x Water out

Appendix A3 Sample spreadsheet to illustrate method of calculation (liquid aqueous layer)

Time			08:00	9:30	11:00	12:30	14:00	15:30	07:00
Mass Organic fraction (g/min)			2.17E+00	3.63E+00	3.99E+00	3.88E+00	4.00E+00	4.05E+00	4.18E+01
Temp. (°C)			400	400	398	400	400	399	398
Area									
hexane			4134819.7	4426559.2	4437503.2	4407159.2	4439161.8	4335758.5	4184393.3
1-hexene			0.00	0.00	0.00	0.00	0.00	0.00	5011.3
3-methylpentane			15364.67	15481.03	14985.54	14566.83	14599.03	14306.64	14067.84
methylcyclopentane			20781.13	19094.9	17002.54	16007.78	15768.62	15400.87	14826.59
1-hexanol			20234.83	8103.02	3390.56	2338.48	1057.24	164.31	
Total			4191200	4469238	4472882	4440072	4470587	4365630	4218299
Corrected area	**Rf**								
hexane	1.0		4134820	4426559	4437503	4407159	4439162	4335759	4184393
1-hexene	1.02		0.00	0.00	0.00	0.00	0.00	0.00	4913
3-methylpentane	1.0		15365	15481	14986	14567	14599	14307	14068
methylcyclopentane	1.0		20781	19095	17003	16008	15769	15401	14827
1-hexanol	1.2		17384	6961	2913	2009	908	141	0.00
Total			4188349	4468096	4472404	4439743	4470438	4365607	4218201
Corrected area %									
hexane			98.72%	99.07%	99.22%	99.27%	99.30%	99.32%	99.20%
1-hexene			0.00%	0.00%	0.00%	0.00%	0.00%	0.00%	0.12%
3-methylpentane			0.37%	0.35%	0.34%	0.33%	0.33%	0.33%	0.33%
methylcyclopentane			0.50%	0.43%	0.38%	0.36%	0.35%	0.35%	0.35%
1-hexanol			0.42%	0.16%	0.07%	0.05%	0.02%	0.00%	0.00%
Total			100.00%	100.00%	100.00%	100.00%	100.00%	100.00%	100.00%
Mol Carbon (mol C/min)	**Mw**	**Carbon no.**							
hexane	86.19	6	1.49E-01	2.50E-01	2.76E-01	2.68E-01	2.76E-01	2.80E-01	2.89E+00
1-hexene	84	6	0.00E+00	0.00E+00	0.00E+00	0.00E+00	0.00E+00	0.00E+00	3.48E-03
3-methylpentane	86	6	5.56E-04	8.78E-04	9.33E-04	8.88E-04	9.11E-04	9.26E-04	9.74E-03
methylcyclopentane	86	6	7.52E-04	1.08E-03	1.06E-03	9.76E-04	9.84E-04	9.97E-04	1.03E-02
1-hexanol	102.2	6	5.29E-04	3.32E-04	1.53E-04	1.03E-04	4.77E-05	7.69E-06	0.00E+00
Total Mol Carbon			1.51E-01	2.53E-01	2.78E-01	2.70E-01	2.78E-01	2.82E-01	2.91E+00

Appendix A3 Sample spreadsheet to illustrate method of calculation (liquid organic layer)

Time	08:00	9:30	11:00	12:30	14:00	15:30	07:00
Time online (h)	1.0	2.5	4.0	5.5	7.0	8.5	24.0
Temp (°C)	400	400	398	400	400	399	398
Organic							
methanol	0.00E+00	0.00E+00	0.00E+00	0.00E+00	0.00E+00	0.00E+00	0.00E+00
hexane	1.49E-01	2.50E-01	2.76E-01	2.68E-01	2.76E-01	2.80E-01	2.89E+00
3-methylpentane	5.56E-04	8.78E-04	9.33E-04	8.88E-04	9.11E-04	9.26E-04	9.74E-03
methylcyclopentane	7.52E-04	1.08E-03	1.06E-03	9.76E-04	9.84E-04	9.97E-04	1.03E-02
1-hexene	0.00E+00	0.00E+00	0.00E+00	0.00E+00	0.00E+00	0.00E+00	3.48E-03
1-hexanol	5.29E-04	3.32E-04	1.53E-04	1.03E-04	4.77E-05	7.69E-06	0.00E+00
ethylene	0.00E+00	0.00E+00	0.00E+00	0.00E+00	0.00E+00	0.00E+00	0.00E+00
propene	0.00E+00	0.00E+00	0.00E+00	0.00E+00	0.00E+00	0.00E+00	0.00E+00
methane	0.00E+00	0.00E+00	0.00E+00	0.00E+00	0.00E+00	0.00E+00	0.00E+00
CO	0.00E+00	0.00E+00	0.00E+00	0.00E+00	0.00E+00	0.00E+00	0.00E+00
CO_2	0.00E+00	0.00E+00	0.00E+00	0.00E+00	0.00E+00	0.00E+00	0.00E+00
Total Mol Carbon	1.51E-01	2.53E-01	2.78E-01	2.70E-01	2.78E-01	2.82E-01	2.91E+00
Light							
methanol	0.00E+00	0.00E+00	0.00E+00	0.00E+00	0.00E+00	0.00E+00	0.00E+00
hexane	5.11E-02	7.76E-02	7.76E-02	7.66E-02	7.31E-02	7.94E-02	7.98E-01
3-methylpentane	0.00E+00	0.00E+00	0.00E+00	0.00E+00	0.00E+00	0.00E+00	0.00E+00
methylcyclopentane	0.00E+00	0.00E+00	0.00E+00	0.00E+00	0.00E+00	0.00E+00	0.00E+00
1-hexene	0.00E+00	0.00E+00	0.00E+00	0.00E+00	0.00E+00	0.00E+00	0.00E+00
1-hexanol	0.00E+00	0.00E+00	0.00E+00	0.00E+00	0.00E+00	0.00E+00	0.00E+00
ethylene	1.39E-02	7.98E-03	3.73E-03	2.04E-03	8.62E-04	4.27E-04	2.20E-03
propene	3.51E-02	1.96E-02	9.86E-03	7.74E-03	3.61E-03	1.62E-03	1.14E-02
methane	1.28E-04	8.27E-05	5.70E-05	0.00E+00	0.00E+00	0.00E+00	0.00E+00
CO	0.00E+00	0.00E+00	0.00E+00	0.00E+00	0.00E+00	0.00E+00	0.00E+00
CO_2	0.00E+00	0.00E+00	0.00E+00	0.00E+00	0.00E+00	0.00E+00	0.00E+00
Total Mol Carbon	1.00E-01	1.05E-01	9.13E-02	8.63E-02	7.76E-02	8.14E-02	8.12E-01
COx							
CO	1.42E-03	2.31E-03	2.33E-03	2.24E-03	2.04E-03	1.99E-03	2.32E-02
CO_2	2.23E-03	3.80E-03	4.09E-03	3.88E-03	3.50E-03	3.38E-03	4.02E-02
Total Mol Carbon	3.65E-03	6.11E-03	6.42E-03	6.12E-03	5.53E-03	5.37E-03	6.34E-02
Aqueous							
methanol	0.00E+00	0.00E+00	0.00E+00	2.37E-05	8.99E-05	2.31E-04	6.39E-03
hexane	0.00E+00	0.00E+00	0.00E+00	0.00E+00	0.00E+00	0.00E+00	0.00E+00
3-methylpentane	0.00E+00	0.00E+00	0.00E+00	0.00E+00	0.00E+00	0.00E+00	0.00E+00
methylcyclopentane	0.00E+00	0.00E+00	0.00E+00	0.00E+00	0.00E+00	0.00E+00	0.00E+00
1-hexene	0.00E+00	0.00E+00	0.00E+00	0.00E+00	0.00E+00	0.00E+00	0.00E+00
1-hexanol	0.00E+00	0.00E+00	0.00E+00	2.70E-06	7.52E-06	2.64E-05	1.72E-04
ethylene	0.00E+00	0.00E+00	0.00E+00	0.00E+00	0.00E+00	0.00E+00	0.00E+00
propene	0.00E+00	0.00E+00	0.00E+00	0.00E+00	0.00E+00	0.00E+00	0.00E+00
methane	0.00E+00	0.00E+00	0.00E+00	0.00E+00	0.00E+00	0.00E+00	0.00E+00
CO	0.00E+00	0.00E+00	0.00E+00	0.00E+00	0.00E+00	0.00E+00	0.00E+00
CO_2	0.00E+00	0.00E+00	0.00E+00	0.00E+00	0.00E+00	0.00E+00	0.00E+00
Total Mol Carbon	0.00E+00	0.00E+00	0.00E+00	2.64E-05	9.75E-05	2.57E-04	6.56E-03

Appendix A3 Sample spreadsheet to illustrate method of calculation

Total mol C out (mol C/min)							
methanol	0.00E+00	0.00E+00	0.00E+00	2.37E-05	8.99E-05	2.31E-04	6.39E-03
hexane	2.01E-01	3.28E-01	3.53E-01	3.45E-01	3.49E-01	3.59E-01	3.69E+00
3-methylpentane	5.56E-04	8.78E-04	9.33E-04	8.88E-04	9.11E-04	9.26E-04	9.74E-03
methylcyclopentane	7.52E-04	1.08E-03	1.06E-03	9.76E-04	9.84E-04	9.97E-04	1.03E-02
1-hexene	0.00E+00	0.00E+00	0.00E+00	0.00E+00	0.00E+00	0.00E+00	3.48E-03
1-hexanol	5.29E-04	3.32E-04	1.53E-04	1.06E-04	5.52E-05	3.41E-05	1.72E-04
ethylene	1.39E-02	7.98E-03	3.73E-03	2.04E-03	8.62E-04	4.27E-04	2.20E-03
propene	3.51E-02	1.96E-02	9.86E-03	7.74E-03	3.61E-03	1.62E-03	1.14E-02
methane	1.28E-04	8.27E-05	5.70E-05	0.00E+00	0.00E+00	0.00E+00	0.00E+00
CO	1.42E-03	2.31E-03	2.33E-03	2.24E-03	2.04E-03	1.99E-03	2.32E-02
CO_2	2.23E-03	3.80E-03	4.09E-03	3.88E-03	3.50E-03	3.38E-03	4.02E-02
Total mol C out (mol C/min)	2.55E-01	3.64E-01	3.76E-01	3.62E-01	3.61E-01	3.69E-01	3.80E+00
Product (mol C/min)							
methanol	0.00E+00	0.00E+00	0.00E+00	2.37E-05	8.99E-05	2.31E-04	6.39E-03
hexane	0.00E+00	0.00E+00	0.00E+00	0.00E+00	0.00E+00	0.00E+00	0.00E+00
3-methylpentane	0.00E+00	0.00E+00	0.00E+00	0.00E+00	0.00E+00	0.00E+00	0.00E+00
methylcyclopentane	0.00E+00	0.00E+00	0.00E+00	0.00E+00	0.00E+00	0.00E+00	0.00E+00
1-hexene	0.00E+00	0.00E+00	0.00E+00	0.00E+00	0.00E+00	0.00E+00	3.48E-03
1-hexanol	5.29E-04	3.32E-04	1.53E-04	1.06E-04	5.52E-05	3.41E-05	1.72E-04
ethylene	1.39E-02	7.98E-03	3.73E-03	2.04E-03	8.62E-04	4.27E-04	2.20E-03
propene	3.51E-02	1.96E-02	9.86E-03	7.74E-03	3.61E-03	1.62E-03	1.14E-02
methane	1.28E-04	8.27E-05	5.70E-05	0.00E+00	0.00E+00	0.00E+00	0.00E+00
CO	1.42E-03	2.31E-03	2.33E-03	2.24E-03	2.04E-03	1.99E-03	2.32E-02
CO_2	2.23E-03	3.80E-03	4.09E-03	3.88E-03	3.50E-03	3.38E-03	4.02E-02
Total Product	5.32E-02	3.41E-02	2.02E-02	1.60E-02	1.02E-02	7.68E-03	8.71E-02
Hexane in Feed (mol C/min)							
Hexane	2.56E-01	3.72E-01	3.83E-01	3.71E-01	3.68E-01	3.78E-01	3.86E+00
Conversion	**21.60%**	**11.79%**	**7.73%**	**6.99%**	**4.98%**	**4.97%**	**4.48%**
Selectivity							
methanol	**0.00**	**0.00**	**0.00**	**0.15**	**0.89**	**3.01**	**7.33**
hexane	**0.00**	**0.00**	**0.00**	**0.00**	**0.00**	**0.00**	**0.00**
3-methylpentane	**0.00**	**0.00**	**0.00**	**0.00**	**0.00**	**0.00**	**0.00**
methylcyclopentane	**0.00**	**0.00**	**0.00**	**0.00**	**0.00**	**0.00**	**0.00**
1-hexene	**0.00**	**0.00**	**0.00**	**0.00**	**0.00**	**0.00**	**4.00**
1-hexanol	**0.99**	**0.97**	**0.75**	**0.66**	**0.54**	**0.44**	**0.20**
ethylene	**26.05**	**23.39**	**18.44**	**12.72**	**8.49**	**5.56**	**2.53**
propene	**65.86**	**57.47**	**48.75**	**48.29**	**35.58**	**21.04**	**13.13**
methane	**0.24**	**0.24**	**0.28**	**0.00**	**0.00**	**0.00**	**0.00**
CO	**2.67**	**6.78**	**11.54**	**13.98**	**20.06**	**25.96**	**26.65**
CO_2	**4.18**	**11.15**	**20.23**	**24.20**	**34.44**	**43.99**	**46.16**
Total	**100.00**	**100.00**	**100.00**	**100.00**	**100.00**	**100.00**	**100.00**
Total mol carbon in feed	2.58E-01	3.75E-01	3.86E-01	3.73E-01	3.70E-01	3.81E-01	3.89E+00
Carbon balance	**99.03%**	**97.22%**	**97.38%**	**97.15%**	**97.60%**	**96.88%**	**97.60%**

Appendix A3 Sample spreadsheet to illustrate method of calculation

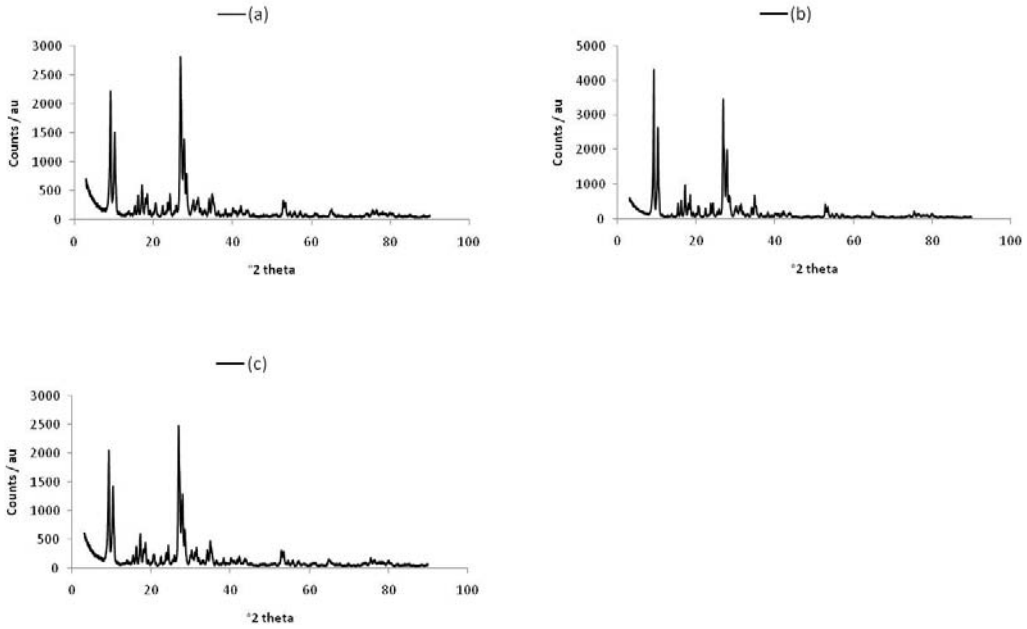

Appendix A4 Diffractograms of (a) H-ZSM-5 (100), (b) H-ZSM-5 (320) and (c) Na-ZSM-5 (100)

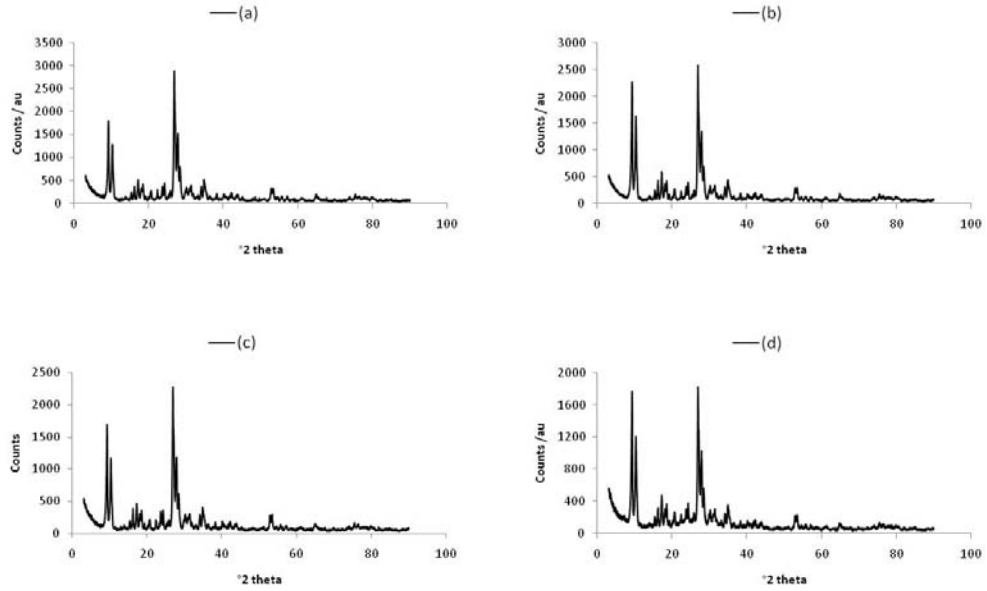

Appendix A5 Diffractograms of (a) Na-V-ZSM-5 (0.4%), (b) Na-V-ZSM-5 (0.9%), (c) Na-V-ZSM-5 (2.0%) and (d) Na-V-ZSM-5 (2.5%)

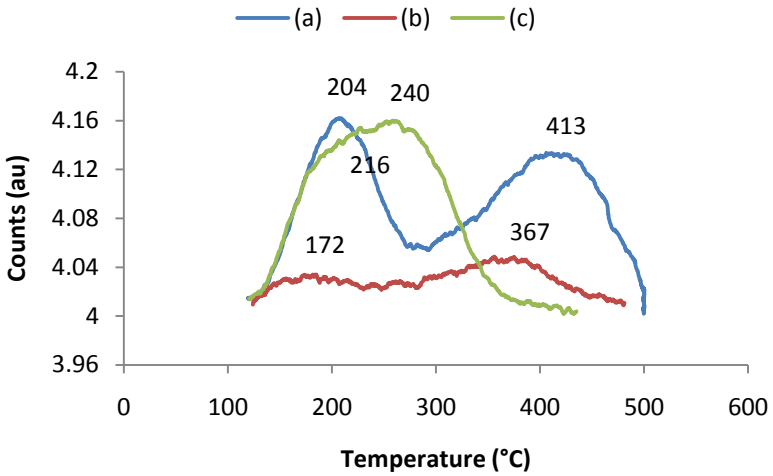

Appendix A6 NH_3-TPD profiles of (a) H-ZSM-5 (100), (b) H-ZSM-5 (320) and (c) Na-ZSM-5 (100)

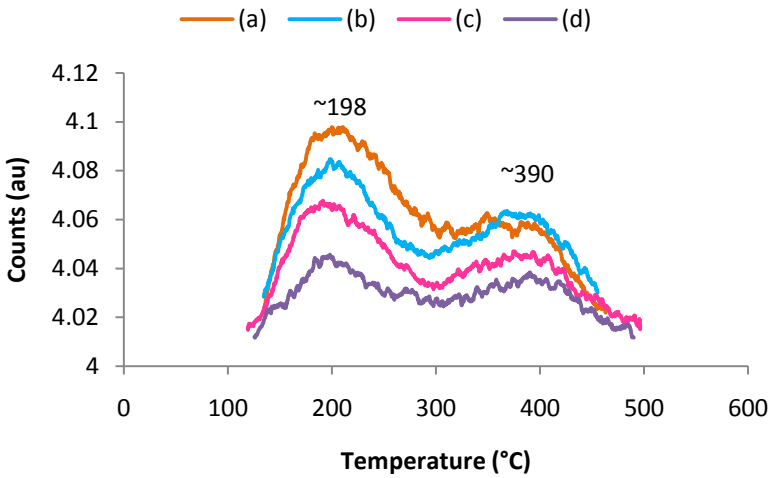

Appendix A7 NH_3-TPD profiles of (a) Na-V-ZSM-5 (0.4%), (b) Na-V-ZSM-5 (0.9%), (c) Na-V-ZSM-5 (2.0%) and (d) Na-V-ZSM-5 (2.5%)

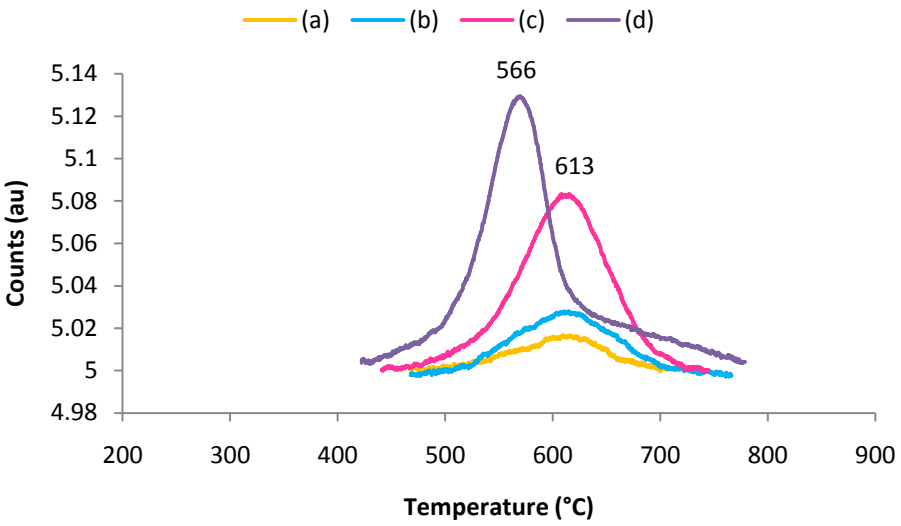

Appendix A8 H_2-TPR profiles of (a) Na-V-ZSM-5 (0.4%), (b) Na-V-ZSM-5 (0.9%), (c) Na-V-ZSM-5 (2.0%) and (d) Na-V-ZSM-5 (2.5%)

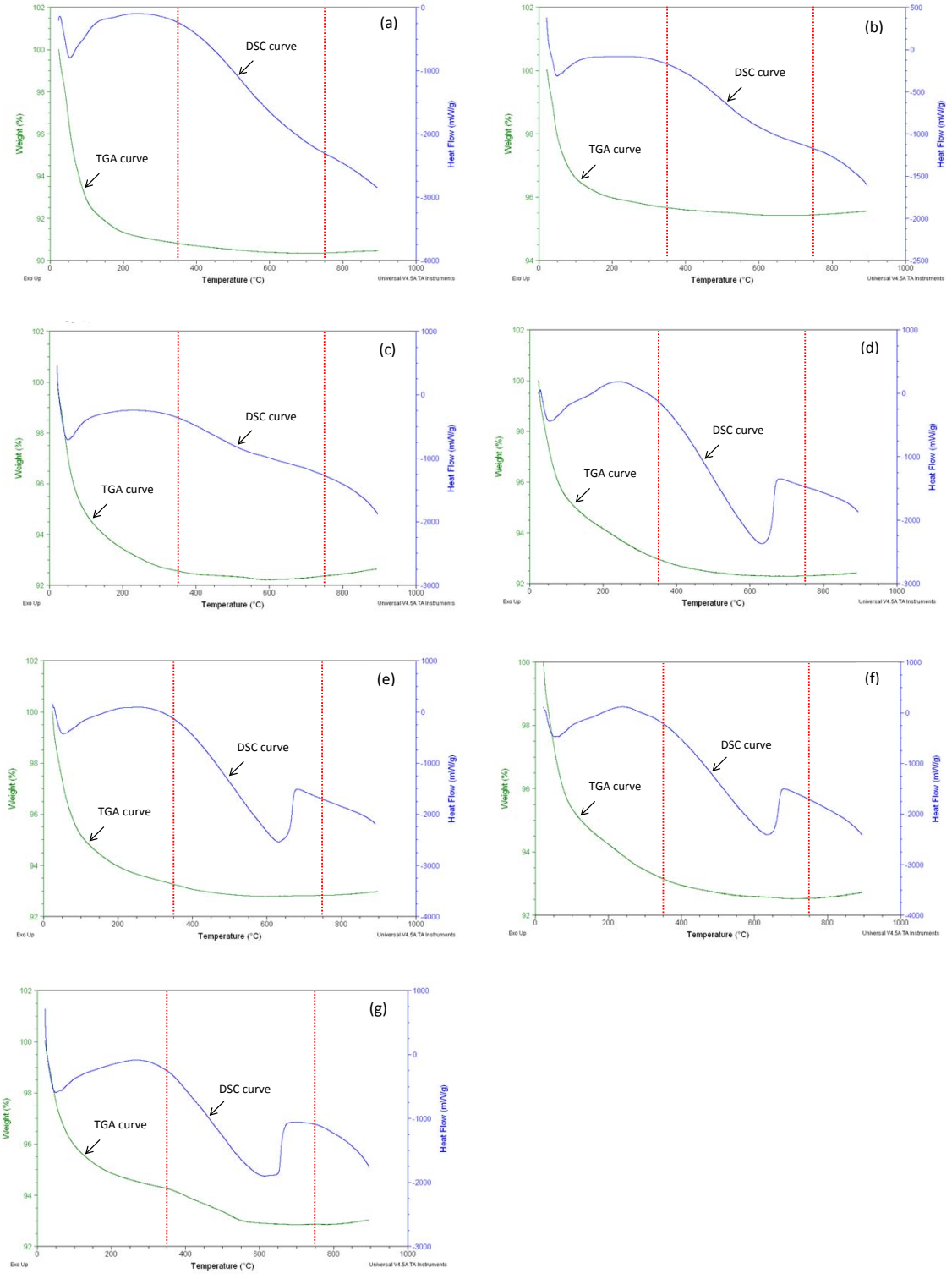

Appendix A9 TGA–DSC curves of (a) H-ZSM-5 (100), (b) H-ZSM-5 (320), (c) Na-ZSM-5 (100), (d) Na-V-ZSM-5 (0.4%), (e) Na-V-ZSM-5 (0.9%), (f) Na-V-ZSM-5 (2.0%) and (g) Na-ZSM-5 (2.5%)

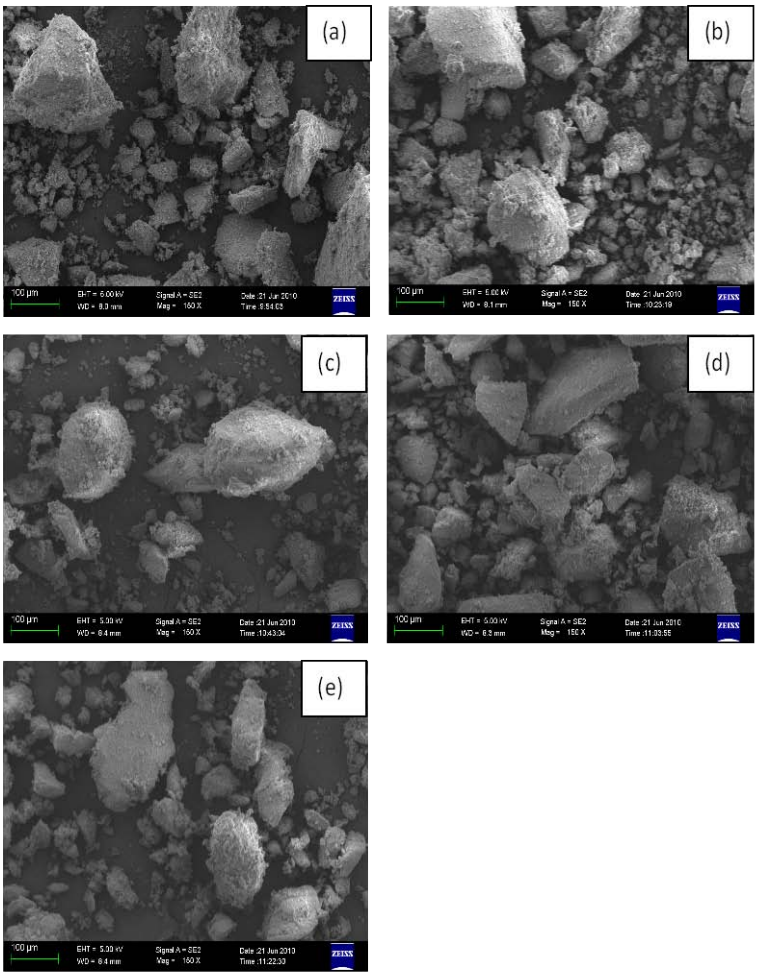

Appendix A10 SEM micrographs of (a) Na-ZSM-5 (100), (b) Na-V-ZSM-5 (0.4%), (c) Na-V-ZSM-5 (0.9%), (d) Na-V-ZSM-5 (2.0%) and (e) Na-ZSM-5 (2.5%)

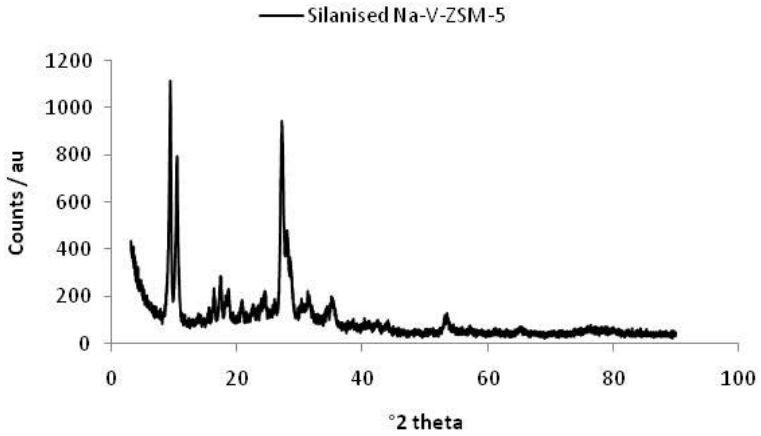

Appendix A11 Diffractogram of silanised Na-V-ZSM-5

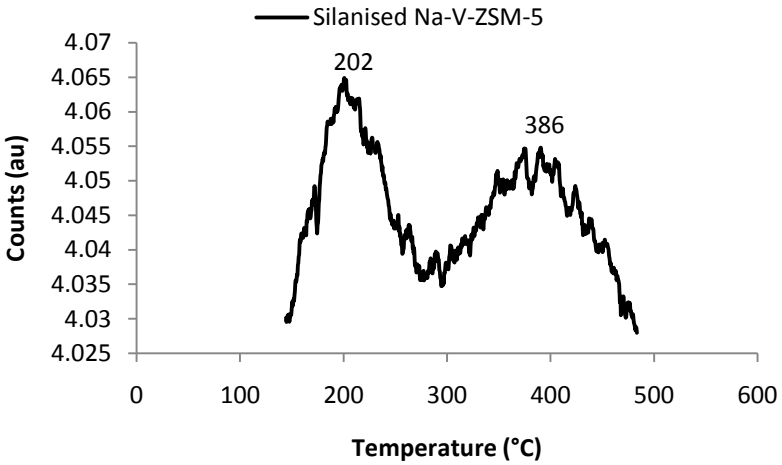

Appendix A12 NH_3-TPD profile of silanised Na-V-ZSM-5

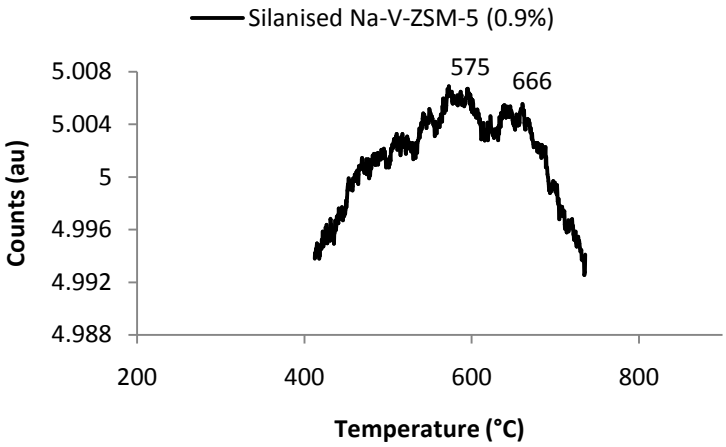

Appendix A13 H_2-TPR profiles of silanised Na-V-ZSM-5

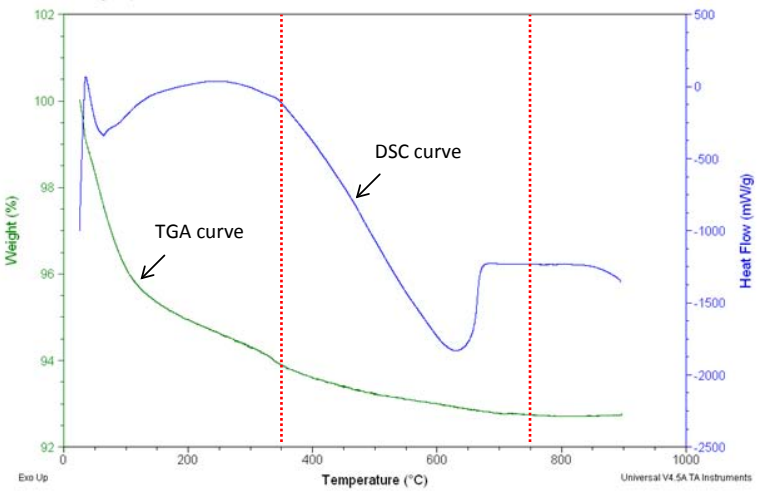

Appendix A14 TGA–DSC curves of silanised Na-V-ZSM-5

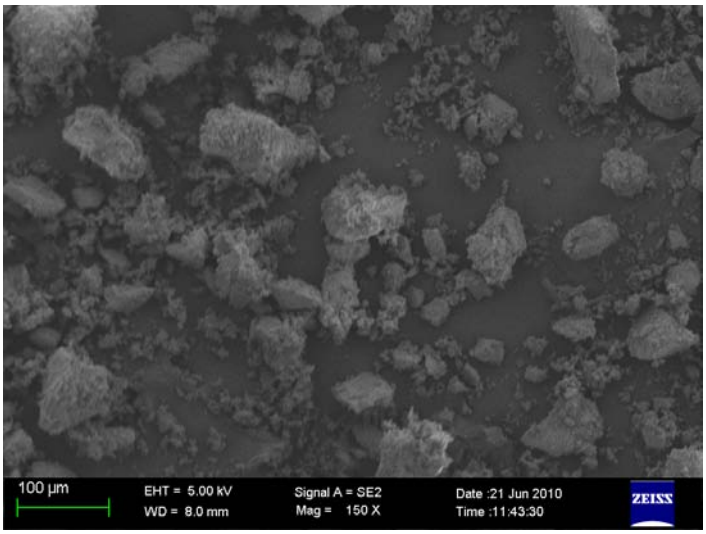

Appendix A15 SEM micrograph of silanised Na-V-ZSM-5

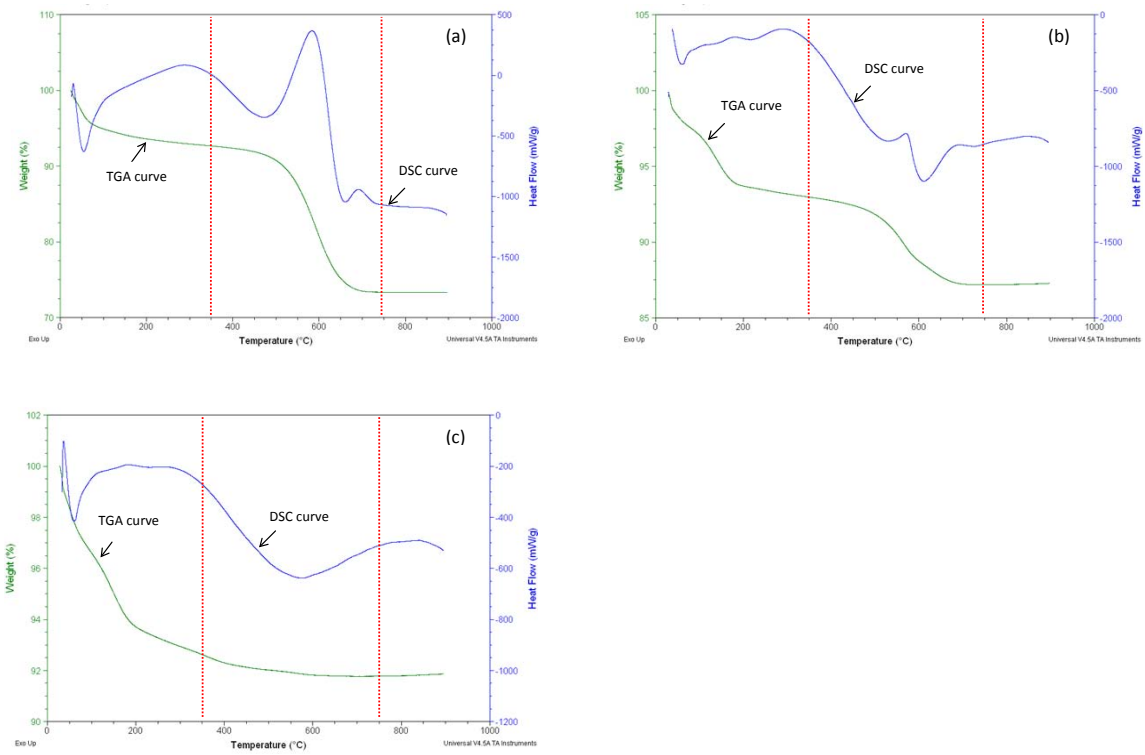

Appendix A16 TGA and DSC curves of spent precursors (a) H-ZSM-5 (100), (b) H-ZSM-5 (320) and (c) Na-ZSM-5 (100

Appendix A17 Summary of products under different reaction conditions and vanadium loadings

						Selectivity (%)[a]													
				Conv.(%)[a]		1-hexanol		Hexanal		Hexanoic acid		1-hexene		Cracked prods.[b]		Cyclics&aromatics[c]		COx	
Temp. (°C)	V loading (%)	Contact time (s)	Fuel-air ratio	1	24	1	24	1	24	1	24	1	24	1	24	1	24	1	24
350	0.9	0.8	1.3	21	17	1.3	0.1	0.0	0.1	4.0	0.2	0.0	1.6	26	40	30	20	17	28
400	**0.9**	**0.8**	**1.3**	**27**	**18**	**1.5**	**0.1**	**0.0**	**0.0**	**1.9**	**0.6**	**0.0**	**1.6**	**35**	**32**	**24**	**9.0**	**19**	**38**
450	0.9	0.8	1.3	24	10	0.9	0.1	0.0	0.0	1.2	0.3	0.0	0.7	31	35	7.0	2.9	30	58
400	0.9	0.5	1.3	5	1	0.7	0.4	0.0	0.0	0.5	0.6	0.0	0.0	57	9	11.8	4.2	24	82
400	0.9	0.8	1.3	27	18	1.5	0.1	0.0	0.0	1.9	0.6	0.0	1.6	35	32	24	9.0	19	38
400	**0.9**	**1.1**	**1.3**	**39**	**27**	**1.6**	**0.1**	**0.0**	**0.4**	**2.1**	**0.2**	**0.0**	**4.6**	**35**	**39**	**35**	**22**	**14**	**22**
400	0.9	1.5	1.3	26	5	1.2	0.0	0.0	0.0	2.0	0.3	0.0	1.1	43	13	24	18	18	62
400	0.9	1.1	0.7	25	20	1.3	0.1	5.8[d]	1.5	0.7	0.2	0.0	0.4	22	26	14	41	52	20
400	**0.9**	**1.1**	**1.3**	**39**	**27**	**1.6**	**0.1**	**0.0**	**0.4**	**2.1**	**0.2**	**0.0**	**4.6**	**35**	**39**	**35**	**22**	**14**	**22**
400	0.9	1.1	2	24	5	1.3	0.6	0.0	0.0	0.9	0.2	0.0	0.0	47	16	28	25	10	47
400	0.4	1.1	1.3	26	16	1.9	0.1	0.0	0.0	0.3	0.5	0.0	2.5	39	38	22	8.0	20	39
400	**0.9**	**1.1**	**1.3**	**39**	**27**	**1.6**	**0.1**	**0.0**	**0.4**	**2.1**	**0.2**	**0.0**	**4.6**	**35**	**39**	**35**	**22**	**14**	**22**
400	2.0	1.1	1.3	23	10	1.4	0.0	0.0	0.0	1.2	0.4	0.0	0.5	33	29	19	8.0	33	48
400	2.5	1.1	1.3	18	11	0.9	0.0	0.0	0.0	1.1	0.2	0.0	0.0	27	24	12	7.0	50	63
400[e]	2.5	1.1	1.3	19	11	0.9	0.1	0.0	0.0	1.0	0.1	0.0	0.0	27	15	11	3.0	50	55
400[f]	0.4	1.1	1.3	18	14	0.3	0.1	0.6	0.2	0.1	0.0	4.2	4.5	38	28	33	38.0	12	15

[a] Initial conversion and selectivities at t = 1 h and t = 24 h are reported. Selectivities to linear C_6 olefins and other C_6 oxygenates are not reported here but in Appendix A, A18

[b] $C_1 – C_5$ linear olefins and oxygenates

[c] Include: cyclopentanone, cyclohexane, benzene, tetrahydrofuran, *cis* and *trans*-2,5-dimethyltetrahydrofuran, 2,5-dimethylfuran, 2-methyl-1-hexene as well as toluene, ethylbenzene, *p*-xylene, *n*-propylbenzene, 2-methyltetrahydropyran, 3,5-dimethyl cyclopentene, 1-ethyl-4-methyl benzene, 1, 2, 4 – trimethylbenzene etc

[d] Time = 2.5 h

[e] Regeneration study – t at completion = 7 h

[f] Silanisation study

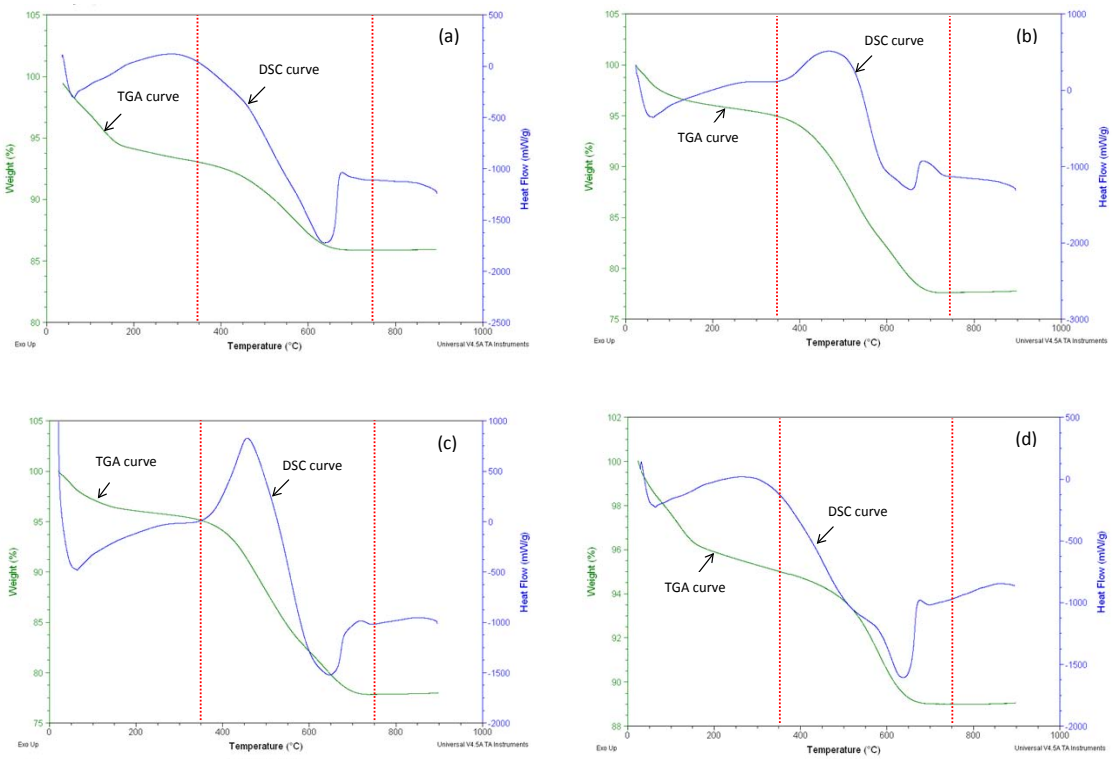

Appendix A18 TGA and DSC curves of spent Na-V-ZSM-5 catalysts (a) 0.5 s, (b) 0.8 s, (c) 1.1 s and (d) 1.5 s

Appendix A19 Selectivities to cracking products formed during the reaction of *n*-hexane with oxygen over Na-V-ZSM-5 catalysts

						Selectivity (%)[a]																			
				Conv.(%)[a]		Methane		Methanol		Ethane		Ethene		Propane		Propene		Butane		Butene		Other cracked[b]		C_6[c]	
Temp. (°C)	V loading (%)	Contact time(s)	Fuel-air ratio	1	24	1	24	1	24	1	24	1	24	1	24	1	24	1	24	1	24	1	24	1	24
350	0.9	0.8	1.3	21	17	0.5	0.6	4.9	12.3	0.3	0.3	5.5	5.0	0.0	0.0	8.5	8.4	0.0	0.0	1.8	4.4	4.5	9.00	2.0	7.8
400	**0.9**	**0.8**	**1.3**	**27**	**18**	**0.4**	**0.6**	**1.2**	**8.7**	**0.8**	**0.0**	**7.1**	**5.6**	**5.6**	**0.0**	**13.3**	**9.8**	**1.6**	**0.0**	**5**	**3.6**	**0.0**	**3.7**	**0.1**	**13.2**
450	0.9	0.8	1.3	24	10	0.6	0.9	0.4	1.4	1.4	1.0	4.6	5.9	2.2	0.0	19.2	22	0.6	0.9	2.5	1.8	0.0	1.1	0.0	1.9
400	0.9	0.5	1.3	5	1.0	0	0.0	0.00	0.00	3.7	0.0	5.7	0.0	13.5	0.0	26	9.00	2.8	0.0	5.2	0.0	0.0	0.0	0.0	0.0
400	0.9	0.8	1.3	27	18	0.4	0.6	1.2	8.7	0.8	0.0	7.1	5.6	5.6	0.0	13.3	9.8	1.6	0.0	5	3.6	0.0	3.7	0.1	13.2
400	**0.9**	**1.1**	**1.3**	**39**	**27**	**0.6**	**0.7**	**2.6**	**6.9**	**0.5**	**0.3**	**6.2**	**5.7**	**5.1**	**0.0**	**9.3**	**9.8**	**2.3**	**0.0**	**5.4**	**6.4**	**2**	**9.2**	**0.2**	**9.3**
400	0.9	1.5	1.3	26	5.0	0.5	0.0	1.1	4.7	2.7	0.0	6.4	2.0	11	0.0	15	5.0	2.1	0.0	3.3	1.0	0.9	0.3	0.1	1.1
400	0.9	1.1	0.7	25	20	0.6	0.0	0.2	4	0.9	0.0	6.2	2.0	2.2	0.0	10.4	2.7	0.0	0.0	1.2	0.9	0.3	13.4	0.1	1.4
400	**0.9**	**1.1**	**1.3**	**39**	**27**	**0.6**	**0.7**	**2.6**	**6.9**	**0.5**	**0.3**	**6.2**	**5.7**	**5.1**	**0.0**	**9.3**	**9.8**	**2.3**	**0.0**	**5.4**	**6.4**	**2**	**9.2**	**0.2**	**9.3**
400	0.9	1.1	2	24	5.0	0.4	0.0	2	5.2	2.6	0.0	5.5	1.1	15.5	0.0	12.9	3.8	3.5	0.0	3.8	1.0	1.8	2.9	0.2	5.1
400	0.5	1.1	1.3	26	16	0.6	0.8	1.1	8.3	0.6	0.3	6.9	6.1	4.7	0.0	13.6	11	1.5	0.0	1.5	0.8	8.5	11	0.2	12
400	**0.9**	**1.1**	**1.3**	**39**	**27**	**0.6**	**0.7**	**2.6**	**6.9**	**0.5**	**0.3**	**6.2**	**5.7**	**5.1**	**0.0**	**9.3**	**9.8**	**2.3**	**0.0**	**5.4**	**6.4**	**2**	**9.2**	**0.2**	**9.3**
400	2	1.1	1.3	23	10	0.6	0.5	1.2	3.8	1.1	0.0	6.2	4.0	5.8	0.0	11.2	6.9	1.6	0.7	3.5	1.4	1.8	12	0.0	5.4
400	2.5	1.1	1.3	18	11	0.8	0.6	1.4	2.6	1.3	0.0	6.1	3.9	6.2	0.0	6.3	5.7	2.0	0.0	0.6	0.4	2.3	9.8	0.0	0.5
400[d]	2.5	1.1	1.3	19	11	0.8	0.7	1.4	2.5	1.3	0.2	6.2	4.2	6.1	0.0	6.3	6.0	1.9	0.0	0.7	0.4	2.3	1.0	0.0	0.0
400[e]	0.9	1.1	1.3	18	14	0.2	0.3	7.7	11.5	0.0	0.0	3.4	3.6	0.0	0.0	6.8	7.0	0.0	0.0	5.6	5.1	11.3	12.5	12	15

[a] Initial conversion and selectivities at t = 1 h and t = 24 h are reported
[b] C_5 and C_2-C_5 oxygenates including acetaldehyde, ethanol, 2-butene etc
[c] C_6 = 1-hexene, *cis* and *trans* 2 and 3-hexene
[d] Regeneration study – t at completion = 7 h
[e] Silanisation study

Appendix A20 Selectivities to linear C_6 olefins and other C_6 oxygenates formed during the reaction of *n*-hexane with oxygen over Na-V-ZSM-5 catalysts

						Selectivity (%)[a]																					
				Conv.(%)[a]		*cis* -2-hexene		*trans* -2-hexene		*trans* -3-hexene		1,5-hexadiene		1,3-hexadiene		2,3-hexadione		2,5-hexadione		3-methyl-2-pentene		2-hexanol		5-hexen-1-ol		*cis* -4-hexen-1-ol	
Temp.	ading (%)	Contact time (s)	Fuel-air ratio	1	24	1	24	1	24	1	24	1	24	1	24	1	24	1	24	1	24	1	24	1	24	1	24
35υ	0.9	0.8	1.3	21	17	0.5	1.9	1.1	4.1	0.5	0.0	1.3	1.0	2.6	1.3	0.2	0.8	3.6	0.5	0.0	0.0	0.2	0.0	0.1	0.2	11.6	0.2
400	**0.9**	**0.8**	**1.3**	**27**	**18**	**0.0**	**2.6**	**0.1**	**8.7**	**0.0**	**0.3**	**2.0**	**1.0**	**2.1**	**1.6**	**0.0**	**0.2**	**3.9**	**0.6**	**0.0**	**3.2**	**0.1**	**0.0**	**0.1**	**0.4**	**10.3**	**0.1**
450	0.9	0.8	1.3	24	10	0.0	0.0	0.0	0.7	0.0	0.5	2.6	0.5	1.2	0.1	17.3	0	2.1	0.5	0.0	0.0	0.4	0.1	0.0	0.1	6.3	0.5
400	0.9	0.5	1.3	5	1	0.0	0.0	0.0	0.0	0.0	0.0	0.0	0.0	0.0	0.0	0.0	0.0	1.4	1.1	0.0	0.0	0.0	0.0	0.0	0.0	4.6	2.7
400	0.9	0.8	1.3	27	18	0.0	2.6	0.1	8.7	0.0	0.3	2.0	1.0	2.1	1.6	0.0	0.2	3.9	0.6	0.0	3.2	0.1	0.0	0.1	0.4	10.3	0.1
400	**0.9**	**1.1**	**1.3**	**39**	**27**	**0.0**	**4.0**	**0.1**	**5.3**	**0.2**	**0.0**	**0.0**	**0.5**	**0.0**	**0.4**	**0.1**	**0.6**	**0.1**	**0.5**	**0.1**	**0.0**	**0.2**	**0.1**	**0.0**	**0.2**	**11.5**	**0.1**
400	0.9	1.5	1.3	26	5	0.0	0.0	0.1	0.0	0.0	0.0	0.0	0.6	0.0	0.0	0.0	0.0	3.0	1.4	0.0	0.0	0.0	0.0	0.0	0.0	8.9	3.6
400	0.9	1.1	0.7	25	20	0.0	0.3	0.1	0.7	0.0	0.0	0.0	1.5	2.1	1.6	0.1	0.9	1.9	1.2	0.0	0.0	0.1	0.0	0.1	0.1	5.5	4.1
400	**0.9**	**1.1**	**1.3**	**39**	**27**	**0.0**	**4.0**	**0.1**	**5.3**	**0.2**	**0.0**	**0.0**	**0.5**	**0.0**	**0.4**	**0.1**	**0.6**	**0.1**	**0.5**	**0.1**	**0.0**	**0.2**	**0.1**	**0.0**	**0.2**	**11.5**	**0.1**
400	0.9	1.1	2	24	5	0.0	1.6	0.0	3.9	0.2	0.0	0.0	0.5	0.0	0.0	0.0	0.6	3.0	0.6	0.0	0.0	0.0	0.0	0.0	0.1	9.0	4.0
400	0.4	1.1	1.3	26	16	0.0	3.4	0.2	6.3	0.0	0.0	0.0	0.0	0.0	0.0	0.0	0.7	3.9	0.8	0.0	0.0	0.1	0.0	0.1	0.2	11.9	0.1
400	**0.9**	**1.1**	**1.3**	**39**	**27**	**0.0**	**4.0**	**0.1**	**5.3**	**0.2**	**0.0**	**0.0**	**0.5**	**0.0**	**0.4**	**0.1**	**0.6**	**0.1**	**0.5**	**0.1**	**0.0**	**0.2**	**0.1**	**0.0**	**0.2**	**11.5**	**0.1**
400	2.0	1.1	1.3	23	10	0.0	1.4	0.0	3.0	0.0	0.5	0.0	0.0	0.0	0.0	0.0	0.0	3.4	2.3	0.0	0.0	0.1	5.8	0.0	0.6	8.5	0.3
400	2.5	1.1	1.3	18	11	0.0	0.0	0.0	0.2	0.0	0.3	0.0	0.0	0.0	0.0	0.0	0.0	2.1	3.0	0.0	0.0	0.0	1.9	0.0	0.4	6.6	0.0
400[b]	2.5	1.1	1.3	19	11	0.0	0.0	0.0	0.1	0.0	0.3	0.0	0.0	0.0	0.0	0.0	0.0	2.0	2.5	0.0	0.0	0.0	1.5	0.0	0.2	6.5	0.0
400[c]	0.4	1.1	1.3	18	14	2.3	3.4	7.6	7.7	0.0	0.0	0.1	0.2	0.0	0.0	0.8	1.3	0.4	0.6	0	0	0	0	0.2	0.3	0.3	0.8

[a] Initial conversion and selectivities at t = 1 h and t = 24 h are reported
[b] Regeneration study – t at completion = 7 h
[c] Silanisation study